NTNU
Norwegian University of
Science and Technology

Low Complexity Antenna Diversity For IEEE 802.15.4 2.4 GHz PHY

Tarjei Aaberge

Master of Science in Electronics
Submission date: June 2009
Supervisor: Torbjørn Ekman, IET

Norwegian University of Science and Technology
Department of Electronics and Telecommunications

Problem Description

Antenna diversity systems can be realized in several ways. Well documented in the literature are polarization diversity, adaptive arrays and transmit/receive diversity. In fact multiple methods are frequently used to further increase reliability in a radio link. However, The most relevant approach for low-power applications is spatial diversity. Spatial diversity employs multiple physical antennas, usually with the same characteristics, that are separated from one another, normally by a space on the order of the wavelength. In addition to the physical requirement of two or more antennas, a diversity system is characterized by the algorithms or techniques that decide how to optimize the signal transmission. Among these techniques are:

- Switching - In a switching receiver, the signal from only one antenna is fed to the receiver for as long as the quality of that signal remains above some prescribed threshold. If and when the signal degrades, another antenna is switched in.

- Selecting - As with switching, selection processing presents only one antenna's signal to the receiver at any given time. The antenna chosen, however, is based on the best signal-to-noise ratio (SNR) among the received signals. This requires that a pre-measurement take place and that all antennas have established connections (at least during the SNR measurement) leading to a higher power requirement. The actual selection process can take place in between received packets of information. This ensures that a single antenna connection is maintained as much as possible. Switching can then take place on a packet-by-packet basis if necessary.

- Combined - Other algorithms are possible, trading between required power/silicon area/receiver complexity. In this case, the possibility of using multiple receivers can be evaluated.

Scope:
- Analyze, implement and test different solutions to low complexity spatial receiver diversity.
- Develop a real system testbed that includes two analog front-ends embedded in TI LPW devices and an external FPGA device where different receiver algorithms and architectures can be implemented and measured (based upon the existing LPW demodulator architectures).
- Establish a test environment where the following scenarios can be analyzed
    * ZigBee system
        - 802.15.4 250 kbps
    * Indoor LOS and non LOS environments
        - Static (multipath effects only)
        - Dynamic (master node moves with TBD m/s speed)
- Produce a set of measurements that show the effects of multiple antenna systems, the algorithms used, and the resulting increase of fading margin in different scenarios.

Assignment given: 16. January 2009

Abstract

This thesis investigates the obtainable performance improvements associated with different fading mitigation techniques using spatial antenna diversity applied to the IEEE 802.15.4 2.4 GHz PHY. The standard possesses modulation properties that inherently provide some multipath resistance. Further resistance is believed obtainable due to the bad and unpredictable fading environments found in typical areas of application. Potential performance increases were theoretically analyzed for different fading channel statistics when two antennas were available for reception. This analysis provided upper bounds for achievable performance improvements that were promising.

Physical testing of selected fading mitigation techniques was performed with hardware from Texas Instruments and means developed by the student. Generally, the PHY has proven itself multipath resistant in the various fading environments tested. PER has been showed to mostly consist of undetected packets. As such, fading mitigation techniques using two receiver chains provide the greatest reduction in PER in a general case, since more packets are detected. PER is observed reduced by a test-dependant factor between 2 and 100 for such techniques. Techniques based on one RF-front end generally provides little performance improvement in dynamic environments, if any. Large spatial differences in received power were observed across distances on the order of a wavelength. A simple technique that switches receiver antenna when detecting an erroneously demodulated packet can exploit this property when RX and TX remain static and hence provide great reductions in PER. This fading mitigation technique is the least complex and power consuming among the ones analyzed and tested.

Contents

List of Tables

List of Figures

Abbreviations

ADC	Analog To Digital Converter
AGC	Automatic Gain Control
BER	Bit Error Rate
CRC	Cyclic Redundancy Check
DSSS	Direct Sequence Spread Spectrum
ED	Energy Detection
FCS	Frame Check Sequence
FPGA	Field Programmable Gate Array
GPIO	General Purpose Input Output
HR-WPAN	High Rate Wireless Personal Area Networks
IEEE	Institute of Electrical and Electronics Engineers
IP	Intellectual Property
LNA	Low Noise Amplifier
LOS	Line of sight
LQI	Link Quality Indicator
LR-WPAN	Low Rate Wireless Personal Area Networks
LVDS	Low Voltage Differential Signaling
MAC	Media Access Control
MLE	Maximum Likelihood Estimates
MR-WPAN	Medium Rate Wireless Personal Area Networks
MRC	Maximal-Ratio Combining
NLOS	No line of sight
NTNU	Norges teknisk-naturvitenskapelige universitet
PAN	Personal Area Network

PER	Packet Error Rate
PHR	PHY Header
PHY	Physical Layer
PPDU	PHY Protocol Data Unit
PPS	Post Packet Switching
PSD	Power Spectral Density
PSDU	PHY Service Data Unit
PSSS	Parallel Sequence Spread Spectrum
RF	Radio Frequency
RSSI	Received Signal Strength Indicator
RX	Receiver
SC	Selection Combining
SHR	Synchronization Header
SNR	Signal-To-Noise Ratio
SOC	System On Chip
SSC	Switch and Stay Combining
TI	Texas Instruments
TX	Transmitter
WPAN	Wireless Personal Area Networks

Chapter 1

Introduction

Envelope fluctuations in the received electromagnetic wave encountered in multipath environments cause performance degradation in wireless systems. The phenomenon is termed fading and has reached a lot of attention since the 1950s. It is believed that different fading mitigation techniques still offers one of the greatest potential performance improvements for current and future wireless standards [17, p. 259]. The use of DSSS specified by [9, p. 27] makes an implementation of the IEEE 802.15.4 2.4 GHz PHY power efficient. Normally, spreading sequences yield multipath and ISI resistance as well. However, these inherent properties of DSSS are not believed to be sufficiently exploited by this standard[4, p. 164] due to relatively long chip periods.

This thesis will investigate the potential performance improvements for the IEEE 802.15.4 2.4 GHz PHY by utilizing spatial antenna receiver diversity with two antennas and different fading mitigation techniques in both dynamic and static indoor environments.

Chapter 2 gives a short introduction to the standard, while chapter 3 deduces a statistical indoor radio channel model. This model is used in chapter 4 to analyze obtainable performance improvements when different fading mitigation techniques are utilized. Analyses are performed for different fading channel statistics, hence capturing possible performance improvements in a range of radio channels likely to be found indoors. The hardware platforms and measurement methodology used to evaluate receiver diversity are presented in chapter 5. Results obtained from tests conducted in four different dynamic indoor environments and one static indoor environment are presented in chapter 6. Key observations and discussion are given in chapter 7, before concluding remarks are stated in chapter 8.

Chapter 2

Zigbee/IEEE 802.15.4

This chapter will give a short introduction to the physical part of IEEE 802.15.4 in general. The major part of the chapter will present information on the 2.4 GHz PHY that is relevant when considering utilization of receiver diversity to mitigate small-scale fading.

2.1 Area of Application

Being part of the IEEE 802.15 family of standards for wireless personal area networks, the IEEE 802.15.4 standard is specified for exchange of information across relatively short distances with emphasis on low power consumption, low complexity/cost and small size. The IEEE 802.15 work group has so far specified the PHY and MAC layers for three such standards. These are HR-WPAN/IEEE 802.15.3, MR-WPAN/IEEE 802.15.1 and LR-WPAN/IEEE 802.15.4. While the MR-WPAN and HR-WPAN supports higher bit rates, the LR-WPAN supports bit rates ranging from 20 Kbit/s to 250 Kbit/s in the ISM bands. The LR-WPAN technology is also intended to be simpler, less expensive and more power-efficient than the other two WPANs.

The targeted properties for IEEE 802.15.4 are ideal for unwired applications that require low data rates and long battery life. This allows for a diverse area of application which can be characterized as wireless network control and monitoring[3]. The ZigBee Alliance is an association of international companies working together to develop a standard with this market as its' target. This wireless standard is called ZigBee, and it is based on the OSI-model. In 2004, the ZigBee Alliance adopted the data link layers defined in the IEEE 802.15.4 standard to provide access to the wireless medium, whereas the rest of the layers, except the application layer, are implemented by the alliance under the name ZigBee Stack. Being incorporated into to this commercial standard, the IEEE 802.15.4 standard is used within building automation, personal health care, industrial control, home control, consumer electronics and computer peripherals[3]

2.2 PHY

The IEEE 802.15.4 standard has been subject to three amendments since the first edition in 2003. Each of these amendments resulted in the addition of optional PHYs. An overview of the PHYs specified by the standard is given in table 2.1. Some parameters are too extensive to present and are hence left out. These can be found by following the reference in the table.

Table 2.1: IEEE 802.15.4 summary, 2009

PHY	Frequency band	Spreading parameters		Data parameters		
		Chip rate	Modulation	Bit rate	Symbol rate	Symbols
(MHz)	(MHz)	(kchip/s		kb/s	ksymbol/s	
IEEE 802.15.4™ -2003						
868/915	868 - 868.6	300	BPSK	20	20	Binary
	902 - 928	600	BPSK	40	40	Binary
2450	2400 - 2483.5	2000	O-QPSK	250	62.5	16-ary ortogonal
IEEE 802.15.4™ -2006 Amendment 1 (optional)						
868/915	868 - 868.6	400	ASK	250	12.5	20 bit PSSS
	902 - 928	1600	ASK	250	50	5 bit PSSS
868/915	868 - 868.6	400	O-QPSK	100	25	16-ary
	902 - 928	1000	O-QPSK	250	62.5	ortogonal
IEEE 802.15.4™ -2007 Amendment 2 (optional)						
UWB(sub GHz)	250 - 750	See table given on page 83 in IEEE 802.15.4™ -2007				
2450 CSS	2400 - 2483.5	?	DQPSK/CSS	250	166.667	64-ary bi-orthogonal
		?	DQPSK/CSS	1000	166.667	8-ary bi-orthogonal
UWB(low band)	3244 - 4742	See table given on page 83 in IEEE 802.15.4™ -2007				
UWB(high band)	5944 - 10234	See table given on page 83 in IEEE 802.15.4™ -2007				

Among the different PHYs specified, the 2.4 GHz DSSS PHY is the most popular. This thesis will analyze and test performance increases given by receiver diversity when applied to this PHY. As such, the 2.4 GHz DSSS PHY will in the following be termed PHY.

2.2.1 Frequency channels

16 frequency channels are specified for the PHY. The center frequency of channel k is given by

$$F_c(k) = 2405 + 5(k-11)MHz \quad \text{for } k = 11,12,...,26 \tag{2.1}$$

which yields 5 MHz channel separation. The spectral mask defined in [9, p. 49] ensures little overlap between channels, so interference from neighbouring channels is kept at low levels. However, this standard will experience coexistence issues with other standards operating in the same frequency band such as the IEEE 802.11b/g/n standards. These standards use channels whose center frequencies also are separated by 5 MHz but each channel occupies approximately 22 MHz of bandwidth. Figure 2.1 shows this standards' channels and the non-overlapping channels for the 802.11-standards which are the ones commonly used around access points.

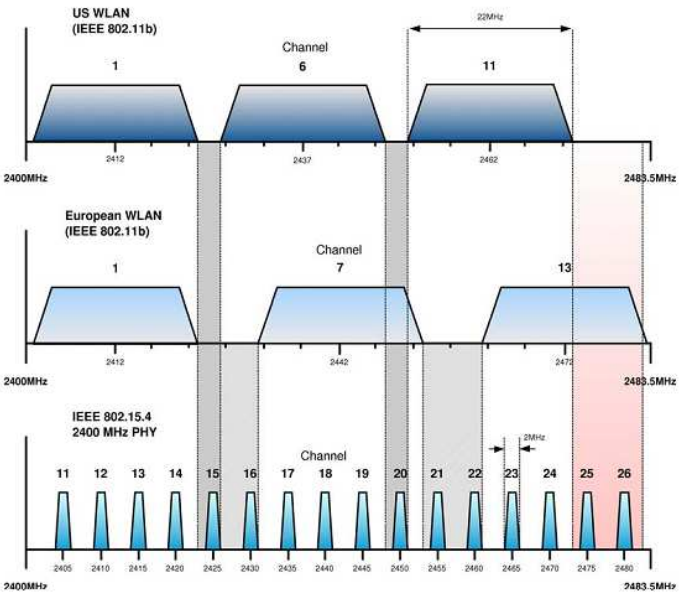

Figure 2.1: IEEE 802.15.4 and 802.11a/b/g/n frequency channels[14]

As can be seen from figure 2.1, channels 15,16,21 and 22 might experience less interference from the IEEE 802.11 standards in European countries while the same applies for channels 15,20,25,26 in the US. This thesis will not attempt to analyze any coexistence issues. As such, analysis will be isolated to only include this standard. For coexistence analysis, the reader is directed to [9, Annex E] or [14].

2.2.2 Coding and Modulation

The PHY uses a quasi-orthogonal modulation scheme, where each symbol corresponds to 4 payload bits and is represented by one of 16 nearly orthogonal PN sequences[9, p. 48] which is modulated onto the carrier by O-QPSK. These PN-sequences consists of 32 chips with half-sine pulse shaping, yielding a chipping rate 32 times the symbol rate which equals 2 Mchip/s. The resulting modulation is equal to MSK. The use of such a DSSS-scheme results in low spectral efficiency due to increased bandwidth and thereby increased multipath resistance. The bandwidth required by this modulation can be deduced from MSK modulation[8, p. 399] or the transmit PSD limits defined in the standard[9, p. 49]. The latter specifies a maximum effective bandwidth of 3.5 MHz which will be used in this thesis for analysis.

2.2.3 Performance Parameters

Performance metrics such as sensitivity, BER and coexistence are given in [9, p. 31,268]. Instantaneous BER in an AWGN channel is given as

$$BER(\gamma) = \frac{8}{15 \times 16} \times \sum_{k=2}^{16} (-1)^k \binom{16}{k} e^{20\gamma(\frac{1}{k}-1)} \tag{2.2}$$

where γ is the instantaneous SNR. The deduction of this formula is given by the same procedure as [9, ch. E.5.5.2] using the chip rate and data rate for the current PHY. The BER performance in AWGN is very good and presented in figure 2.2 together with PER and the sensitivity limit defined by[9, p. 31].

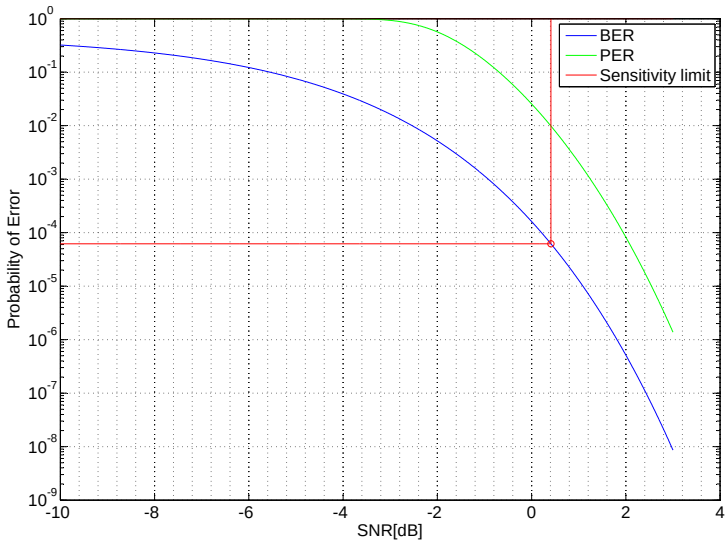

Figure 2.2: Error performance in AWGN channel

The packet error rate in figure 2.2 is a hypothetic packet error rate that might not be entirely correct modeled. The problem is that a packet error occurs if one or more bit errors are detected. Bit errors occur only when a wrong symbol decision is made. Since a symbol contains 4 bits, a symbol error might result in 4 bit errors. The question is how to map BER to PER or vice versa. The graph in figure 2.2 assumes that all packets are detected and that packet error occurs if at least one bit error occurs. This yields the following instantaneous PER in an AWGN channel

$$PER(\gamma) = 1 - (1 - BER(\gamma))^N \tag{2.3}$$

where N equals number of bits in the packet. In practice, lost packets can give a self-chosen amount of bit errors limited from above by the number of bits in a packet and from below by one. Or one might even remove the lost packet from the statistics, considering only bit errors occurring in erroneously received packets. However, the last option can be hard to investigate if the demodulator does not provide such information.

2.2.4 Channel Parameters

The PHY is required to perform two measurements that deal with the state of the radio channel[9, p. 65].

2.2.4.1 Energy Detection

The ED is an estimate of the received signal power within the bandwidth of the radio channel. As such, it measures the total received noise, interferer and wanted signal power. This measure is intended for use by the network layer to select one of the different channels specified in equation (2.1). The ED measurement is required to average the received signal power over 8 consecutive symbols, which equals 128us.

2.2.4.2 Link Quality Indicator

'The LQI measurement is a characterization of the strength and/or quality of a received packet. The measurement may be implemented using receiver ED, a signal-to-noise ratio estimation, or a combination of these methods. The use of the LQI result by the network or application layers is not specified in this standard.'[9, p. 65]

2.2.5 Data Transmission

Data transmissions occur in packets according to the PPDU with the format given i table 2.2

Table 2.2: PPDU

Octets				
4	**1**	**1**		**Variable**
Preamble	SFD	Frame length	Reserved	PSDU
SHR		**PHR**		**PHY Payload**

The PPDU contains the PSDU which holds the variable length payload of the packet. The maximum PSDU size is 128 bytes. Even though it's possible to continuously transmit packets using the PHY, this typically will not happen since the standard is ment for low data rate systems with nodes that produce relatively little data. Thus, activity in a given frequency channel can be viewed as in figure 2.3 where a ACK/NAK scheme is used.

The IEEE 802.15.4 standard defines several data transfer models[9, p.18] and these will not be

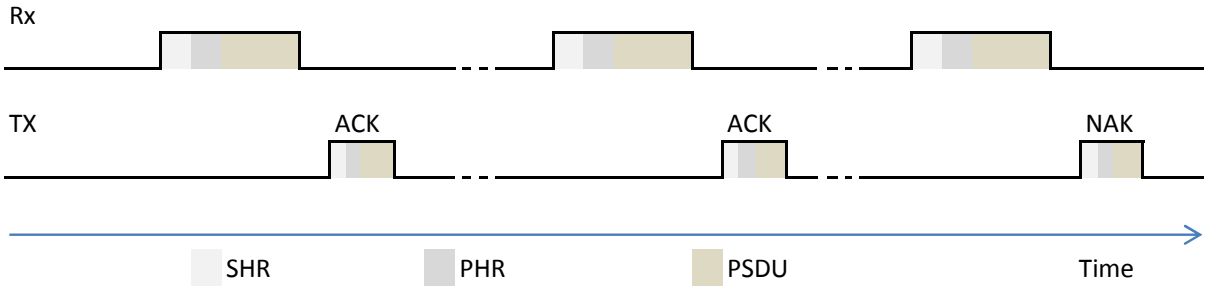

Figure 2.3: Transmission of packets

given any further attention here. Noteworthy about figure 2.3, is that the receiver has a time limited to the duration of the preamble to achieve synchronization and hence detect the packet. This time window is interesting in the context of diversity analysis.

Chapter 3

Description of the radio channel

Being the sum of effects that influences the signal of interest between a transmitter and a receiver, the radio channel is a complex medium for signal propagation. This is due to the contamination of the wanted signal by noise, interference, attenuation by obstacles and multipath propagation, all of them generally being time-variant due to a dynamic environment and movement. To cope with the difficulties imposed by the nature of the radio channel, it's helpful to split the analysis of the radio channel into the small and large scale effects it has on the signal propagation. These effects are dependant on the wavelength of the signal of interest. Receiver diversity is deployed to mitigate multipath effects which constitutes the small scale effects in the radio channel. Hence, the description of the radio channel given in this chapter will mainly deal with these effects. The mathematical notation used in this chapter conforms with that in [5].

3.1 Large-Scale Propagation Effects

Large-scale propagation effects deal with the variations in the received signal power as a function of the separation between transmitter and receiver in a given environment and variations due to shadowing. These variations in signal power can be described with different accuracy. A completely correct description would require perfect knowledge of the environment in which propagation takes place and the solution of Maxwell's equations with appropriate boundary conditions. This approach is rarely used. Instead, the use of statistical models based on empirical measurements are common as well as ray-tracing techniques.

3.1.1 Path Loss

Given a wireless communication link the linear path loss of the channel is defined to be

$$P_L = \frac{P_t}{P_r} \tag{3.1}$$

where P_t is the power of the transmitted signal s(t) and P_r is the averaged power of the received signal r(t) along a line with the same distance to the transmitter. By doing this, effects caused by shadowing are separated from that of path loss. The path loss is simply the value of linear path loss in dB. However, in text books it's more common to use path gain, which naturally is the inverse of path loss. The sources to path loss are many. Examples are free-space path loss, absorption, diffraction, scattering and atmospheric attenuation. There are basically two categories of techniques to model path loss.

3.1.1.1 Ray Tracing

Ray tracing is an analytical technique that models electromagnetic wavefronts as particles, not waves. As such, the effects of scattering, reflections and diffraction are only approximated. The technique models the received signal as a sum of received rays, each with its own path of propagation caused by a finite number of reflectors. It is assumed that the location of the transmitter, receiver and the reflectors with their dielectric properties are known at all time. To describe the received and transmitted signals the equivalent lowpass representations of bandpass signals is used. This assumes that the bandwidth of the modulated signal is significantly lower than the carrier frequency. By adopting such representation the transmitted signal can be expressed as

$$s(t) = \Re\left\{u(t)e^{j2\pi f_c t}\right\} \tag{3.2}$$

where u(t) is the complex envelope of s(t). Neglecting noise and interference, the received signal can similarly be expressed as

$$r(t) = \Re\left\{v(t)e^{j2\pi f_c t}\right\} \tag{3.3}$$

where the equivalent lowpass signal v(t) is dependent on the radio channel, through which s(t) propagates. If both transmitter and receiver is located in free space with no obstacles interfering with signal propagation the received signal is[5, p. 31]

$$r(t) = \Re\left\{\frac{\lambda\sqrt{G_l}e^{\frac{j2\pi d}{\lambda}}}{4\pi d}u(t)e^{j2\pi f_c t}\right\} \tag{3.4}$$

where d is the distance between transmitter and receiver and G_l is the product of the antenna gains in LOS direction. Thus, the ratio of the received power to the transmitted power, path gain, is

$$\frac{P_r}{P_t} = \left[\frac{\lambda\sqrt{G_l}}{4\pi d}\right]^2 \tag{3.5}$$

This equation shows that the received signal power follows an inverse square-law in free-space with respect to distance. However, when not in free space it falls of more rapidly as distance increases.

To illustrate the ray tracing technique a simple two-ray model is described. In figure 3.1 a simple environment is depicted, showing a LOS-path and a reflected path that is being detected by the receiver.

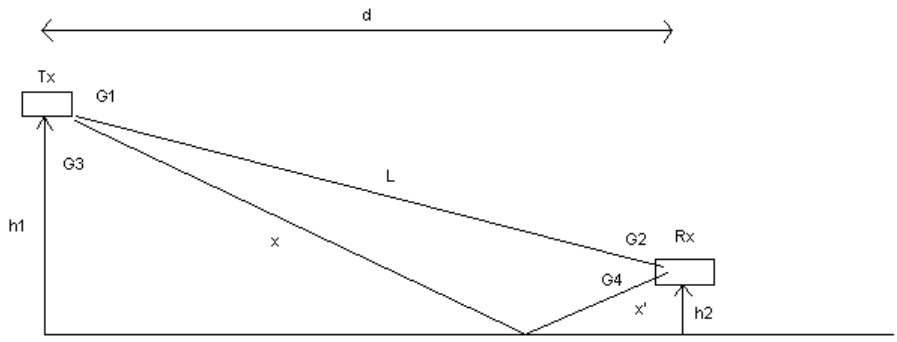

Figure 3.1: Simple two-ray model

The received signal r(t) is modeled as

$$r(t) = \Re\left\{\frac{\lambda}{4\pi}\left[\frac{\sqrt{G_l}u(t)e^{\frac{-j2\pi l}{\lambda}}}{l} + \frac{R\sqrt{G_r}u(t-\tau)e^{\frac{-j2\pi(x+x')}{\lambda}}}{x+x'}\right]e^{j2\pi f_c t}\right\} \tag{3.6}$$

where τ = (x+x'-l)/c and symbolizes the difference in time of arrival between LOS and the reflected path. This quantity is the delay spread of this channel. Further, G_l and G_r are the combined antenna gain in the LOS and reflected path, respectively. R is the ground reflection coefficient. For large separations between transmitter and receiver the path gain can be approximated as[5]

$$\frac{P_r}{P_t} = \left[\frac{\sqrt{G_l}h1h2}{d^2}\right]^2 \tag{3.7}$$

Equation 3.7 shows that power falls off inversely with forth power of d on large distances. Figure 3.2 shows the path gain as function of distance for this scenario.

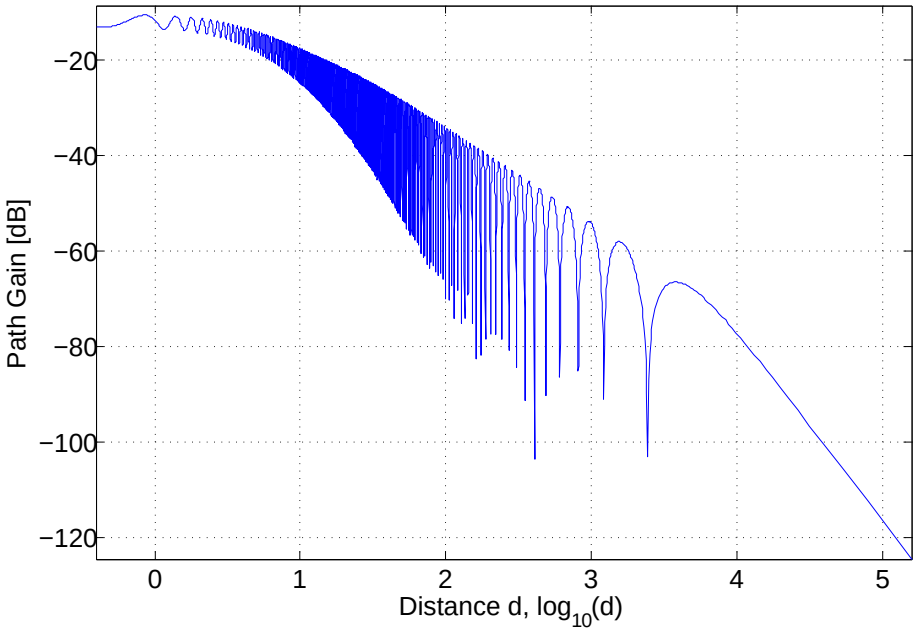

Figure 3.2: Two-ray path gain

Even though this scenario is very simple it captures both path loss and the constructive and destructive effects of multipath wave propagation. As can be seen from figure 3.2, the mean path gain falls off inversely with the second power of d, then with the forth power while strongly varying around this mean. Ray tracing is often used to predict the local mean received power $\overline{P}_r$ in a close area surrounding the receiver. When doing this the squared magnitude of all the received rays are summed to average out local spatial variations due to phase variations in the received rays as seen i figure 3.2.

3.1.1.2 Empirical models

Application of ray tracing is bound to a given environment for the results to be accurate. To model every scenario using ray tracing would be impossible when it comes to system analysis. Instead, when the wireless channel becomes too complex to model or when the analysis should be valid for many environments with similar characteristics, empirical models are used. Empirical

models on the mean path loss as a function of distance differ from ray tracing by including both path loss and shadowing for a certain type of propagation environment. When such models become complex, simplified models are often used to capture the tendency in the path loss. In the far field of the transmitter antenna, the received power are often modeled as

$$P_r = P_t K \left[\frac{d_0}{d}\right]^{\gamma} \tag{3.8}$$

The reference distance of the far field is d_0 while K is a unitless constant accounting for antenna characteristics and average channel attenuation at distance d_0. When using this model, values for γ, K and d_0 have to be determined by fitting the model to either analytical or empirical models. Description on how this is done can be found in [5]. The values of the path-loss exponent γ reflects the environment in which communication takes place. The table below summarizes some typical path-loss exponents.

Table 3.1: Typical path loss exponents

Environment	γ-range
Urban macrocells	3.7-6.5
Urban microcells	2.7-3.5
Office building(same floor)	1.6-3.5
Office building(multiple floors)	2-6
Store	1.8-2.2
Factory	1.6-3.3
Home	3

3.1.2 Shadowing

Blockage of the signal and changing propagation environment will cause random variations in the received signal power at a specific distance. Properties of the sources causing these variations are generally unknown, so this phenomena is modeled statistically. The log-normal distribution is a well accepted model to account for the shadowing attenuation. In this model the transmit-to-receive power $\psi = \mathrm{P}_t/\mathrm{P}_r$ is a random variable with a log-normal distribution. However, when expressed in dB this ratio becomes Gaussian with mean μ_{dB} and standard deviation σ_{dB}

$$p(\psi_{dB}) = \frac{1}{\sqrt{2\pi}\sigma_{\psi_{dB}}} e^{-\frac{(\psi_{dB}-\mu_{\psi dB})^2}{2\sigma^2_{\psi dB}}} \tag{3.9}$$

To model the large scale propagation effects μ_{dB} must include both average path loss and attenuation due to shadowing. When using empirical techniques μ_{dB} equals the path loss. When using analytical models this does not necessarily hold, since these aim to model the path loss alone and not attenuation due to shadowing. In this case it's possible to use a combined model for path loss and shadowing.

$$\frac{P_r}{P_t} dB = 10 log_{10} K - 10\gamma log_{10} \frac{d}{d_0} - \psi_{dB} \tag{3.10}$$

In equation 3.10 the simple path loss model in equation (3.8) has been applied to describe path loss with the addition of a zero-mean Gaussian random variable ψ_{dB} with variance $\sigma^2_{\psi_{dB}}$.

3.2 Small-Scale Propagation Effects

Small-scale propagation effects constitute the constructive and destructive effects of the multipath radio channel. These effects are clearly shown in figure 3.2, where the averaged received signal power fluctuates around a local mean. However, the underlying scenario in this figure is based on an ideal and simplified model of the multipath phenomenon which makes it deterministic. As described in previous sections, reallife radio environments are rarely found to be simple and deterministic.

In order to describe the fading process in multipath channels a general time-variant channel impulse response will be described. The general form of this impulse response will then be reduced to match various indoor radio environments where the PHY is designated to operate. This reduction will provide a statistical and simplified channel model on which anaysis are carried out on in the next chapter.

3.2.1 General Channel Impulse Response

Following the same notation used in [5] and generalizing the two-ray model introduced in section 3.1.1.1 to include movement of the receiver as well as more propagation paths, the received signal in a general multipath channel can be written as

$$r(t) = \Re\left\{\sum_{n=0}^{N(t)} \alpha_n(t)u(t-\tau_n(t))e^{j(2\pi f_c(t-\tau_n(t))+\phi_{D_n}(t))}\right\} \tag{3.11}$$

when noise is neglected. τ_n(t), ϕ_{D_n}(t) and α_n(t) represents the time-varying delay, Doppler phase shift and amplitude of received multipath component n, respectively. This equation contains several unknowns which all are functions of time. N(t) represents the time-varying number of multipath components, while n = 0 corresponds to line-of-sight. This number is time-varying when the environment is dynamic, i.e the transmitter, receiver or obstacles are moving in some fashion causing different propagation paths with time. The mathematical expressions for τ_n(t) and ϕ_{D_n}(t) are given by

$$\tau_n(t) = \frac{r_n(t)}{c} \tag{3.12}$$

$$\phi_{D_n}(t) = \int_t 2\pi \frac{vcos\theta_n(\tau)}{\lambda} d\tau \tag{3.13}$$

where r_n(t) and θ_n(t) are the propagation distance and the angle of arrival relative to the velocity vector of the receiver associated with multipath component n, respectively. α_n(t) is a function of path loss, reflections and shadowing for multipath component n. As an example, comparing equation (3.6) to equation (3.11) gives

$$\alpha_0 = \frac{\lambda\sqrt{G_l}}{4\pi l} \tag{3.14}$$

$$\alpha_1 = \frac{\lambda R\sqrt{G_r}}{4\pi(x+x')} \tag{3.15}$$

Setting τ_0(t) to zero gives

$$\tau_1(t) = \frac{x+x'-l}{c} \tag{3.16}$$

Equation (3.6) modeled a static environment, giving ϕ_{D_n}(t) = 0 for n = 1,2.

The general model of the received signal reduced nicely to the special case of a deterministic environment. However, this is usually not the case. For indoor channel modeling purposes it's both convenient and common to consider τ_n(t), ϕ_{D_n}(t) and α_n(t) to be stationary and ergodic random processes within a horizontal circle of diameter 10λ due to unpredictable movement in the environment.

The equivalent lowpass impulse response c(τ,t) of the general time-varying radio channel at time t can be derived by rewriting equation (3.11) as[5]

$$r(t) = \Re\left\{\left(\int_{-\infty}^{\infty} c(\tau,t)u(t-\tau)d\tau\right)e^{j2\pi f_c t}\right\} \tag{3.17}$$

which by comparison with equation (3.11) gives the impulse response as

$$c(\tau,t) = \sum_{n=0}^{N(t)} \alpha_n(t)e^{-j(2\pi f_c \tau_n(t) - \phi_{D_n}(t))}\delta(\tau - \tau_n(t)) \tag{3.18}$$

Equation (3.18) represents the general time-varying impulse response of an arbitrary radio channel and will now by subject to reduction to fit indoor radio channels of interest.

3.2.2 Reduction of General Time-Invariant Impulse Response

Equation (3.18) captures both wideband and narrowband radio channels. This section will reduce the channel impulse response in equation (3.18) to make it both realistic and suitable for diversity analysis in the next chapter. This can be done by considering measurements of power delay profiles, signal bandwidth and multipath environment.

3.2.2.1 Power Delay Profile

The power delay profile, A(τ), is defined as

$$A(\tau) = E\left\{c^*(\tau)c(\tau)\right\} \tag{3.19}$$

and represents the expected received power as a function of multipath delay τ. The PDP is easily measured if high-bandwidth equipment is available. When empirical data is not at hand, it's useful to analytically model A(τ). A popular model is the one-sided exponential distribution, which frequently has gained justification by measurements[7, p. 2],[20, p. 4]. A measurement of A(τ) in a LOS-scenario[7, p. 2] is reproduced in figure 3.3a and compared to a normalized one-sided exponential distribution if figure 3.3b.

The shape of the PDP is heavily dependant on the surroundings and the composition of LOS and NLOS components. One important feature of the PDP is the delay spread which deals with the extent of the received power in time. There are several ways to characterize delay spread. However, it is assumed that the demodulator synchronizes to the average delay spread, defined as

$$\mu_{T_m} = \frac{\int_0^\infty \tau A(\tau)d\tau}{\int_0^\infty A(\tau)d\tau} \tag{3.20}$$

In this case the most common measure on delay spread is the RMS delay spread, defined by

$$\sigma_{T_m} = \sqrt{\frac{\int_0^\infty (\tau - \mu_{T_m})^2 A(\tau)d\tau}{\int_0^\infty A(\tau)d\tau}} \tag{3.21}$$

Larger room dimensions generally result in larger delay spreads. The extent of the delay spread is also determined by output power, receiver sensitivity and noise floor. Arrival of waves with

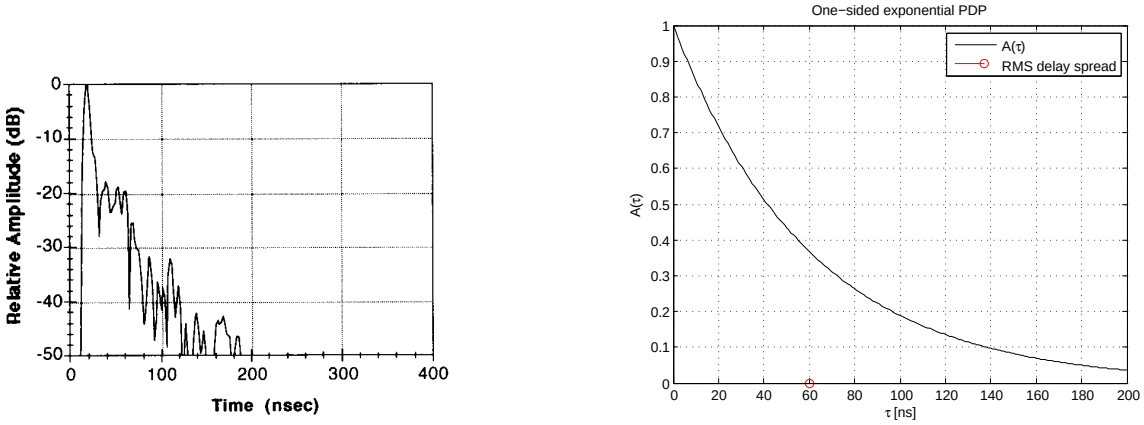

(a) PDP measurement in medium-size office building(LOS) **(b)** Normalized one-sided exponential PDP

Figure 3.3: Power delay profiles

undetectable powers are not a part of the PDP. Numerical values for delay spread for various indoor radio channels are found ranging from 10 ns - 150 ns for the 2.4 GHz band[7],[16],[19, p. 3],[20, p. 5] and [6, sl. 7-9].

A receiver cannot resolve different multipath components that differ in time by less than the inverse baseband bandwidth[5, p. 65]. In this case this equals 500 ns which corresponds to 150 m of propagation. The maximum time difference between arrivals of signal power can roughly be deduced as a small integer number of the delay spread[5, p. 86]. For an indoor, low-power radio link it's thus fair to say that all multipath components are resolved as one. The amount of ISI experienced in an indoor radio channel by the current PHY can also be deduced from the delay spread. A common rule of thumb predicts that a wireless link will experience negligible ISI if the symbol time exceeds ten times the delay spread which is very likely to occur in various indoor environments. Even though this might not hold for all indoor radio channel realizations, it will be assumed in the following. These assumptions yield a narrowband channel and equation (3.18) is reduced to

$$c(\tau, t) = \sum_{n=0}^{N(t)} \alpha_n(t) e^{-j(2\pi f_c \tau_n(t) - \phi_{D_n}(t))} \delta(\tau) = h(t)\delta(\tau) \tag{3.22}$$

The equation reflects the fact that all received multipath components are resolved as one by letting $\tau_n(\mathrm{t}) = 0$ for all n. It's important to note that since all multipath components are resolved as one the resulting channel filter coefficient will be time-variant due to the constructive and destructive addition of multiple signal components. As an example, multipath components that differ by 0.2 ns will cancel each other due to opposite phases. The superposition of all multipath components leads to fading, which will be discussed further in the next section for the given channel model in a specific environment.

3.2.2.2 Type of Fading

By applying DSSS to the data symbols, the PHY has gained some multipath resistance in its transmission of data. A bitrate of 250 Kbit/s would require a minimum bandwidth of 125 KHz when using O-QPSK. Because of the rapid fluctuating phase in equation (3.22), this would likely induce flat narrowband fading in many environments causing frequent outage periods. The

effect of using a spreading sequence widens the signal bandwidth, making it more resistant to frequency flat fading while still experiencing performance degradation from frequency-selective fading. This type of fading will somewhat be averaged out in the receiver. However, this PHY can still experience flat fading since flat fading implies that the symbol time greatly exceeds the delay spread. Considering the low delay spreads reported in section 3.2.2.1 this scenario is not unlikely. In the following a flat fading, narrowband channel will be assumed. This is consistent with the ISI-free channel assumed in section 3.2.2.1

3.2.3 Statistical Characterization of the Received Signal

The channel coefficient described in equation (3.22) is characterized as a complex stationary Gaussian process when a receiver moves within an area of ten λ in an environment with high density of multipath components. As such, the envelope of the received signal can also be characterized as a stationary random process described by it's autocorrelation and pdf.

3.2.3.1 Autocorrelation

To describe the autocorrelation of the received signal the uniform scattering model[5, p. 73] is chosen since it provides the shortest coherence time obtainable for a radio channel. This model also assumes that the power in all multipath component are uniformly distributed. The autocorrelation of the received signal in this scenario is presented in figure 3.4

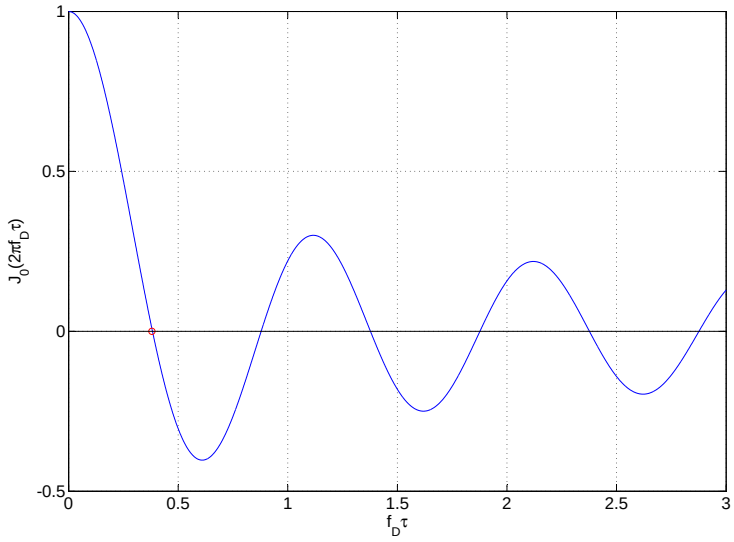

Figure 3.4: Zero-order Bessel function of first kind

Two important observations can be made by observing figure 3.4. For $f_D\tau = 0.38$ the received signal becomes uncorrelated. As such, observations taken 0.38λ apart in space or $0.38/f_D$ in time are uncorrelated. Firstly, for slow indoor movement at speeds ranging from 1 ms^{-1} to 2 ms^{-1} the latter implies a coherence time of 45.6 - 22.8 ms which supports an assumption of block fading independent of PSDU size. Since this channel has the shortest coherence time obtainable, this assumption is likely to hold for all other scattering environments with high density of multipath components as well. Secondly, observations of the signal taken 0.38λ apart are uncorrelated. Both of these observations are interesting when later analyzing and simulating fading mitigation techniques.

3.2.3.2 Envelope and Power Distributions

Indoor radio channels are often modeled as Rayleigh fading channels because of the uncertainty in the in-phase and quadrature components of the channel coefficient. This reflects the high density multipath environment often encountered indoors where no LOS is present. The power distribution in such channels are exponential distributed according to

$$p_{\Omega}(\Omega) = \frac{1}{\overline{\Omega}} e^{-\Omega/\overline{\Omega}} \quad , \Omega > 0 \tag{3.23}$$

where $\overline{\Omega}$ is the total average received power within an area of 10 λ given by path loss and shadowing, as described in the beginning of this chapter. In a LOS scenario on the other hand, the complex channel will contain a strong multipath component yielding a Rician distributed envelope and a corresponding power distribution parameterized by $\overline{\Omega}$ and the K-factor defined as

$$K = \frac{\Omega_{LOS}}{\Omega_{NLOS}} \tag{3.24}$$

The severity of fading is limited by the Rayleigh case with K = 0 and the AWGN case by K = ∞. Fading mitigation in Rician fading channels are challenging to analyze. Rician distributed variables can, however, closely be approximated by Nakagami-m distributed variables when

$$m = \frac{(K+1)^2}{(2K+1)} \tag{3.25}$$

This is convenient since fading mitigation in Nakagami-m fading channels are easier to analyze. The power distribution of a Nakagami-m channel is Gamma distributed as

$$p_{\Omega}(\Omega) = \left(\frac{m}{\overline{\Omega}}\right)^m \frac{\Omega^{m-1}}{\Gamma(m)} e^{-m\Omega/\overline{\Omega}}, m \geq \frac{1}{2}, \Omega \geq 0 \tag{3.26}$$

The Nakagami-m distribution also reduces to Rayleigh for m = 1. Noteworthy about the Nakagami-m distribution is that it captures more severe fading than Rayleigh fading by supporting values of m less than 1.

Chapter 4

Fading Mitigation

Diversity, or microdiversity, is a well-known concept of combating the effects of multipath fading. It is believed that diversity combining still offers one of the greatest potential performance improvements for current and future wireless standards [17]. This performance improvement could be more reliable radio links or the ability to lower the output power. The latter would increase battery life time and lower radio interference to other devices in the 2.4 GHz band. Since the PHY is designated to operate in areas of possible significant multipath fading the application of diversity combining at the receiver is interesting to investigate. Other techniques that cannot be classified as diversity combining but still mitigates fading will also be investigated.

This chapter will start by giving a short introduction on how to achieve multiple observations of the signal of interest on the receiver side, known as receiver diversity, in a general case along with some pros and cons associated with the different methods. The latter and major part of the chapter will theoretically analyze and present simulation results for a selection of well-known diversity combining techniques as well as two other possible fading mitigation methods.

4.1 Possible Receiver Realizations

To achieve receiver diversity multiple observations of the same signal of interest must be a available at the receiver. The different fading signals can be obtained at the receiver by use of various methods. Common for these methods is the goal of extracting uncorrelated fading signals from different radio channel realizations.

4.1.1 Antenna Diversity

Diversity can be achieved by using multiple antennas in different configurations. This is commonly known as antenna diversity.

4.1.1.1 Adaptive Array Diversity

An adaptive array of antennas can be used to obtain path-diversity by resolving multipath components with different incident angles [21] and thereby providing multiple observations of the wanted signal. An adaptive array can also be used to provide angle-diversity where the strongest multipath components fall within the antenna pattern's main lobes. Both of these methods work better with an increasing number of antennas resulting in higher cost due to many RF-front ends. This also leads to a system with higher off-chip area and power consumption. Using an adaptive array also implies more on-chip silicon area due to beam steering which would add to the silicon used for fading mitigation algorithms.

4.1.1.2 Polarization Diversity

Polarization diversity is the use of yet another dimension in the diversity space. It can be combined with any number of antennas. Just double the number of antennas in any array to take the polarization into account. Polarization diversity exploits the fact that multiple random reflections distribute the signal power relatively equal with respect to two orthogonal polarizations. Diversity is achieved because of the unlikely scenario of both polarizations entering a deep fade due to the fact that scattering angles relative to each polarization are random. Polarization diversity possess the property of potential small-size implementation since antenna separation can be made small. The number of RF-front ends needed to achieve polarization diversity is equal to the number of antennas used.

4.1.1.3 Spatial Diversity

Spatial diversity utilizes multiple antennas to ideally extract uncorrelated fading signals as function of distance. The antennas usually possess equal characteristics and are spaced apart by a fovourable distance. By using omni-directional antennas the separation distance can be at a minimum. This concept is quite easy to visualize by looking at figure 3.4 for the theoretical case of a uniform spreading environment with equal signal powers received from all directions. Neglecting the effects of coupling between antennas, two observations of the wanted signal would be totally uncorrelated if observed 0.38λ apart. This situation is, however, never encountered in practice. Spatial diversity allows a great number of antennas on the receiver side while complexity is dependant on the fading mitigation algorithm used.

4.1.2 Frequency Diversity

In a frequency diversity scheme the same information signal is transmitted in different frequency bands, typically separated by at least the coherence bandwidth of the channel. This diversity scheme results in large increase in hardware, total output power and bandwidth. It is thus not compliant with the requirements of the IEEE 802.15.4 standard

4.1.3 Time Diversity

When using time diversity the same information is transmitted multiple times in different time slots. The time slots are separated in time by more than the coherence time of the channel. This way the signal of interest has been obtained from different channel realizations. Even though the transmit power does not increase during transmission of a packet, the total transmit power could easily be larger than necessary when compared to a system only using ACK/NAK to request a potential retransmission. This is dependant on packet lengths and channel conditions. The total data rate is also lowered, but this does not necessarily conflict with the packet rates experienced in a Zigbee system. What mostly makes this diversity scheme not useful is the increase in total output power, incompatibility with higher layer transmission protocols[9, p. 18] and worst-case performance in stationary channels. In a traficated 2.4 GHz band this scheme would also increase collision rates and lower coexistence with other standards. A realization would, however, result in no extra hardware, only protocol change.

4.2 Performance Analysis

How multiple observations of the wanted signal are obtained can be abstracted away when analyzing possible performance increases by diversity reception. This section provides the basis on how performance increases are analyzed and simulated in this thesis for the fading mitigation techniques described in the next sections. The slow small-scale fading channel discussed in section 3.2.2 will be assumed. A PSDU length of 21 bytes will be considered. This gives a frame length of 22 bytes, which conforms with coexistence analysis in[9, p. 268]. The analysis provided here will not deal with coexistence issues.

4.2.1 Diversity Gain

By mitigating fading the transmission power can be lowered while at the same time providing the same system performance. This possible reduction in transmission power is termed diversity gain. Diversity gain can be realized as reduced transmission power, increased fading margin or a combination of both. When not all the gain is realized through reduced transmission power, throughput will also be increased. This concept is depicted in figure 4.1 for the case of optimal diversity combining, known as Maximal-Ratio Combining using 4 diversity branches.

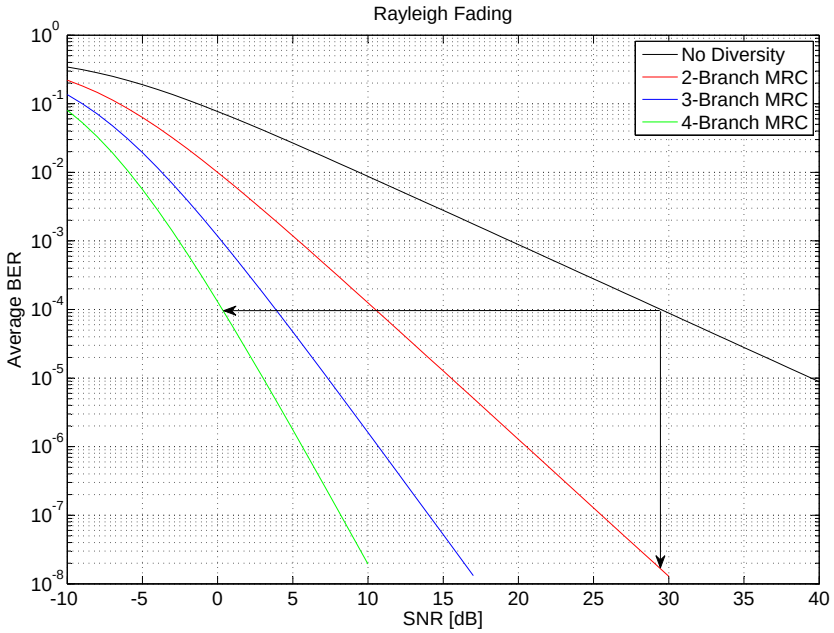

Figure 4.1: Diversity gain

The targeted system performance in this case is an average BER of 0.01%. The horizontal arrow indicates the diversity gain achieved by using different orders of MRC. It's important to note that the largest diversity gain is achieved by going from no diversity to 2-branch diversity. The vertical line indicates the maximum reduction in average BER for 2-branch MRC which can be translated to increased throughput.

The underlying mechanism providing diversity gain is the decreasing probability of simultaneous deep fades on all diversity branches with increasing number of diversity branches. Figure 4.2 illustrates this concept by displaying the instantaneous SNR in two independant diversity branches obtained from a Rayleigh fading channel with uniform scattering. Assuming two receiver antennas separated by 0.38λ, this plot corresponds to transmitter movement of 10λ at a velocity of 0.5 m/s while transmitting 100 packets each second.

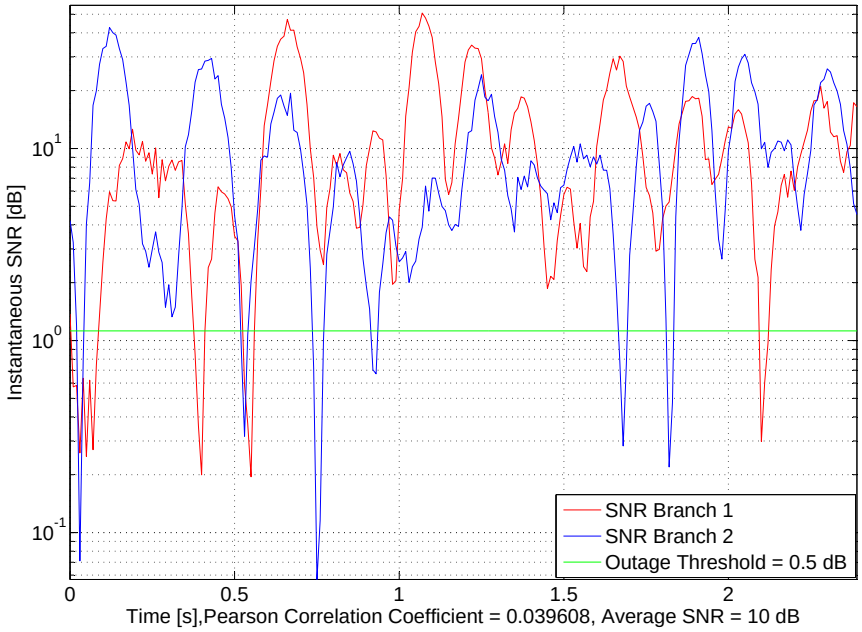

Figure 4.2: Two independant Rayleigh fading channels

The small-scale fading in this environment will occasionally result in deeps fades in the received signal power. Supposing a deep fade occurs if the instantaneous SNR falls below 0.5 dB, as indicated by the green line, it's clear that the probability of deep fades can greatly be reduced if exploiting the two diversity branches.

The probability of simultaneous deep fades is highly dependant on the cross-correlation between the signal envelopes, increasing with cross-correlation. Further, for a given cross-correlation, the potential diversity gain will decrease with increasing unbalance in the average SNRs in the diversity branches [17, p. 347]. This effect can be substantial in polarization diversity schemes, and it's therefore risky to assume balanced SNR distributions in such diversity branches. The probability of a simulataneous deep fades will decrease as the average SNR in the branches increase, and as such provide great performance improvments when fading mitigation techniques are used. This can be seen in figure 4.1.

4.2.2 Analytical Analysis

The performance of fading mitigation techniques will be analyzed by considering BER and PER in various slowly fading channels. The instantaneous SNR in symbol decisions, γ, is considered known to the different fading mitigation techniques later discussed. The analysis neglects the use of AGC in the receiver and assumes error-free synchronization with the preamble.

To obtain the average BER given a specific fading environment, equation (2.2) is averaged over the fading distribution of the instantaneous SNR. The latter is obtained by replacing Ω with γ in equations (3.23) and (3.26). This gives the average BER as

$$BER(\overline{\gamma}) = \int_0^\infty BER(\gamma) p_\gamma(\gamma) d\gamma \tag{4.1}$$

Inserting equation (2.2) into equation (4.1) and rearranging the order of summation and integration yields

$$BER(\overline{\gamma}) = \frac{8}{15 \times 16} \sum_{k=2}^{16} (-1)^k \binom{16}{k} \int_0^\infty e^{20(\frac{1}{k}-1)} p_\gamma(\gamma) d\gamma \tag{4.2}$$

By using the MGF approach described in [17, p. 18], equation (4.2) takes the following form.

$$BER(\overline{\gamma}) = \frac{8}{15 \times 16} \sum_{k=2}^{16} c_k \times M_\gamma(d_k) \tag{4.3}$$

where

$$M_\gamma(d_k) = \int_0^\infty p_\gamma(\gamma) e^{s\gamma} d\gamma \tag{4.4}$$

$$c_k = (-1)^k \binom{16}{k} \tag{4.5}$$

$$d_k = 20 \times (\frac{1}{k} - 1) \tag{4.6}$$

Equation (4.3) provides a very handy way of analyzing average BER performance since closed form expressions for equation (4.4) are provided for many different distributions in [17].

The analysis of average PER in a given fading environment can be obtained in a similar way as

$$\begin{aligned} PER(\overline{\gamma}) &= \int_0^\infty \left(1 - (1 - BER(\gamma))^N\right) p_\gamma(\gamma) d\gamma \\ &= 1 - \int_0^\infty (1 - BER(\gamma))^N \, p_\gamma(\gamma) d\gamma \end{aligned} \tag{4.7}$$

where N equals the number of bits in the packet. The nature of this equation makes it very hard to solve when inserting equation (2.2) and an appropriate fading distribution. As can be seen from the equation, PER is a highly non-linear function of instantaneous BER and the fading distribution. In a packet-based system diversity gain in PER is somewhat more meaningful than diversity gain in BER. As such, to evaluate this gain a simulation model has been constructed.

4.2.3 Simulation Model

A block-fading simulator has been programmed in Matlab to provide PER simulation results for different fading mitigation techniques. This simulation model generates SNR samples corresponding to Rayleigh and Nakagami-m fading envelopes with an underlying autocorrelation corresponding to the uniform scattering environment. By providing an underlying autocorrelation of the envelope samples, it's possible to investigate and take advantage of the time dynamics in the channel.

The model is limited to generating an arbitrary number of SNR sequences where the stochastic components are independent between the sequences. Further, the model also provides equal mean SNR for all the generated sequences, even though this easily could be altered to a general case where this does not hold. As such the model provides diversity results for an ideal case of uncorrelated channels with equal mean SNRs which correspond to a case of maximal diversity gain, thus providing an upper bound for the diversity gain possibly achievable for the PHY. Being a block fading simulator, the results are not guaranteed to conform with reality for long packet lengths, since PER increases with packet length.

When invoked, the model will generate a sequence of complex envelope samples corresponding to a movement of 10λ given the desired packet rate and velocity of transmitter or receiver, according to the autocorrelation specified. Independent of the desired envelope distribution the model will start by generating Rayleigh fading envelope samples by AR-modeling, according to [2]. If a Nakagami-m envelope distribution is desired, such a sequence is derived from samples matching the Nakagami-m distribution. This sequence is then rearranged to match the

wanted Nakagami-m autocorrelation according to the rank statistics of the previously generated Rayleigh sequence with the desired autocorrelation. This method is completely described in [15]. After the complex envelope sequences are generated, the squared module of the envelope is obtained and then scaled to get the desired SNR sequence for the given environment. The different diversity combining techniques can be simulated with these sequences as input. Average PER in a given fading environment is then simulated by averaging the instantaneous PER over all SNR samples.

4.3 Diversity Combining Techniques

Figure 4.3 shows a general linear, narrowband, multi-channel diversity combiner which can be used to describe several well-known diversity combining techniques.

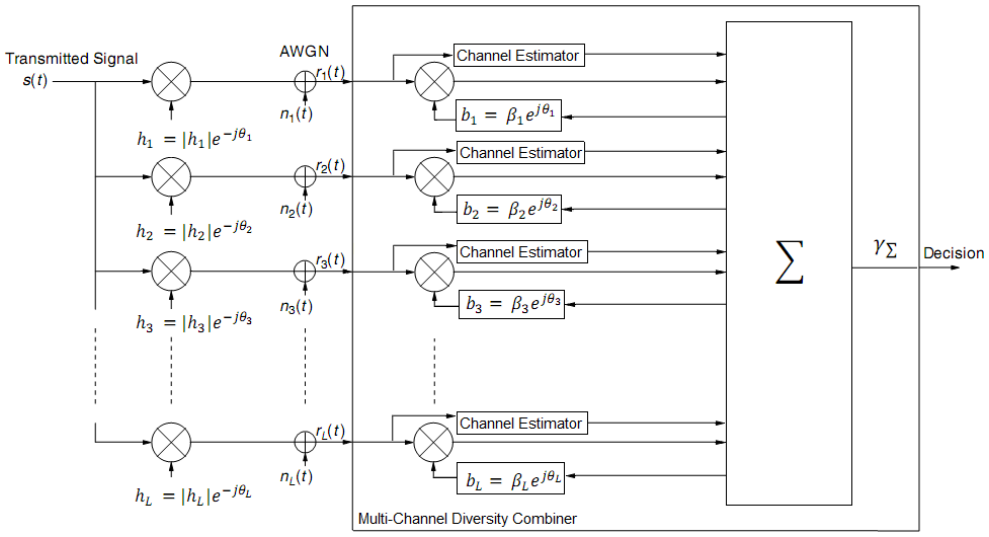

Figure 4.3: Narrowband multi-channel diversity combiner

In this figure, $r_i(t)$, for i = {1,L}, is the received signal envelope plus noise in the L different diversity branches obtained in any of the ways described earlier. The sets $\{h\}_1^L$ and $\{\theta\}_1^L$ are the random channel fading amplitudes and phases, respectively. These sets are assumed to be mutually independant and constant during packet receptions. The fading amplitudes $\{h\}_1^L$ are statistically described by Rayleigh or Nakagami-m distributions, while the noise PSD is assumed constant and independant between different channels and the different fading amplitudes. The combiner output should possess a statistically better distribution of the instantaneous SNR when the input signals are properly combined which would leads to both diversity and array gain. The latter is defined as the increase in SNR in the absence of fading and is not treated in this thesis.

In figure 4.3, the combiner, Σ, and the fading distribution on the different channels determines the distribution of the intantaneous SNR at the combiner output. The combiner can affect this distribution by specifying the set $\{\beta\}_1^L$ and/or perform co-phasing. What mainly seperates the different techniques is how many signals that are combined. If more than one signal is combined, this requires post- or predetection co-phasing indicated by the set $\{\theta\}_1^L$. In the following, two diversity branches will be assumed available due to cost and power requirements.

4.3.1 Maximal-Ratio Combining

This fading mitigation technique is not targeted by the problem description. It is, however, included in this analysis to provide an upper bound for what diversity gain to expect from other combining techniques. The output of the combiner is a weighted sum of all the signals in the different branches, where high SNR branches are weighted more than low SNR branches. As such, this technique requires knowledge of the sets $\{|\mathrm{h}|\}_1^2$ and $\{\theta\}_1^2$ to co-phase the different signals as well as to obtain the appropriate scaling factors[5, p. 214]. This is indicated in the figure by each branch having a channel estimator whose outputs are used by the combiner to control the sets $\{\beta\}_1^2$ and to perform co-phasing specified by $\{\theta\}_1^2$. Assuming equal noise PSD in all branches and independent branches the instantaneous output SNR of the combiner is given by[5, p. 265] as

$$\gamma_\Sigma = \sum_{i=1}^{2} \gamma_i \tag{4.8}$$

when optimal $\{\beta\}_1^2$ are chosen. Figure 4.4 shows the input SNRs in two branches and the output SNR of the combiner when it is realized as MRC.

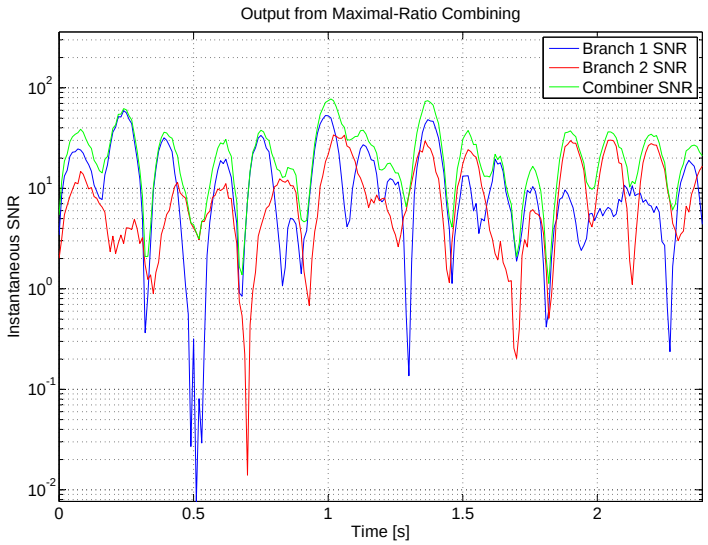

Figure 4.4: Output SNR from MRC

The SNR distribution of the combiner output is easily obtained in closed MGF form. This is due to the fact that equation (4.8) is a sum of independent variables which gives

$$M_{\gamma_{MRC}}(s) = \prod_{i=1}^{2} M_i(s) \tag{4.9}$$

where $\mathrm{M}_i(\mathrm{s})$ is the MGF of the fading distribution on branch i. This makes it easy to evaluate the resulting average BER when MRC is utilized even when the branches exhibit different SNR distributions.

4.3.1.1 Implementation Considerations

MRC constitute the most complex and optimal form of diversity combining. In the case of this PHY it requires 2 full receiver chains giving 2 times higher power requirement and silicon area. An implementation could be relaxed if the block fading assumption holds. In this case, the

estimation of the instantaneous SNR could be made during preamble and then kept fixed when scaling the samples in the combiner. If this assumption does not hold, estimation could be performed every Kth received symbol, still leading to power consumption reduction if averaging is not required.

4.3.2 Selection Combining

The output of the combiner in this combining scheme is the signal with the highest instantaneous SNR in the two branches, giving only one non-zero element in the set $\{\beta\}_1^2$. The channel estimators are still required to do this measure, which results in the need of continuously monitoring the two branches. However, the channel estimator can have low complexity if equal noise powers are assumed in the branches since the decision then is based on which branch has the highest total power. Co-phasing is not performed.

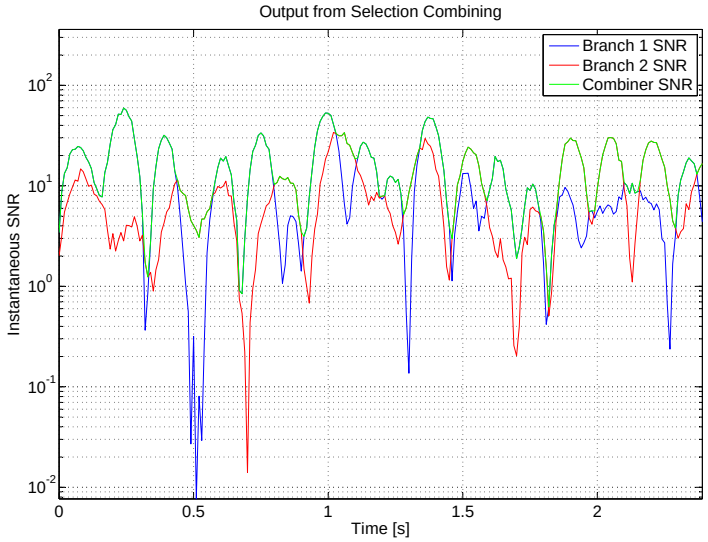

Figure 4.5: Output SNR from SC

The SNR distribution of the combiner output is quite complex. The MGF for two correlated Nakagami-m fading channels is given in equations [17, eq 9.182-9.187]. Assuming identical mean SNR in the branches and uncorrelated fading, this MGF can be simplified and expressed as

$$\begin{aligned} M_{\gamma_{SC}}(s) &= \frac{2^{3m+1}\Gamma(2m)m^{2m}(-2s)^{-2m}}{\Gamma(m)\Gamma(m+1)\bar{\gamma}^{2m}} \\ &\times \left[W(1+W)\right]^{-m} \times_2 F_1(1-m,m;1+m;\frac{1}{2}(1-\frac{1}{W})) \qquad (4.10) \\ W &= 1-\frac{2m}{\gamma s} \qquad (4.11) \end{aligned}$$

, where ${}_2F_1$(a,b;c;d) is the Gauss hypergeometric function. This expression for the Nakagami-m fading channel can be used to analyze BER performance in both Rayleigh and Rician fading channels with appropriate values for m.

4.3.2.1 Implementation Considerations

Selection Combining is a far simpler combining method than MRC. However, it still requires the monitoring of two signal branches yielding two full receiver chains since a packet is detected

through a preamble sequence. The ED measure provided by the PHY can be used to select what branch to use in demodulation assuming the current channel model holds. The savings going from MRC to SC would in this case be reduced power consumption and silicon needed for the channel estimator. The current channel model implies that the selection should be done during preamble leading to a minimal power consumption. Reduced power consumption is achieved by turning off the receiver chain not selected.

4.3.3 Switch and Stay Combining

The combiner output signal is equal to one of the branch inputs which gives only one non-zero element in the set $\{\beta\}_1^2$. The difference between SC and SSC is that the SSC combiner will output its' current input signal as long as its' instantaneous SNR remains above a given threshold or as long a downward crossing of this threshold does not occur. This essentially leads to three different realizations of the SSC combiner[1], named SSC-A, SSC-B and SSC-C. Relative performance analysis among these three will not be given here, but [1] reports SSC-A giving best error performance while suffering from higher switching rates in the case where subsequent packets experience nearly independent fading conditions.

SSC-A is not only the SSC scheme that gives best error performance, it is also the least complex versions of the SSC schemes. SSC-A is from now on termed SSC. The SNR is estimated once per packet and compared to a given threshold. If the SNR estimate is below the given threshold, the combiner switches to the other branch regardless of the SNR on that branch. Figure 4.6 shows how the instantaneous output SNR from SSC would be in a situation equal to those in figures 4.4 and 4.5. From this figure it is seen that the diversity gain provided

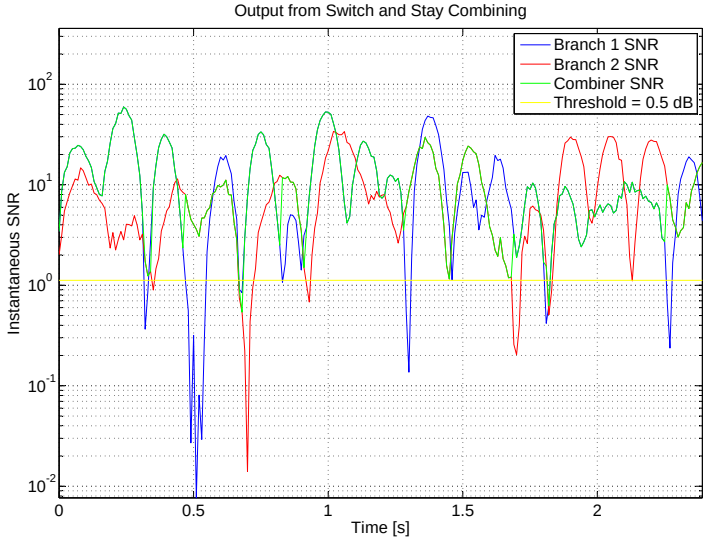

Figure 4.6: Output SNR from SSC

by SSC is less than SC, since the instantaneous SNR often is less than SC. An important consideration when implementing SSC is the targeted switching threshold. SSC gives the same outage probability as SC when setting the switch threshold equal to the outage threshold[17, p. 355]. Outage is the probability that γ_Σ falls below a given threshold. This strategy does, however, not minimize the average BER. The MGF of SSC in uncorrelated and SNR balanced Nakagami-m fading channels is given by[17, p. 351] as

$$M_{\gamma SSC}(s) = (1 - \frac{s\overline{\gamma}}{m})^{-m} \times \left[1 + \frac{\Gamma(m, (1 - (\frac{\overline{\gamma}}{m}))s(\frac{m\gamma_T}{\overline{\gamma}})) - \Gamma(m, \frac{m}{\overline{\gamma}})\gamma_T)}{\Gamma(m)}\right] \tag{4.12}$$

where Γ(a,b) is the complementary, incomplete Gamma function and γ_T is the switching threshold. Optimum switching thresholds can theoretically be found by solving

$$\frac{dBER(\overline{\gamma})}{d\gamma_T}|_{\gamma_T=\gamma_{T*}} = 0 \tag{4.13}$$

with equation (4.12) as input for the MGF in equation (4.3). Figure 4.7, 4.8 and 4.9 shows the optimum simulated switching thresholds to minimize BER for selected average SNRs in three Nakagami-m fading channels.

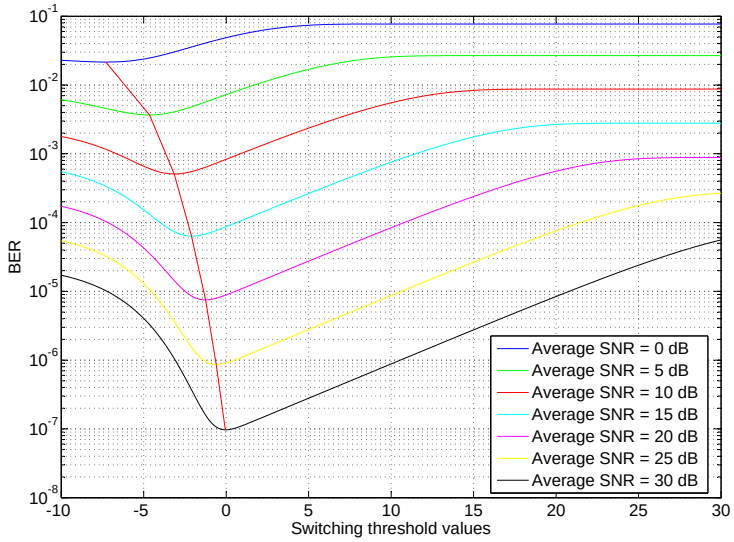

Figure 4.7: Minimum BER switching thresholds, K = 0

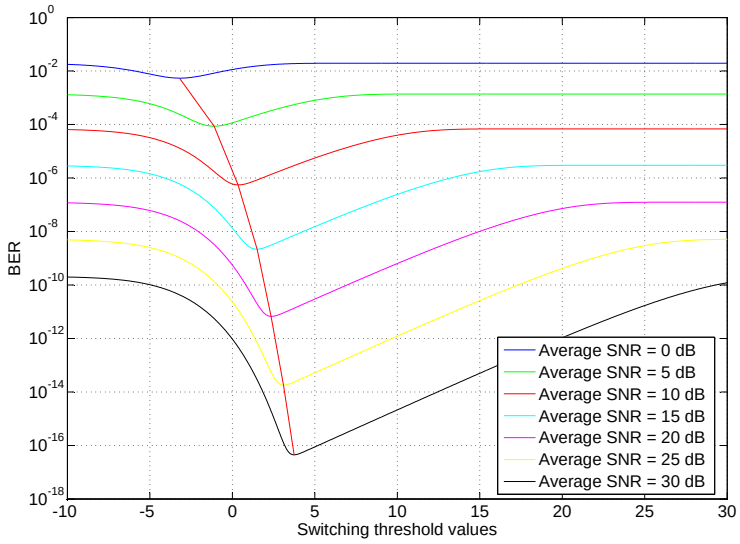

Figure 4.8: Minimum BER switching thresholds, K = 4

These figures show that the solution to equation (4.13) will vary with the fading channel and average SNR. An implementation of SSC that reaches the optimal BER in an arbitrary fading channel will hence be very complex if not impossible to realize. It is, however, important to remember that when the K value increases diversity gain will decrease in the case of SSC due to the unlikelihood of deep fades and the frequency of these. As such, these optimal switching

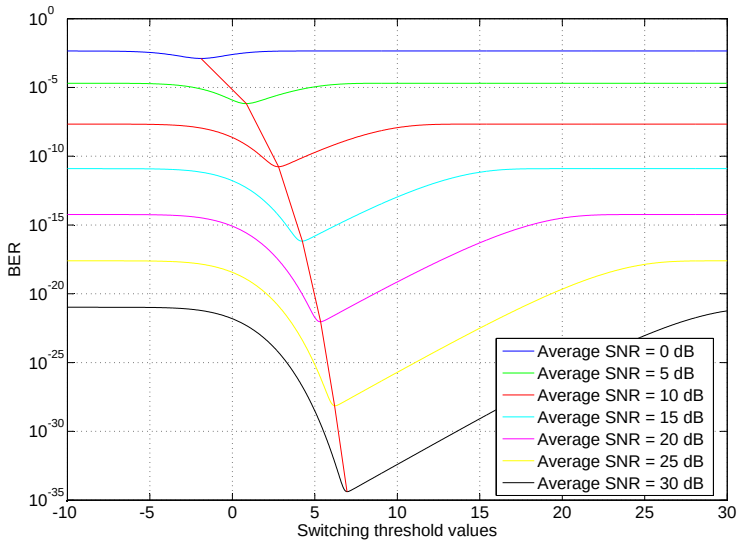

Figure 4.9: Minimum BER switching thresholds, K = 12

thresholds are mostly interesting for low K-values. In the case of K = 0, Rayleigh fading, and K = 4, a fixed threshold value could be used. If not estimating the channel to determine K, an engineer would have to decide where diversity gain is most wanted. A threshold value of 0 dB would in the Rayleigh case provide diversity gain for reasonable values of average SNR. The Rayleigh case is also the worst practical fading scenario where SSC has greatest potential to increase system performance.

4.3.3.1 Implementation Considerations

The time window for switching gives two possible implementations, on-chip and off-chip. These will be termed preamble-switching and PSDU-switching. As witch SC, the ED measurement performed by the PHY can be used as switch argument if the assumed channel model holds.

PSDU-Switching

After preamble synchronization is found, the algorithm can decide whether or not a switch should be performed. There are unwanted effects when initiating this kind of switching. Most RF-front ends utilize an AGC-loop to provide a constant level of signal quality within the demodulator. Hopefully, the instantaneous SNR will be better when using the other antenna. If so, the received signal power should be correspondingly larger. When switching, this would ideally present a stronger signal to the LNA which in theory can clip the signal. In this case, the packet is likely to be lost. In addition, RF-transients caused by switching might induce this behavior as well. If a switch is utilized, both switching and attenuation of transients should be fast compared to the duration of a chip.

The switching process can be modeled as an additive noise process, which has the potential of causing packet errors. This process is most pronounced in bad fading scenarios, and is hence likely to reduce possible diversity gain in these. Using a switch would also imply some increase in noise figure due to insertion loss which would generally reduce receiver sensitivity. The modulation scheme used by the PHY is however likely to overcome some of these problems.

Assuming these problems solved, SSC can be implemented with one RF-front end, a RF-switch and two antennas. When the signal degrades, the other antenna can be switched in. The channel model assumed will, however, cause the instantaneous SNR to remain constant

throughout a packet. As such, one switch per packet will be enough to mitigate fading. In very unfriendly fading environments, there is however a great chance that preamble synchronization is not achieved. This leads to another possible implementation of SSC.

Preamble-Switching

Two receiver chains can be used during preamble reception. This way, the probability of preamble synchronization would be increased. SSC can be performed after both receiver chains are synchronized to the preamble. The receiver chain not selected can then be inactivated to save power due to channel assumptions. This implementation would resemble SC but performance would be degenerated. The switching will cause no problems in this case.

4.4 Other Fading Mitigation techniques

This section briefly discusses two other options to fading mitigation, not generally considered as diversity combining. The literature is limited, and the following represents the student's reasoning on the two techniques.

4.4.1 Double Receiver

Diversity gain can be achieved by using a double receiver. By ideally demodulating the same packet independently two times the instantaneous PER is reduced. This is captured by the following equation

$$PER_2 = \prod_{i=1}^{2} PER_i \tag{4.14}$$

A low-cost implementation of a fading mitigation technique is not likely to justify the use of more than two receiver chains. In this case the performance of a double receiver chain is bounded from below by SC in all fading environments. The double receiver can be modeled as an extended SC-scheme, where one combiner is implemented as SC while the other combiner is implemented as the compliment of SC, $\overline{SC}$, which always selects the branch with the lowest instantaneous SNR. Each combiner output is then demodulated separately. The PER in this case is

$$PER_2 = PER_{SC} \times PER_{\overline{SC}} \tag{4.15}$$

In a Rayleigh fading environment the distribution of $\gamma_{\overline{SC}}$ is given by Appendix A as

$$\gamma_\Sigma = \gamma_{\overline{SC}} = \frac{2}{\overline{\gamma}} e^{-\frac{2\gamma}{\overline{\gamma}}} \tag{4.16}$$

Replacing Ω by γ in equation (3.23) and comparing it to equation (4.16) yields an exponential distribution with half the average SNR. The advantage of a double receiver over SC in Rayleigh fading is thus the availability of a signal branch with statistically half the average SNR as a single branch receiver.

The upper bound of performance is harder to analyze. This should somewhat be a function of both the fading environment and the average SNR in the two branches. MRC will outperform the other combining techniques in all fading channels. The question is if it will outperform the double receiver as well, being an optimal combining technique. Some general remarks can be made by looking at figures 4.4 and 4.5. This scenario represents a Rayleigh fading channel with an average SNR of 10 dB. The increased instantaneous SNR in MRC does not differ that much from the instantaneous SNR in SC in this scenario, especially at times where one of the

branches experiences a deep fade and the other doesn't. Since deep fades occur frequently in a Rayleigh fading channel it's therefore probable that a double receiver can perform better than MRC. The reasoning is as follows. At very low average SNR the diversity gain added by the option to demodulate a packet with half the average SNR is low. This can be understood from equation (2.3), which reduces to a value close to 1 for low instantaneous SNR due to high values of N. Low values of the instantaneous SNR is more likely at low average SNR and equation (4.15) reduces to

$$PER_2 \approx PER_{SC} \tag{4.17}$$

As the average SNR increases so will the probability of high instantaneous SNR. As such, equation (2.3) will start in a non-linear fashion to take values closer to 0 and equation (4.15) must be used to describe the instantaneous PER. When this happens, the PER curve corresponding to a double receiver should be steeper than the one corresponding to SC. As such, it will intersect the MRC PER curve at some average SNR making the double receiver more effective in mitigating fading than MRC.

However, as the fading environment becomes more friendly due to a deterministic and strong multipath component, the probability of deep fades will decrease. As such, the instantaneous γ_Σ in the MRC case will become much greater than the γ_Σ in the SC case. This yields larger separation in diversity gain between the two compared to the Rayleigh case. Due to the bigger separation the double receiver will have a harder time beating the MRC diversity gain. A potential crossing might happen for very large average SNR. In a strong LOS environment the double receiver will hence be bounded from above by MRC.

4.4.1.1 Implementation Considerations

The argumentation for using two full receiver chains to demodulate the received signal from two different antennas can be strong if the combining schemes analyzed earlier are based on preamble-switching. In this case two RF-front ends will be needed on-chip either way, and the extra cost of adding signal processing corresponding to an extra digital demodulator in silicon might not be high. Another important argument is the low time spent implementing such a system, since nearly all design modules exists. Power consumption might be more critical, but as processing technology reduces the power dissipation in CMOS-circuits this might not be critical either, especially when considering the low duty cycle of transmissions. In fact, total power consumption might go down when compared to a system not trying to mitigate fading since such a system might have a higher re-transmitting rate in fading environments.

4.4.2 Post-Packet Switching

When a corrupt packet is received the PPS technique switches to the other antenna. Another option is to let the switching be decided by the instantaneous SNR and a given threshold, as in SSC. This way, the next packet will be received on a different antenna with perhaps better instantaneous SNR.

This strategy is very unlikely to achieve success in all fading channels when applied to the current PHY. Considering the autocorrelation in figure 3.4 it can be seen that, in this special case, the channel experiences successive correlations and decorrelations over time. However, the channel samples in one diversity branch would represent a fairly uncorrelated sequence at low packet rates since the time between packets exceeds the coherence time. When assuming uncorrelated branches in the first place, this implies no greater probability of successful packet reception the next time a packet is being demodulated, yielding no diversity gain.

However, this strategy might provide diversity gain when coherence time is long and/or packet rates are high. The channel samples in one diversity branch can in this case represent

a correlated sequence. As such, subsequent packet demodulation will become correlated and vulnerable to errors in periods of signal fades. Assuming uncorrelated branches, this might be avoided by post-packet switching hence yielding diversity gain. This can be visualized by looking at figure 4.6. Assuming instantaneous SNR under the threshold value corresponds to detected and erroneously received packets, a PPS strategy will provide diversity gain. However, as the fading environment becomes more friendly, such deep fades becomes less likely and PPS will provide very little diversity gain. The potential diversity gain will also decrease with increasing average SNR, since the probability of a packet error or of a deep fade crossing the threshold value will decrease.

4.4.2.1 Implementation Considerations

The least complex fading mitigation technique discussed involves PPS using two or more antennas and a regular switch. Requirements to switching speed and transients are dependant on packet rates. These requirements can in general be very relaxed, and a low-cost switch will most likely meet the requirements. It is, however, believed that PPS will be more effective at mitigating fading in wireless systems with higher duty cycle of transmissions since coherence time is more likely to be exploited.

4.5 Analysis and Simulation Results

This section will present and compare results on diversity gain for the different fading mitigation techniques previously described. Even though diversity gain for PER is more interesting in a packet-based system, analytical diversity gain for BER will be presented for the different combining techniques described. The simulated diversity gain in BER will be compared to the theoretical and as such provide confidence in the diversity gain in PER resulted from simulations. The simulated BERs have solid lines while the theoretical BERs are marked with *. Using the simulation model constructed, each pair of (K,$\overline{\gamma}$) resulted in at least 1.920.000 correlated (K,γ) pairs which were input to diversity algorithms.

As described in section 3.2.3.2 Rician fading channels will be approximated by Nakagami-m fading channels with m given by equation (3.24). Since Rayliegh fading channels are equal to Nakagami-m fading channels with m = 1, or K = 0, all results will be presented for Nakagami-m fading channels with the corresponding K-value. Further, the simulation results are valid for a Doppler of 8.33 Hz.

4.5.1 Rayleigh Fading Channel, K = 0

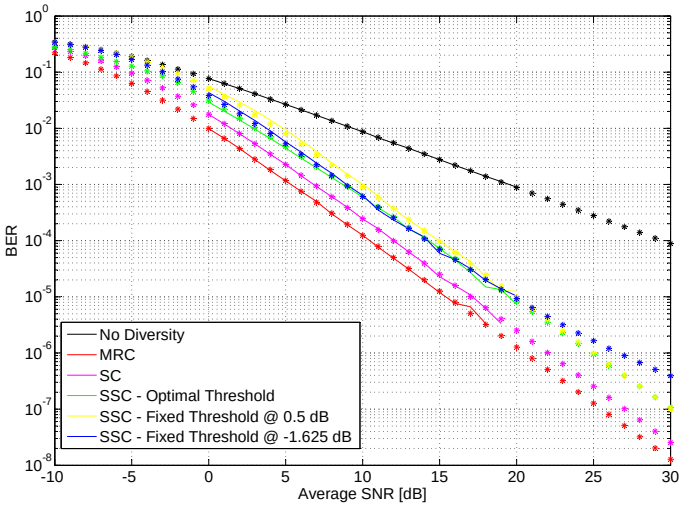

Figure 4.10: Nakagami-m fading channel BER, K = 0

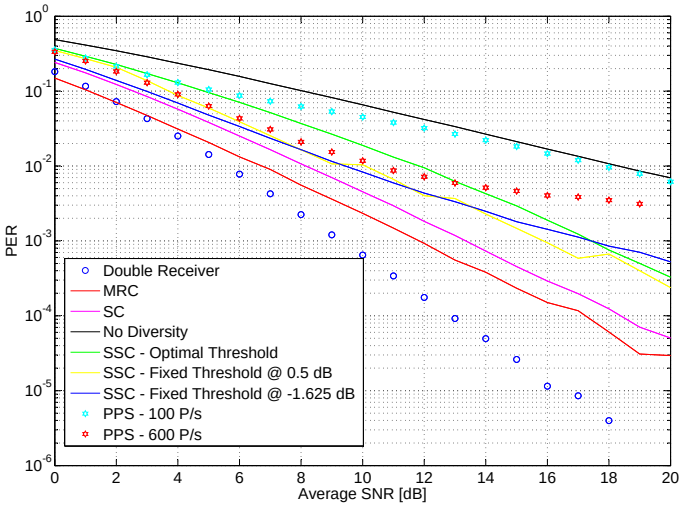

Figure 4.11: Nakagami-m fading channel PER, K = 0

4.5.2 Nakagami-m Fading Channel, K = 2

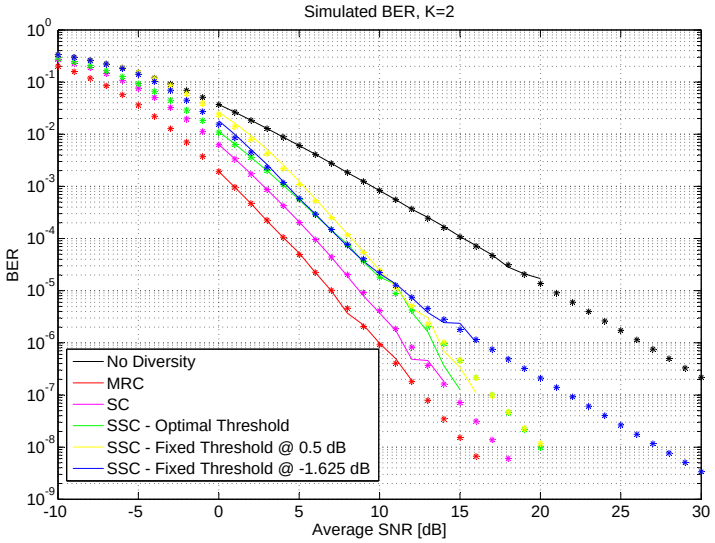

Figure 4.12: Nakagami-m fading channel BER, K = 2

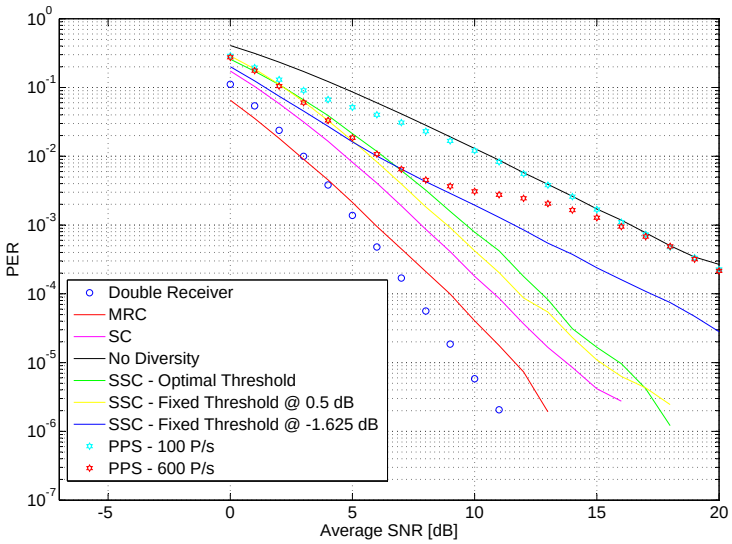

Figure 4.13: Nakagami-m fading channel PER, K = 2

4.5.3 Nakagami-m Fading Channel, K = 4

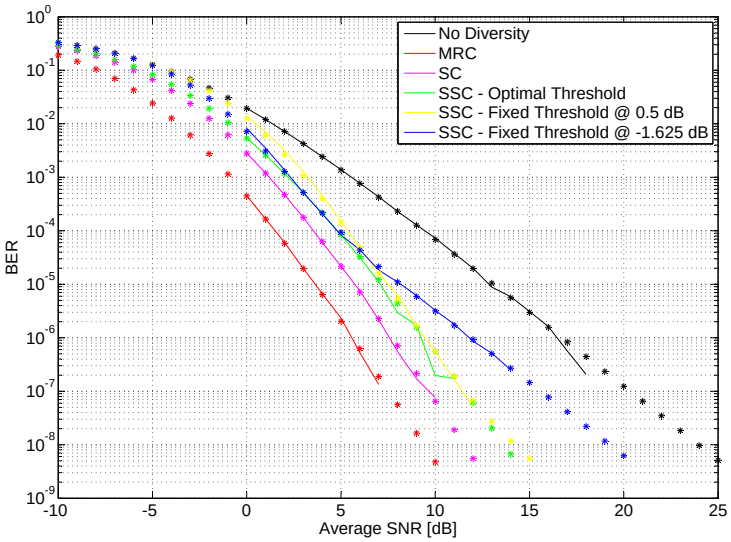

Figure 4.14: Nakagami-m fading channel BER, K = 4

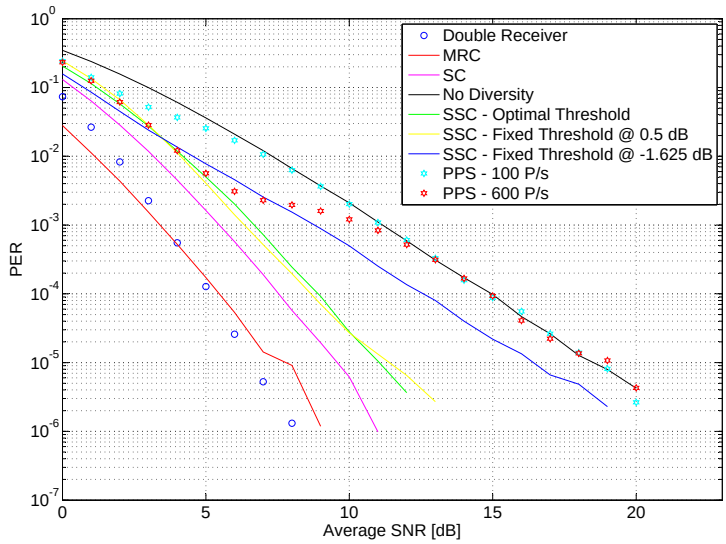

Figure 4.15: Nakagami-m fading channel PER, K = 4

4.5.4 Nakagami-m Fading Channel, K = 8

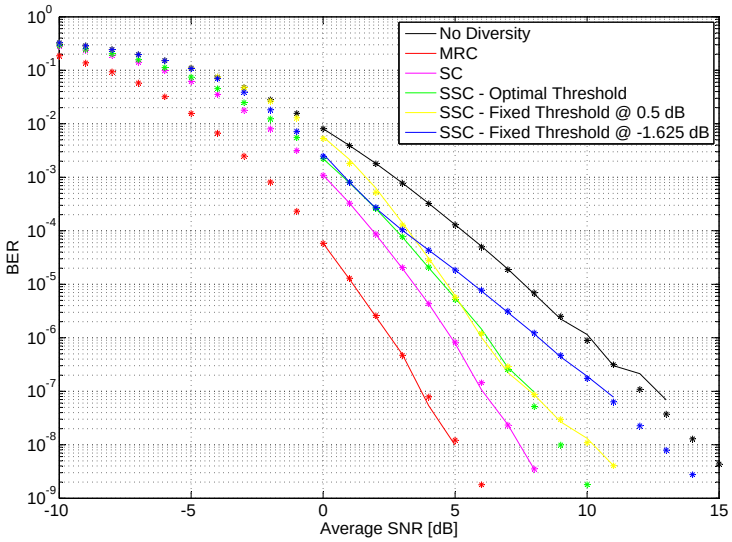

Figure 4.16: Nakagami-m fading channel BER, K = 8

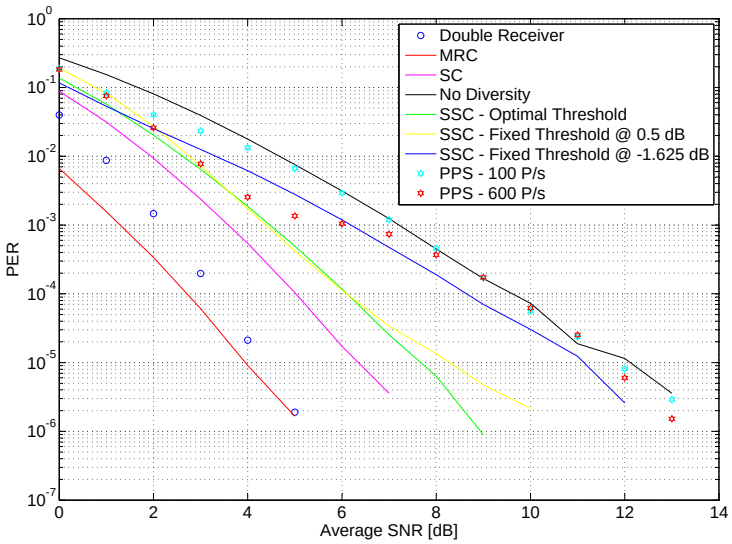

Figure 4.17: Nakagami-m fading channel PER, K = 8

4.5.5 Nakagami-m Fading Channel, K = 16

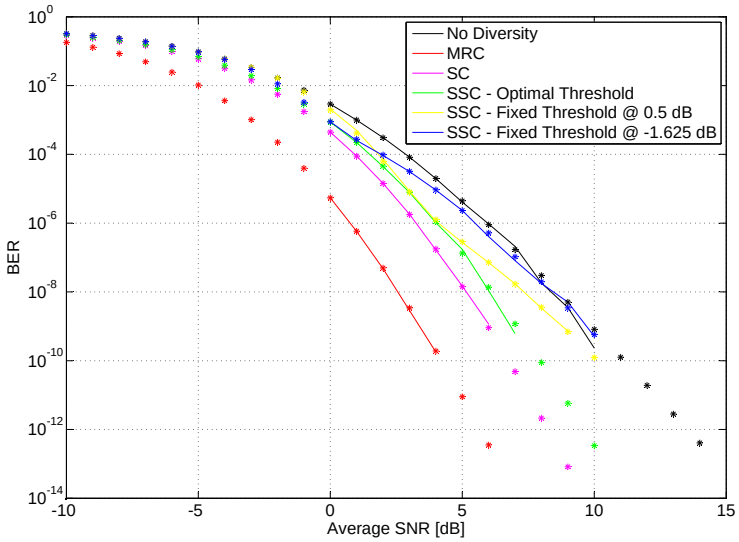

Figure 4.18: Nakagami-m fading channel BER, K = 16

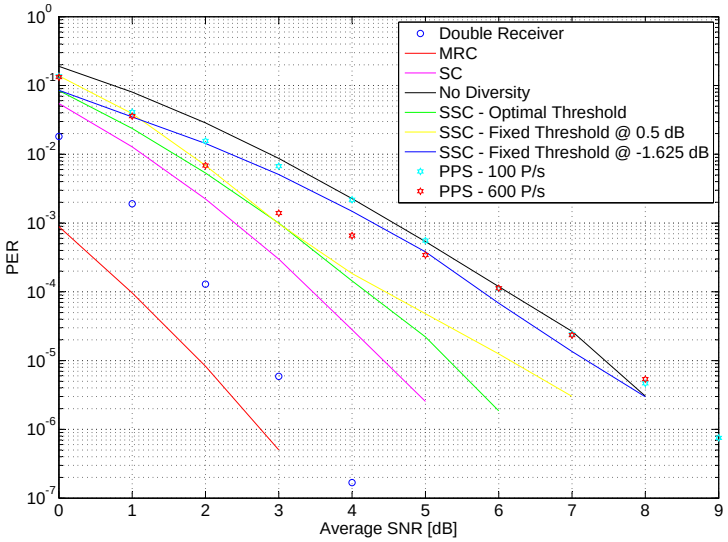

Figure 4.19: Nakagami-m fading channel PER, K = 16

4.5.6 Discussion

The following to subsections discuss the simulation results on a BER and PER basis.

4.5.6.1 Diversity Gain in BER

The simulated and theoretical BERs for the combining techniques described in section 4.3 correspond well in all fading channels presented. Some general remarks can be made about MRC, SC and minimum-BER SSC as function of average SNR and the fading channel. As average SNR increases, diversity gain increases. This is explained by the vanishing probability of deep fades. However, the diversity gain is reduced for all values of average SNR as the fading environment becomes more friendly. This is due to the presence of a relatively stronger and deterministic multipath component. As this deterministic component gets stronger, the possibility of deep fades is further reduced. MRC is affected less by this than SC and minimum-BER SSC. The reason is that all the diversity combining techniques are associated with an array gain, as explained in section 4.3. As the K-factor goes to infinity, the the channel will approach the characteristics of an AWGN channel, since the channel coefficient can be described deterministicly. However, the array gain of 2-branch MRC constantly equals 2 for all values of K while it's a decreasing function of K for both SC and SSC[17, p. 354].

Two values of switching thresholds are provided for SSC in addition to the optimal variable case. A switching threshold of 0.5 dB correspond to the sensitivity limit as showed in figure 2.2 while a switching threshold of -1.625 dB corresponds to a PER of 40%. As can be seen from the BER-figures, the threshold value of -1.625 dB approximates the optimal case the best for low values of K. As average SNR increases it will deviate more and more from the optimal curve. Figures 4.7, 4.8 and 4.9 predicts this behaviour, as the fixed threshold will dodge the minimas of the BER curve with increasing average SNR and K-values. The behaviour of both the fixed threshold SSC schemes will in the limit assume a no diversity system since thresholds are too low to be crossed.

4.5.6.2 Diversity Gain in PER

The simulated diversity gain in PER for the combining techniques described in section 4.3 behaves similar to the theoretical and simulated gains in BER, with one exception. For lower values of K, the minimum BER strategy does not correspond to minimum PER. As such, this strategy provides less diversity gain in PER than BER. This behavior can be explained from the non-linear mapping from instantaneous BER to instantaneous PER and the distribution of the instantaneous SNR given in equation (4.7). As K increases though, minimum BER corresponds to minimum PER. The switching threshold of 0.5 dB yields very good results on PER basis. This justifies the use of a fixed threshold instead of implementing an optimum threshold algorithm.

The behavior of the double receiver outlined in section 4.4.1 is verified by these simulation results. There is very little difference in PER between MRC and the double receiver for K-values of 2, 4 and 8. MRC performs significantly better in terms of PER for a K-value of 16, while the difference in diversity gain between the two is very little. Further, the double receiver performs best in the Rayleigh fading channel.

The predicted behavior of PPS is also verified by these results. When exploiting the coherence time of the channel by increasing the packet rate, diversity gain is achieved. This gain collapses with increasing average SNR and tends to get smaller as the fading environment gets more friendly. Since the fading environment assumed in these simulations represents the

lowest possible coherence time, diversity gain is likely to be observed in a real-life scenario with this strategy given that packet rates are high enough to exploit the coherence time.

Chapter 5

Measurement Platforms and Methodology

Test equipment, software and hardware IP provided by Texas Instruments have been utilized in various configurations together with hardware and software developed by the student to assess the potential performance increase for a Zigbee compatible PHY that utilizes spatial 2-branch antenna diversity and the combining schemes presented in section 4.3. These means and the methodology used to achieve relevant test data are presented in the latter part of this chapter. The theory provided in earlier chapters cannot directly be adapted to TI Zigbee compatible PHYs due to the lack of perfect SNR estimation which the analysis were built on. Consequently, this chapter begins with a treatment of relevant and possibly suitable arguments for diversity combining algorithms.

5.1 Diversity Combining Arguments

The theoretical analysis given in section 4.3 treated the diversity combining algorithms as having only one input argument upon which decisions were made, besides the two diversity branches. This analysis represented the ideal diversity combining situation where the instantaneous SNR in the diversity branches were available to the combiner. By performing combining based on this ideal input argument the diversity gain and/or the throughput was maximized for the various theoretical fading channels considered. It is so since the SNR is the only parameter exactly capturing the signal transmission quality. On the other hand, the simulations involving the double receiver showed that this strategy of combating the fading gives good results while at the same time requiring no knowledge of the signal quality to optimize transmissions. The following discusses three arguments that fading mitigation techniques can operate on when the instantaneous SNR is not at hand.

5.1.1 RSSI

The implementation of ED found in TIs Zigbee compatible chips is termed RSSI. No attempt to demodulate the data is made, and the RSSI represents only a measure of the total power within the channel bandwidth averaged over the 8 first symbols following the SFD. In a narrowband channel, this includes noise and interferer power as well as the wanted signal power. As such, it might represent a good decision argument for SC and SSC if the noise and interferer power are equally distributed and constant in the two diversity branches.

However, the assumption of an ideal narrowband channel might fail in many radio environments of interest. ISI will to some extent be introduced when the chip duration no longer

exceeds approximately ten times the RMS delay spread. When this happens, actual channel quality degrades while RSSI still might indicate good channel quality if interpreted this way. Contemplating RSSI as a channel quality measure and using it as an argument for diversity combining is therefore considered to possible give bad results. Nevertheless, since this channel measure is provided the benefits gained in diversity combining algorithms by use of it will be investigated by the physical testbed.

5.1.2 Correlation

A better measure than RSSI on the channel quality is provided by an averaged correlation value reported by the PHY for each received packet[10, p. 84]. As with RSSI calculation, the window used for averaging corresponds to the 8 first symbols following the SFD. By using the formula given in [10, p. 84], this correlation value can be converted to the LQI measure required by the standard. The correlation value corresponding to maximum quality received packets is reported by [10, p. 84] to be ∼110 while a value of ∼50 corresponds to packets barely detectable. As such, the correlation value is believed to be a better argument for diversity algorithms than the RSSI since it is obtained at the sampling instants of the correlator.

This estimate cannot be directly mapped to SNR since the input to the correlator is filtered and saturated to provide a fixed bit representation width. As such, noise power is removed. Mapping a symbol correlation value to SNR using signal space analysis can also suffer from decision errors causing better SNR estimates in cases where a symbol error occurred, which obviously is wrong.

5.1.3 LQI

The LQI measurement required by the standard does not specify how it should be implemented. The correlation value described above might be used, or it might be realized in a different way. To provide a third argument that diversity algorithms can operate on, the input to the correlator can be used to compute a measure on channel quality that is separated from the correlator. Such a measure will still be affected by the filtering performed prior to the correlator and might provide an estimate on the channel quality that is quite as good as the correlation value. This third argument will from now on be termed LQI. Figure 5.1 shows two conceptual input sequences of chips to the correlator. Referenced to this figure the LQI will be computed as

$$LQI = \frac{1}{N}\sum_{n=1}^{N}(X_n - \mu_n)^2 \tag{5.1}$$

by performing hard decision for each chip relative to the threshold value. This decision yields the expected value μ_n. N determines the averaging window and should equal one or more symbols to lower the variance associated with the LQI. The LQI will still not resemble a true SNR measurement, since incorrect hard decisions will cause wrong expected values and hence lead to an incorrect measure on SNR if interpreted this way. However, while receiving with high instantaneous SNR the inverse of the LQI will be proportional to SNR. The problem is that these situations most likely will not benefit from diversity combining. Interpreting LQI as SNR in situations where reception would benefit from diversity combining would therefor be wrong.

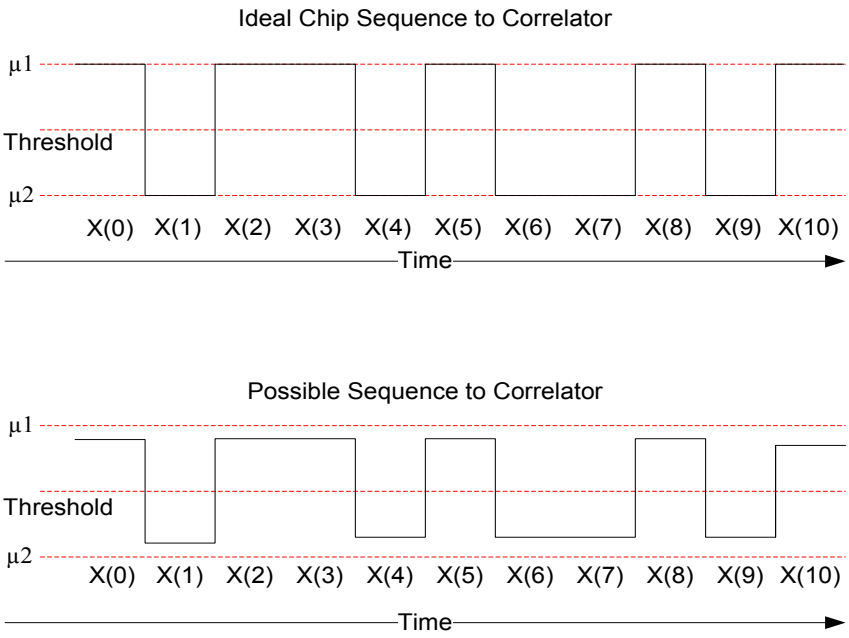

Figure 5.1: Conceptual view on input to correlator

5.2 Tx - Hardware Platform

To generate PHY compatible packets a SmartRF05EB revision 1.7[12] board equipped with an CC2530EM[11] were used as a hardware platform. The CC2530 SOC ran a program heavily based on the PER-tester available by downloading the software examples for CC2530[11]. The chip were programmed by following the steps in the user guide attached to these software examples. The functionality of the program was almost identical to the original PER-tester. The only difference in code was the specification of the payload bytes as well as the MAC header's address fields. The address fields were changed to be able to filter out received packets that belonged to other ZigBee networks, while the payload contained a counter which was incremented for each packet. By doing this, the receiver could be able to place received packets in time.

In brief, this transmitter setup can be configured to use different channels, output powers, packet rates and number of packets transmitted by following a menu displayed on the SmartRF05EB LED. The PSDU used in the tests gives a packet frame length of 22 bytes which conforms with [9, p. 268]. The PSDU is depicted in table 5.1

Table 5.1: PSDU

Octets	2	1	2	2	2	10	2
What	Frame Control	Sequence Number	Destination PAN ID	Destination Address	Source Address	Frame Payload	FCS

5.3 Rx - Hardware Platform

The problem description dictated the development of a real physical testbed that can be used to evaluate different receiver algorithms and architectures used to mitigate fading based on existing demodulator IP provided by Texas Instruments. Because each combining scheme yields one specific receiver architecture it would be impractical and time consuming to implement and verify the different receiver architectures in a FPGA separately. To acquire the data needed to assess any performance increase, a generic hardware solution has been chosen instead. This generic hardware solution must provide data which software can post-process to verify potential performance improvements for a given radio environment by using different methods to fading mitigation. MRC will be neglected for implementation since the problem description emphasized the less complex versions of the diversity combining schemes to be implemented and tested. Since MRC requires co-phasing, two full receiver chains would have been needed in addition to combining circuitry, which makes MRC more complex than a double receiver, SC, SSC and PPS. A second argument for disregarding MRC is the need for a dedicated hardware platform to test it and the absence of a good estimate on the instantaneous SNR. The latter makes such an implementation sub-optimal in either case and has not been analyzed in section 4.3. A third argument is that the performance of MRC can be approximated by the double receiver, which in turn is easy to implement.

5.3.1 FPGA Implementation

The main target for physical testbed development was a FPGA realization of a diversity receiver which could be used to evaluate potential increase in throughput for different fading scenarios and different combining algorithms. Texas Instruments Norway provided an Virtex-4 FPGA development kit and the digital demodulator IP for their newly released CC2530 Zigbee SOC. RF-front ends responsible for downconversion and analog-to-digital conversion were provided by using two CC2530 in ADC debug mode. When operated in this mode, the chip outputs ADC data for I- and Q-channels together with a ADC clock that is used to sample the data. The relation between these signals internal in the CC2530 chip when not operated in ADC debug mode is shown in figure 5.2

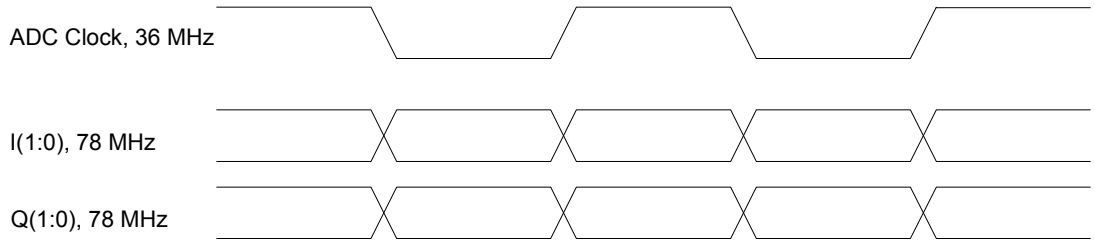

Figure 5.2: ADC data interface

The system architecture chosen for evaluation of diversity combining algoritms is shown in figure 5.3.

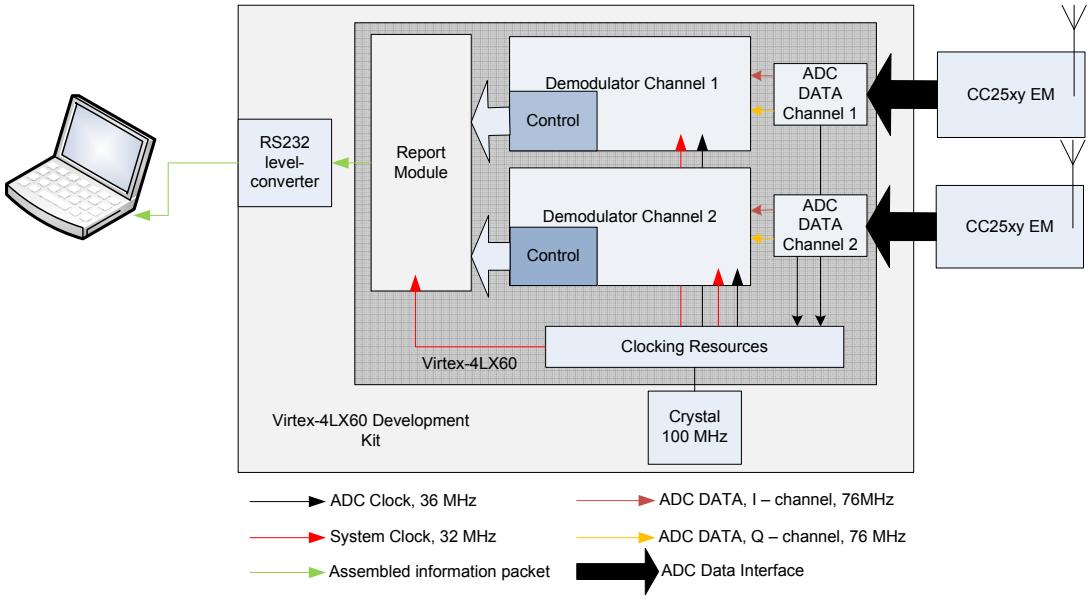

Figure 5.3: FPGA system architecture

The system architecture contains two full receiver chains that are slightly modified. To provide the relevant parameters that the diversity algorithms can use, each digital demodulator is extended by a module that controls the reception of packets in each channel by

- Performing packet filtering to discard demodulated packets from other ZigBee systems that does not belong to the diversity test
- Extracting and temporarily storing packet number, RSSI, correlation and CRC for each packet in registers
- Computing and storing a LQI value for each packet in a register
- Signaling the state of demodulation and the validness of the contents in the registers used to hold received packet information to the report module.
- Restarting, initializing and reseting the demodulator logic at appropriate times according to the specification of the demodulator

The top-level design contains IOs, clocking resources, the two extended demodulators and a report module that assembles data packages containing the stored packet information from each demodulator. The report module also implements a UART that is used to transmit the assembled packages to a computer using a RS232 level-converter and serial port located on the development kit. The packages were read, parsed and saved to files by a Matlab program for post-processing by different fading mitigation algorithms.

5.3.1.1 Verification of Design

To verify the design ADC data was sampled from a CC2530 chip in ADC debug mode by a logic analyzer and used as input to a VHDL testbench containing the above FPGA architecture as VHDL code. These ADC samples contained noise as well as packets according to the PSDU format given in table 5.1. Correct behavior of the architecture was verified by simulations in Modelsim.

5.3.1.2 Practical Problems

This measurement platform was not successful in practice. Physical tests of the platform showed that the PER was very high compared to the PER-tester mentioned in section 5.2. Analysis of the data received by the computer also showed that the RSSI was reported being 30-40 dB lower than what the PER-tester reported. Several factors have possibly contributed to this:

- ADC data was outputted on regular single-ended GPIO pins which yielded bad signal integrity at the frequencies given in figure 5.3. The cables connecting the chip with the FPGA would have to support the 10th harmonic to transfer such signals.
- The ADC clock needed to be outputted on a 20 mA pad, while the data was outputted on pads supporting 4 mA. The chip's voltage supply was measured and found time-varying and strongly correlated with the ADC clock.
- Sources at TI explained that no timing requirements was specified to the pads outputting the ADC data. As such, the relation between the ADC clock and the data signals shown in figure 5.2 could not be guaranteed, hence yielding bad signal integrity.
- Sources at TI explained that the ADC very likely could behave badly when the chip is operated in ADC test mode. This incorrect behavior could lead to increased noise being added to the ADC data. This would affect the chip's sensitivity and thereby lower the range between TX and RX that give satisfying throughput. The student have followed the advice given from technical staff at TI to configure internal registers in the chip to reduce this problem.

The problems affecting the signal integrity between the chip and the FPGA made sampling of the ADC data on the FPGA side very difficult and erroneous. Using an oscilloscope that were triggered on the rising edge of the ADC clock revealed severe problems at the relevant sampling instants that can be characterized by very bad eye-diagrams. This problem was tried worked around by increasing the signal integrity between the source of ADC data and the FPGA using the setup showed in figure 5.4

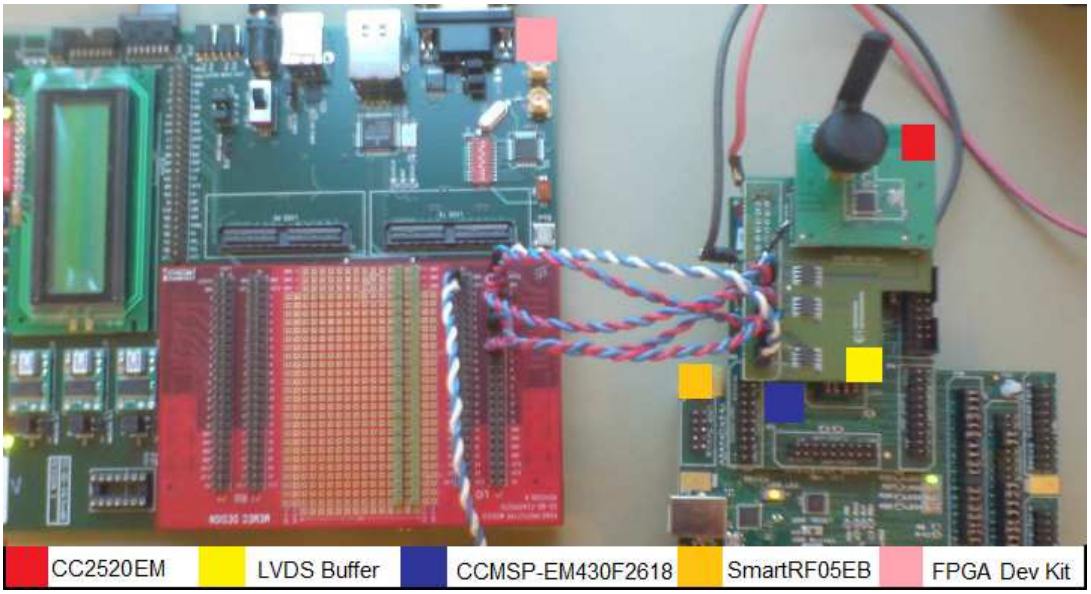

Figure 5.4: Test-setup with LVDS buffer

This test setup used a LVDS buffer compatible with the CC2520EM to convert the single-ended ADC signals to LVDS signals and thereby increasing signal integrity. This was possible since the ADC signals and RF-front end in CC2520 are equal to those found in CC2530. The microcontroller on CCMSP-EM430F2618 was programmed to set up the CC2520 tranciever in ADC test mode by SPI-programming, while the SmartRF05EB was used to power the CCMSP-EM430F2618 during programming. This strategy yielded better range and PER results compared to the single-ended interface. However, this solution was still inferior to the PER-tester regarding both PER and range.

The problem described above was considered too serious to use this platform to evaluate the different fading mitigation algorithms. The reason was the high packet loss, most likely introduced by the ADC interface, and the reduced range of operation. Packet loss increased dramatic as function of range compared to the PER-tester. To evaluate the fading mitigation algorithms with higher confidence a new platform had to be constructed. This platform is described in the next section.

5.3.2 Packet Sniffer Implementation

By using the Packet Sniffer[13] application developed by TI it was possible to acquire the RSSI and correlation values associated with each detected packet together with the total contents of the packet shown in table 5.1. This information was stored in a binary file by the application according to the format given in figure 5.5, where each packet corresponds to 151 bytes.

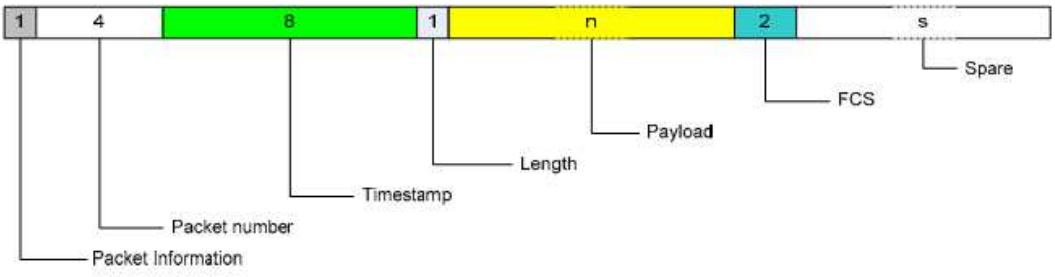

Figure 5.5: Format of binary file

The information contained in this binary file was used to construct arrays containing RSSI, correlation, payload counter and CRC as a function of time with a resolution of 10ms, the inverse of the packet rate. These actions were performed by a channel builder algorithm. PHY packets not belonging to the test and packets caused by demodulation of noise was removed by the algorithm by filtering packets with wrong address fields. Erroneously demodulated packets with correct address fields but failed FCS could reliably be resolved with respect to RSSI and correlation. When neither address fields nor FCS were correct, the packet could not be resolved as part of the test. As such, RSSI and correlation were given default values corresponding to -111 dBm and 0, respectively. Each run of the channel builder algorithm consisted of searching forward in time for the next correctly demodulated packet. When found or no more received packets available, the algorithm rebuilt the channel backwards in time by filling in the resolved values or defaulted values.

The address filtering will impact the rebuilt channel parameter arrays in an unwanted way by defaulting the RSSI and correlation values when both FCS and address fields are wrong. In environments with significant fading this can lead to many defaulted channel parameter values, which is highly unwanted when investigating the relation between packet loss, RSSI and correlation. Filtering cannot, however, be completely removed. Without providing all the

details of the channel builder algorithm, this can be explained by a little example. Starting at the last correctly received packet, the algorithm will start searching forward among the received packets for the next correctly received packet belonging to the test. When found, the algorithm will determine the number of lost packets belonging to the test that were corrupted or lost. The channel parameter arrays are then rebuilt backwards in time, inserting the determined RSSI and correlation values at correct places by using the reported timestamps in figure 5.5. When a packet that does not belong to the test is not filtered out in this process, the algorithm will process more packets than expected and hence overload the preallocated channel arrays. This will cause indexing problems, and the algorithm will fail. This problem can be worked around by lowering the degree of address filtering or totally remove it if testing in areas with no other Zigbee-systems.

Even though the Packet Sniffer implementation had the above described issues, measurements using this platform could be done more effectively than what the FPGA approach allowed by using many instances of the application. This allowed emulation of a setting with multiple receiver chains. This provided more measurements from each test allowing the diversity algorithms, explained in the next section, to be evaluated with higher confidence by averaging the results than the FPGA approach would allow. Performance improvements as function of antenna separation could also be investigated for the same channel realizations, since channel information was synchronized as described above. As such, much more data for analysis would be available to evaluate diversity gain and PER in a given environment.

5.3.3 Algoritms To Be Tested

The SC and SSC algorithms could be evaluated with RSSI and correlation as input arguments when using the Packet Sniffer implementation. As such the following 9 fading mitigation algorithms were chosen to be tested.

1. Double Receiver

2. SC - Choose highest correlation. If equal, choose highest RSSI. If equal, keep current diversity branch.

3. SC - Choose highest RSSI. If equal, choose highest correlation. If equal, keep current diversity branch.

4. SC - Choose highest correlation. If equal, keep current branch.

5. SC - Choose highest RSSI. If equal, keep current branch.

6. PPS - If packet was received with errors, receive the next packet on the other branch.

7. SSC - Switch to other branch if RSSI is under given threshold value.

8. SSC - Switch to other branch if correlation is below given threshold value.

9. SSC - Switch to other branch if both correlation and RSSI is below their respective thresholds.

The SSC algorithms were implemented as if using PSDU-switching since this only yields one RF-front end. Switching thresholds were determineded by measurements in the next chapter.

5.4 Measurement Setup

This section explains how relevant measurements were conducted to obtain multiple data sets on which diversity algorithms could be evaluated and other statistics extracted.

5.4.1 RX - FPGA Implementation

The test performed with the FPGA implementation were conducted with an RX setup as showed in figure 5.4. As explained, this RX configuration was chosen not to evaluate fading mitigation algorithms due to PER not only being a function of wave propagation and possible interference but also the ADC interface. As such, only one office environment test was conducted to extract statistics regarding the relation between packet errors, RSSI, correlation and LQI.

5.4.2 RX - Packet Sniffer Implementation

Test were performed by using 4 SmartRF05EB revision 1.7[12] with 4 CC2520EMs connected. The CC2520EM was spaced in a manner yielding an antenna separation of 0.5 λ. Figure 5.6 shows the somewhat non-ideal RX setup in one of the environments where tests were conducted. This setup was used to evaluate diversity gain with an antenna spacing of 0.5 and 1.0 λ. As

Figure 5.6: RX setup

such, the confidence of the 0.5λ measurements were higher than the 1.0λ measurements, due to more averaging. In addition to being more reliable and effective compared to the FPGA setup, the Packet Sniffer setup was also much more portable since all the SmartRF05EB were powered by batteries.

5.4.3 TX

When analyzing diversity gain in chapter 4, all results were valid for a given average SNR and fading environment. To obtain the same statistic foundation when doing field tests, small-scale measurements within an area of 10λ diameter must be taken with random movement of either TX or RX. This way, large-scale propagation effects will be the same and the variation in received signal power will be caused by multipath effects only. An alternative to obtain the data set could be to move TX along a straight line in the variable fading environment. This strategy can, however, be victim to possible shadowing effects caused by large elements often found in buildings, such as metal plates, elevators etc. As such, the measurements cannot be related to a specific fading environment since received power varies as well as the statistics of the channel coefficient. These scenarios are showed in figure 5.7 were the Packet Sniffer RX setup is used. As showed in the figure, TX was chosen to be randomly moved within a diameter of 10λ to achieve the measurement properties as described above. Speeds of approximately 1ms^{-1} was targeted but were hard to verify accurately due to movement along curves.

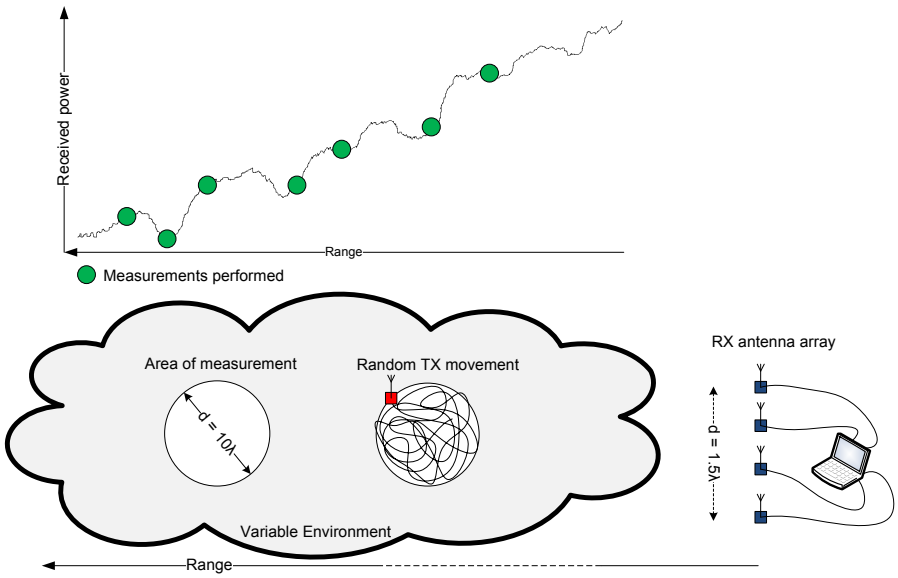

Figure 5.7: Measurement setup

Time available to testing was shortened due to the development complications described in section 5.3.1.2. As such, the number of environments tested was limited. Typical indoor radio environments were seeked out to gain insight in the performance improvements obtainable for the PHY. There were, however, problems finding ranges with guaranteed radio LOS, given by no obstructions in the first Fresnel zone. On small distances radio LOS was obtained, but as range increased some of the LOS environments tested might have had structures a little bit inside the first Fresnel zone. However, all environments seeked out represented typical indoor multipath environments. As such, the significance of these possible and small violations were considered negligible. The following multipath environments were used to conduct the procedure described above

- Forskningsparken, main cafeteria NLOS
- Forskningsparken, main cafeteria LOS
- Rikshospitalet, garage house NLOS
- Rikshospitalet, garage house LOS

In addition to the measurement procedure outlined above, tests where both TX and RX remained static were conducted in the Forskningsparken main cafeteria NLOS environment. Each test in a given environment, static as well as dynamic, consisted of a transmission of 10.000 packets at a rate of 100 per second.

Presence of WLAN activity constitutes an additional source to packet errors due to packet collisions. The strategy to counteract the effects of this error source in the measurements consisted of using frequency channel 15 in the tests, as shoved in figure 2.1. To further counteract the possibilities of collisions in the Forskningsparken environment, test were conducted during holiday when few people were using the building and hence the wireless networks. No WLAN activity was detected in the garage house environment.

Chapter 6

Practical Results

This chapter will start by presenting samples of available data on channel statistics obtained by using the Packet Sniffer platform and the FPGA platform. These samples will provide an understanding of what determines the success of different fading mitigation algorithms. All samples presented will be given a short discussion.

The gained insight obtained by analyzing the data material collected, will in the last section be used to reduce the number of algorithms subject to test. Results on diversity gain and reductions in PER given by the different algorithms will be discussed in the end of the chapter. Time available to measurements was heavily reduced by the problems described in section 5.3.1.2. As such, it's natural to question the confidence in the results given here. This topic will be treated in the discussion in chapter 7.

Further, all tests were performed by using -3 dBm output power. This choice was based on an assumption that measurements should be performed at relatively low signal powers. One reason is that the AGC loop will have variable gain for a certain range of RSSI values. As such, it will become harder to analyze the effect of fading mitigation algorithms. Another reason is the fact that delay spreads are reduced when lowering the signal output power. ISI will as such be reduced. Tests were performed with a variable separation of 10-50 meters between RX and TX.

6.1 Channel Statistics

This section presents the channel statistics obtained from the two measurements platforms. Data obtained from the Packet Sniffer platform were not filtered, as discussed in section 5.3.2. As such, the channel parameters were unaltered by the channel builder algorithm. Packets not received have the default RSSI and correlation values of -111 dBm and 0, respectively. All packets received belonged to the test.

Random movement within an area of 10 λ diameter, as shown in figure 5.7 was targeted with a speed of approximately 1ms^{-1}. This resulted in a Doppler of approximately 8.3 Hz. The accuracy of the speed/Doppler is not that high due to curved random movement. Figure 6.1 shows the numbering of the branches relative to the antennas used when displaying data.

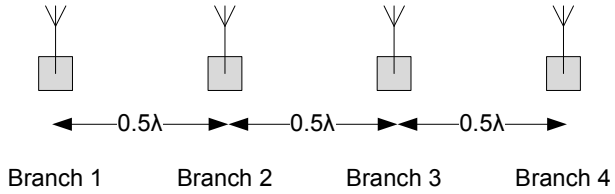

Figure 6.1: Diversity branch numbering

The different scenarios will be analyzed in terms of RSSI dynamics and statistical distributions using the reported RSSI and correlation values. These analyses are somewhat problematic with respect to the measurement platform, the reported RSSI and the limited sample population. Firstly, the measurement platform only reports RSSI values for detected packets. Secondly, the reported RSSI values possess an uncertainty of +/- 4 dBm[10, p. 13], which means that the reported RSSI values actually can be more than twice as high or twice as low as the real values. Thirdly, the RSSI values are burdened with non-linear quantization noise. High RSSI values will as such have high variance, whereas small values will have low variance. Fourthly, a RSSI measurement represents all the power in the frequency band of interest. As such, it contains noise, interference and wanted signal power. RSSI measurements were taken before tests were conducted in a specific environment. All branches reported the same RSSI values. As such, noise can, on average, be regarded as constant and equal for all branches. The interference, however, cannot be treated the same way. Packets subject to interference that are not lost, will hence contribute to uncertainty when analyzing results in terms of RSSI.

These RSSI properties will affect analyses in different ways. Statistics on RSSI distributions within a small area cannot in either way be regarded as correct. For example, RSSI distribution estimation will be affected by packets that are lost, especially if all lost packets correspond to low RSSI values. The uncertainty and noise associated with the RSSI values will also affect the correctness of distribution estimates. Interference will in general not necessarily cause packet errors due to good interference rejection. The estimated RSSI will, however, be larger than samples without interference. The distribution estimates will be affected by such RSSI values. In dynamic tests corresponding to section 5.4.3, distribution estimates should therefore not be interpreted and compared between branches. The limited data set will also restrict the accuracy of distribution estimation. The key conclusion to draw from such estimates is the tendency in the estimates which describes the environment. All RSSI distribution estimation will be done with the gamfit-function[18] provided by Matlab. This function returns the MLEs for the Gamma distribution parameters m and $\frac{\overline{\Omega}}{m}$ with a 95% confidence interval.

The error and uncertainty sources described above will also affect estimates on envelope covariance between the branches. These estimates are generated as Pearson's product-moment coefficient. Input to this estimator is the root of the RSSI[mW] samples in the different branches. This is a highly non-ideal input to such an estimator.

6.1.1 Forskningsparken, Main Cafeteria NLOS

This section presents a sample of obtained channel statistics taken from one of the measurements in the main cafeteria at Forskningsparken. There was no LOS between TX and RX.

6.1.1.1 RSSI Dynamics

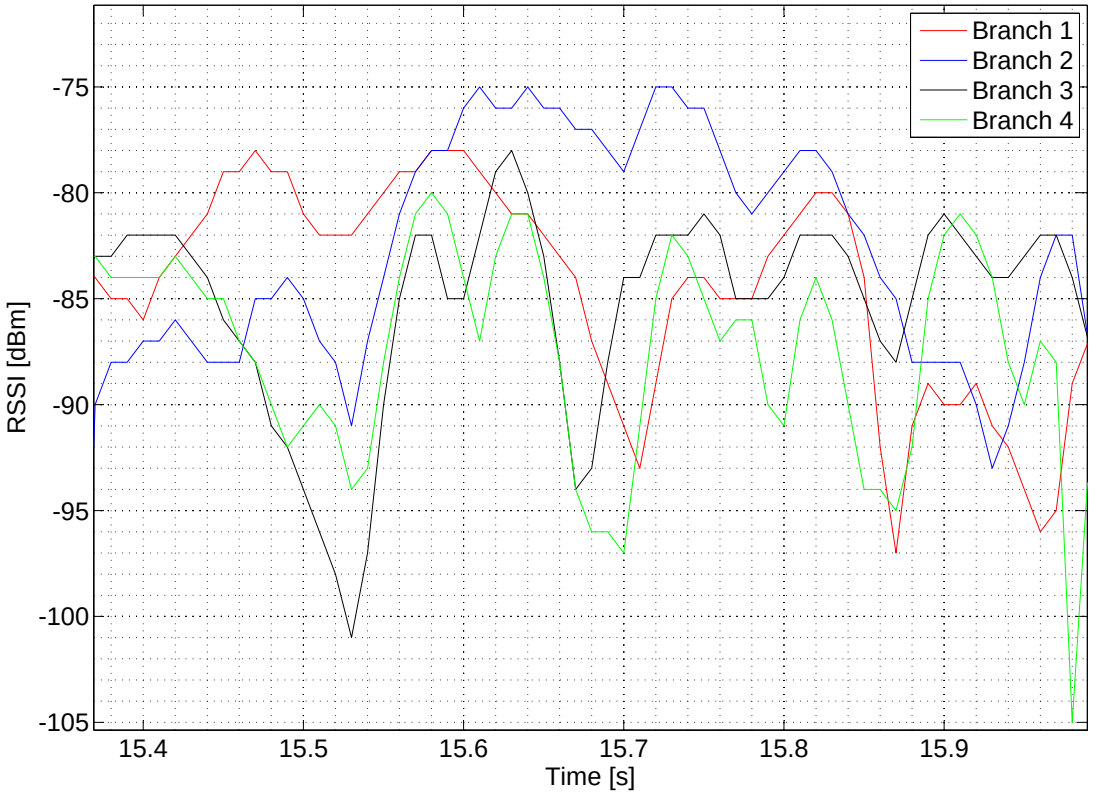

Figure 6.2: RSSI measurements in a NLOS evironment

This sample of the reported RSSI is quite interesting but not special compared to the rest of the collected RSSI values from this environment. All branches experience large variations in RSSI, some more than others. Branch 4 is subject to faster variations than for instance branch 2 in this segment, while being fairly correlated to branch 3, only separated by 0.5λ. The fastest variation in RSSI is observed on branch 3 in the right part of the figure where it drops 18 dB in 10 ms, which is the time resolution of the samples. A velocity of x ms^{-1} would in this case represent a movement of x/12 λ. The velocity of TX in all samples were approximately 1 ms^{-1} yielding a movement of 1/12 λ which is fairly little. The covariance between the branches are presented in table 6.1.

Table 6.1: Envelope covariance between branches

	Branch 1	Branch 2	Branch 3	Branch 4
Branch 1	1	0.5426	0.3873	0.3639
Branch 2	0.5426	1	0.5817	0.5105
Branch 3	0.3873	0.5817	1	0.5314
Branch 4	0.3639	0.5105	0.5314	1

These values are calculated as outlined in previous section. Envelope covariance between branches drops with distance as expected. A separation of 0.5λ causes the branches to decorrelate the most, while little decorrelation is achieved by increasing the antenna separation.

6.1.1.2 Channel Parameter Distributions

Histograms of the received RSSI[mW] and correlation values on branch 2 and 4 during this test are given in figure 6.3

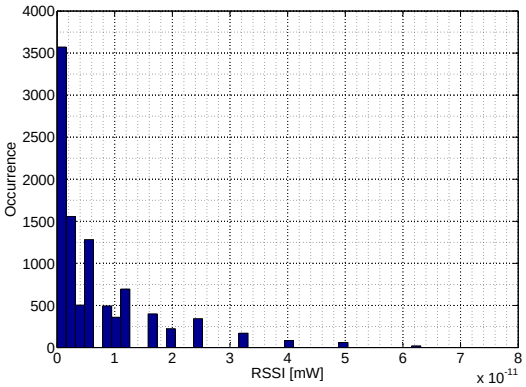

(a) RSSI distribution on branch 2

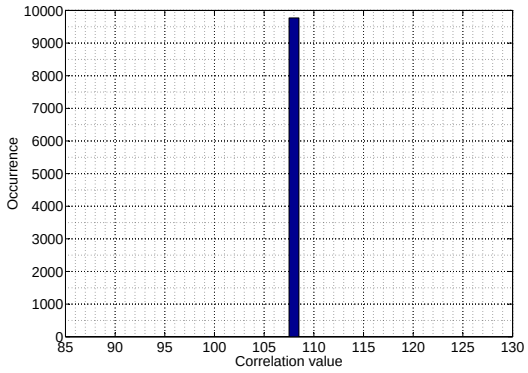

(b) Correlation value distribution on branch 2

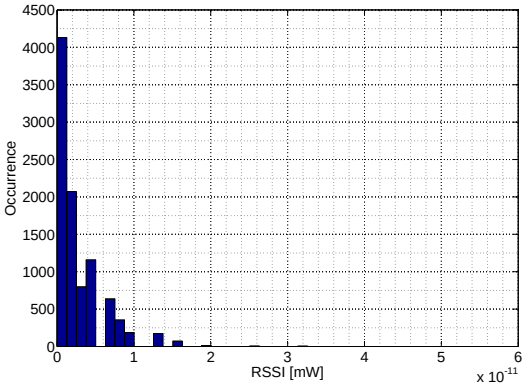

(c) RSSI distribution on branch 4

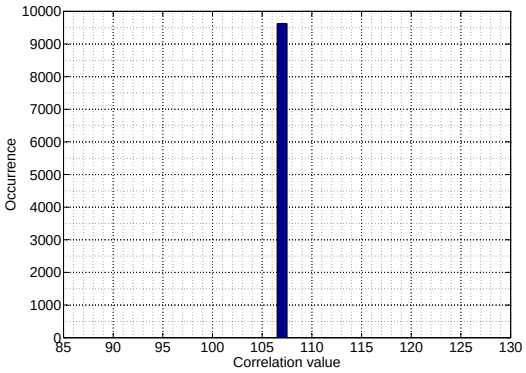

(d) Correlation value distribution on branch 4

Figure 6.3: Channel parameter distributions

The distribution of the RSSI and correlation values are very different, the latter only containing correlation values of 108 for branch 2 and 107 for branch 4. The reported difference in correlation value might come from differences in the CC2520EMs used when measuring. The MLEs for the Gamma distribution parameters are provided in table 6.2.

Table 6.2: MLE for Gamma distribution parameters

Branch	m			$\frac{\overline{\Omega}}{m}$		
	MLE	Confidence Interval		MLE	Confidence Interval	
1	0.8675	0.8467	0.8888	6.1738e-012	5.9781e-012	6.3759e-012
2	0.6904	0.6742	0.7071	9.6568e-012	9.3364e-012	9.9882e-012
3	0.9281	0.9056	0.9512	4.7418e-012	4.5923e-012	4.8962e-012
4	0.8895	0.8679	0.9117	3.1218e-012	3.0220e-012	3.2249e-012

The values of m in table 6.2 indicate a more severe fading channel than Rayleigh since these are beneath 1. Further, the different branches experience slightly different fading channels with small differences in RSSI. Using the MLE values, the mean RSSI in the channels vary from -85.56 dBm to -81.76 dBm. This is not expected from the measurement methodology outlined in section 5.4.3 and can be explained by the sources of errors described at the beginning of this chapter.

6.1.1.3 Packet Error Dependencies

Packet errors among the 10.000 packets transmitted to branch 2 and 4 were distributed between RSSI and correlation values as showed in figure 6.4

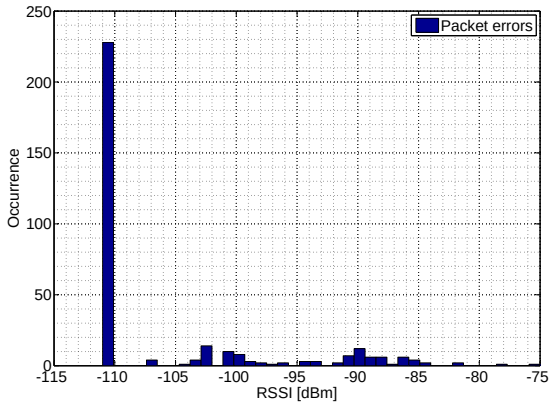

(a) Packet error as function of RSSI, branch 2

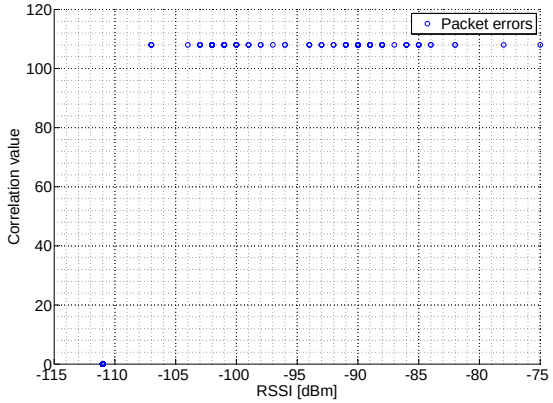

(b) Packet error as function of RSSI and correlation, branch 2

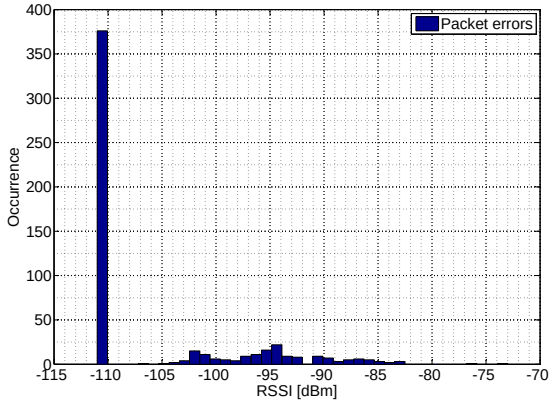

(c) Packet error as function of RSSI, branch 4

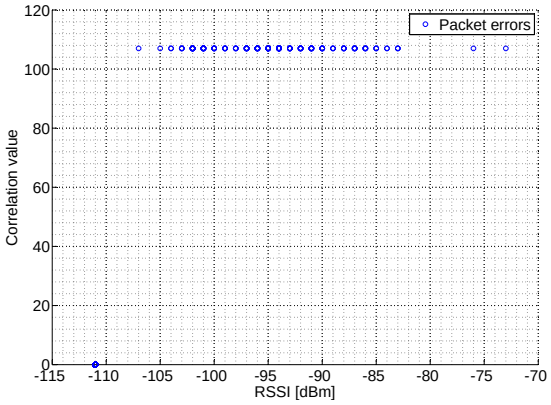

(d) Packet error as function of RSSI and correlation, branch 4

Figure 6.4: Packet error dependencies NLOS

There are several interesting remarks about this figure. Packet errors are distributed over a range of RSSI values whereas only three correlation values. The packet errors corresponding to a RSSI of -111 dBm and a correlation value of 0 originates from undetected packets. These points are made by the channel builder algorithm. As can be seen from figures 6.4b and 6.4d the correlation values for all erroneously received packets are constant and equal to 108 and 107, for branch 2 and 4 respectively. This observation is important when considering the effectiveness of correlation as an input argument to a fading mitigation algorithm. An SC algorithm always choosing the branch with the largest correlation value would in this case always choose branch 2. This would imply no diversity gain. Using the MLE Gamma parameters in table 6.2 gives a mean RSSI of -81.76 dBm for branch 2 and -85.56 dBm for branch 4. From figures 6.4a and 6.4c it can be seen that packet errors are not particular concentrated around the corresponding means. Further, the high amount of undetected packets in this test implies great uncertainties in the RSSI distributions given in figures 6.3a and 6.3c since it is quite possible that many packets associated with low RSSI values are lost. The high amount of undetected packets would in this

example reduce the effectiveness of SSC algorithms implemented with one RF-front end, since PER mostly consists of undetected packets.

6.1.2 Rikshospitalet, Garage House LOS

This section presents a sample of obtained channel statistics taken from one of the measurements in the garage house at Rikshospitalet. There was a clear LOS between TX and RX in this measurement. The environment in the garage house can be classified as highly reflective due to the cars parked on the same floor as well as the floors above and below.

6.1.2.1 RSSI Dynamics

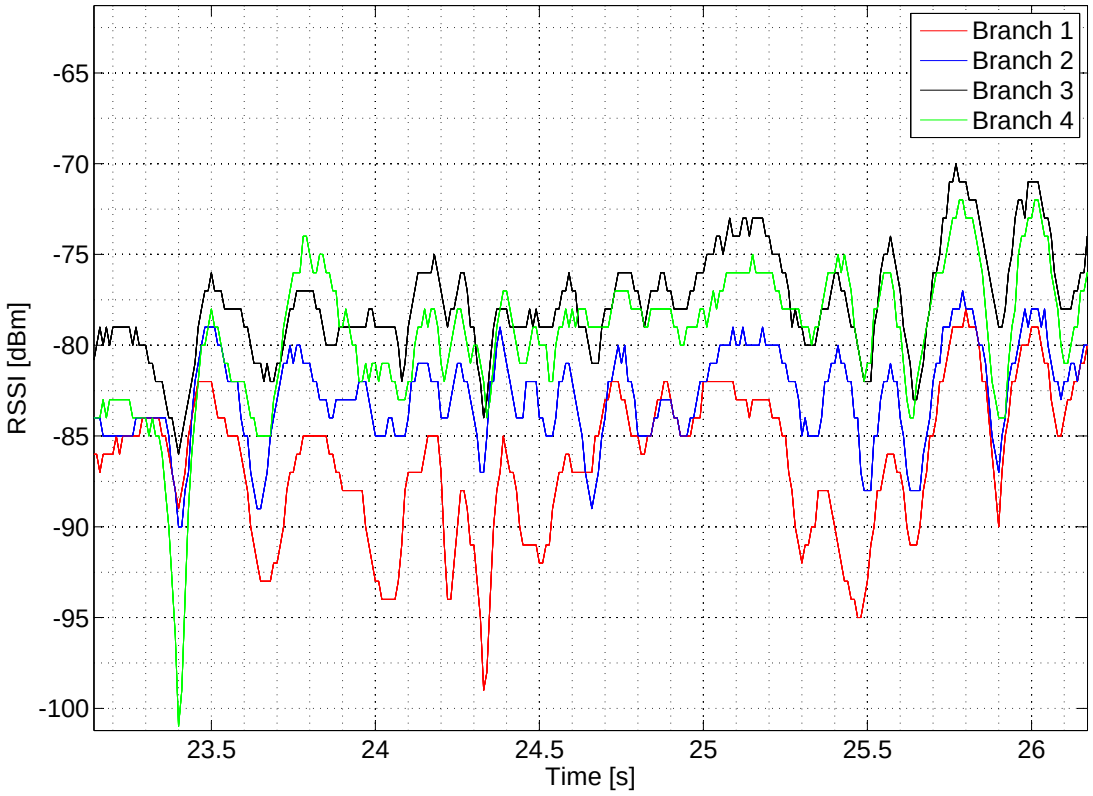

Figure 6.5: RSSI measurements in a LOS evironment

This sample correspond to a larger time window than the similar plot given in figure 6.2. The larger time window was chosen so that the correlation between the branches become more visible. The RSSI values all behave similar, even though they differ from each other with an offset in this time window. Rapid and relatively large variations in RSSI are visible in this case as well. This can probably be explained by the highly reflective environment consisting of cars and the limited spaces encountered in such garage houses. These two factors will contribute to many and relatively strong multipath components compared to the direct component. As such, this type of environment is likely to possess properties corresponding to NLOS environments when range increases. The envelope covariance between the branches is presented in table 6.3.

Table 6.3: Envelope covariance between branches

	Branch 1	Branch 2	Branch 3	Branch 4
Branch 1	1	0.7049	0.7762	0.6399
Branch 2	0.7049	1	0.8106	0.7450
Branch 3	0.7762	0.8106	1	0.8124
Branch 4	0.6399	0.7450	0.8124	1

The covariance values given in table 6.3 are very different than the ones presented in table 6.1. Covariance between branches are stronger and does not vary that much with antenna separation. This is characteristic for a LOS environment. Fading mitigation algorithms will not perform optimally in such scenarios due to strong correlations between branches. The SSC algorithm with one RF-front end will be degraded the most due to the likelihood of switching to a worse branch.

6.1.2.2 Channel Parameter Distributions

Histograms of the received RSSI[mW] and correlation values on branch 3 and 4 during this test are given in figure 6.6.

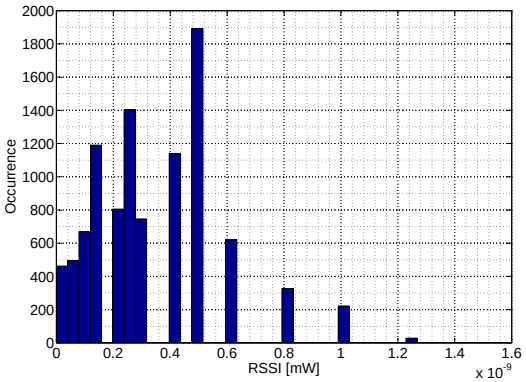

(a) RSSI distribution on branch 3

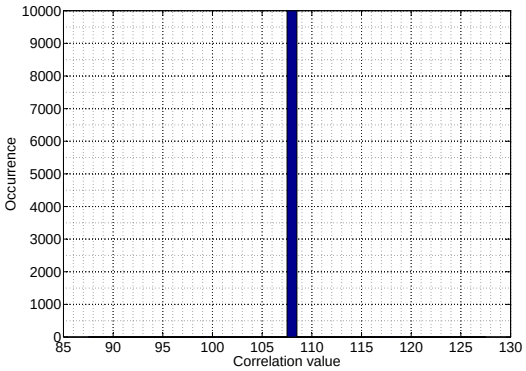

(b) Correlation value distribution on branch 3

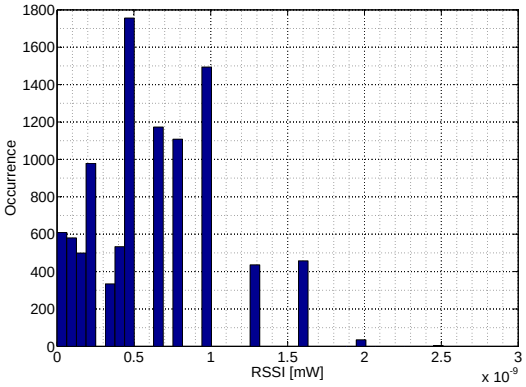

(c) RSSI distribution on branch 4

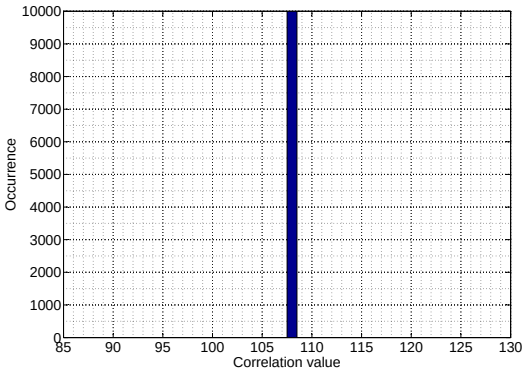

(d) Correlation value distribution on branch 4

Figure 6.6: Channel parameter distributions

Once again, the RSSI values are very differently distributed compared to the corresponding correlation values. The correlation values in both branch 3 and 4 are constant and equal to

108. This is interesting since branch 4 had a constant value of 107 in the NLOS test presented in previous section. This possibly implies time variation in the test setup due to movement of the equipment. Differences due to the multipath environment should be averaged out when performing testing as described in section 5.4.3. As such, the differences seen in correlation values on branch 4 in the two tests should not occur. This fact strengthens the suspicion regarding variations in the test equipment.

As can be seen from figure 6.6, the received RSSI values differ quite much from the ones observed in figure 6.3. This corresponds well with the MLE for the Gamma distribution parameters given in table 6.4. Using equation (3.24) and the MLE values for m for branch 3 and 4 yield K-values of approximately 1.8 and 1.47, respectively. These K-values indicate a LOS environment with the presence of a stronger multipath component. Further, the RSSI distribution for the different branches differ quite much, as seen from table 6.4. Branch 2 has a K-value nearly equal to 0.

Table 6.4: MLE for Gamma distribution parameters

Branch	m			$\frac{\overline{\Omega}}{m}$		
	MLE	Confidence Interval		MLE	Confidence Interval	
1	1.1483	1.1203	1.1770	8.9725e-011	8.7009e-011	9.2525e-011
2	1.0560	1.0304	1.0822	8.6561e-011	8.3913e-011	8.9292e-011
3	1.7138	1.6707	1.7581	1.9410e-010	1.8845e-010	1.9992e-010
4	1.4776	1.4408	1.5153	4.0788e-010	3.9586e-010	4.2027e-010

Using the MLE values, the mean RSSI in the channels vary from -70.39 dBm to -62.2 dBm. Even though this particular measurement was taken with a clear LOS, the highly reflective multipath environment caused the RSSI distributions not to really reflect this fact. In general, as the separation between TX and RX increased in the garage, the environment resembled more and more the NLOS environment in section 6.1.1. What is particular interesting with this measurement is the large difference in RSSI distribution between branch 2 and 3, only separated by 0.5λ. This makes an example of the problems estimating Gamma distribution parameters this way, since these are expected to be the same between branches when using the test methodology outlined in section 5.4.3.

6.1.2.3 Packet Error Dependencies

Packet errors among the 10.000 packets transmitted to branch 3 and 4 were distributed between RSSI and correlation values as showed in figure 6.7

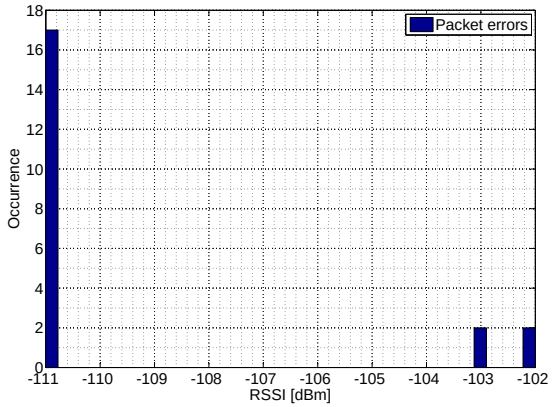

(a) Packet error as function of RSSI, branch 3

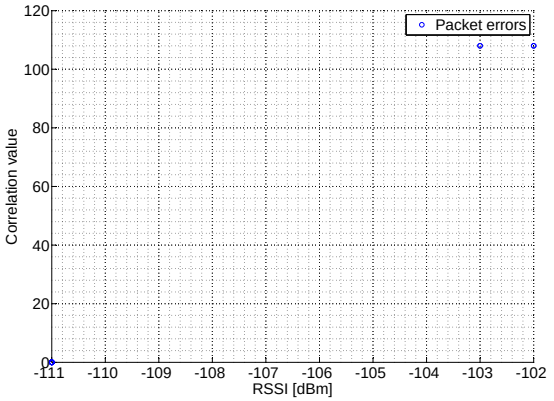

(b) Packet error as function of RSSI and correlation, branch 3

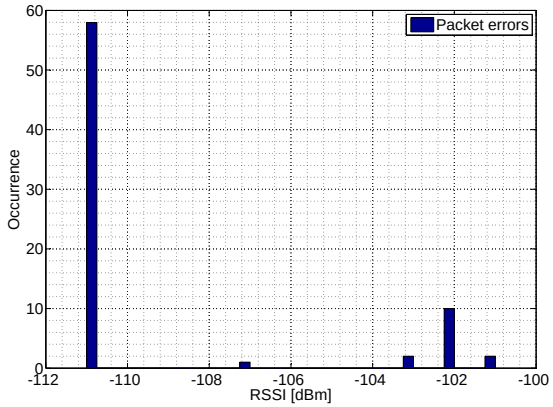

(c) Packet error as function of RSSI, branch 4

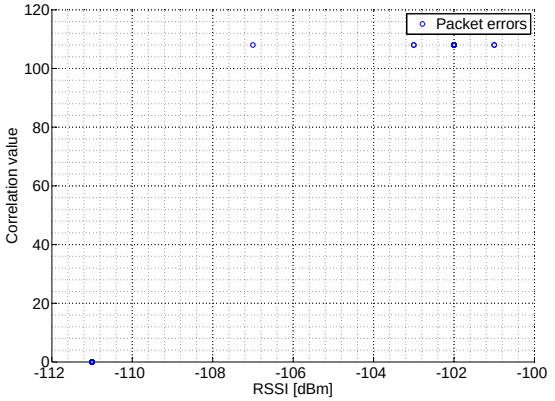

(d) Packet error as function of RSSI and correlation, branch 4

Figure 6.7: Packet error dependencies LOS

The amount of undetected packets once again dominates the composition of PER and all the erroneously demodulated packets are reported having a constant correlation value of 108. Using the MLEs for branch 3 and 4, the average RSSI values are -64.78 dBm and -62.20 dBm, respectively. Erroneously demodulated packets are not distributed around the mean RSSI in the branches and occur for very low RSSI values.

From figure 6.7 it is also seen that branch 3 experience a less amount of undetected packets than branch 4. This could be connected to the higher value of K in this branch which in theory would give lower probability of fading dips. However, K is affected by the amount of lost packets, so this reasoning is subject to errors.

6.1.3 Static RX and TX

Situations where both TX and RX remain static while the environment is characterized by slow movement or bursts of movement are likely to be encountered in the areas of application for this PHY. This section presents a sample of such a scenario taken in the main cafeteria at Forskningsparken. The test were conducted with no LOS. The channel parameters from branch 2 were lost due to some technical problems encountered at the end of the project. As such, only channel parameters for the remaining branches are showed. Since the measurement methodology described in section 5.4.3 is not used, different RSSI distributions on the branches are quite probable. As such, the distribution estimation presented in this section can, with higher confidence, be used to analyze differences between branches. The higher confidence is due to expected differences in branch distributions.

6.1.3.1 RSSI Dynamics

Two figures showing how the RSSI varies with time are given below. Figure 6.8 shows the entire lapse of the test, while figure 6.9 displays a segment of figure 6.8.

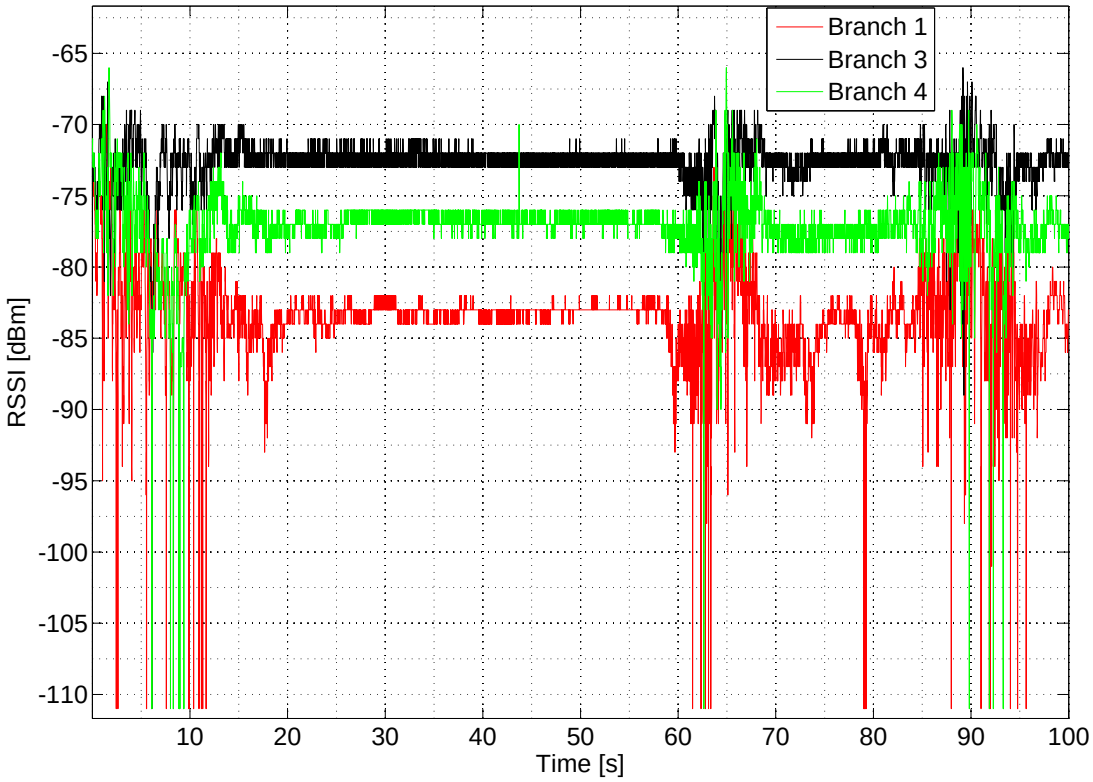

Figure 6.8: Static RSSI measurements for the entire lapse of transmission

This plot is highly different from similar plots given in figures 6.2 and 6.5. As can be seen, the RSSI levels on all three branches remain somewhat constant over a large period of time while periods of variations occur simultaneously due to movements in the environment. During this test, the only movements registered by the student were two moving elevators in addition to the student walking around slowly. Even though RX and TX remain static, the environment is still a multipath environment. This is easily seen by the different mean RSSI between the branches. The separation of 1.0λ between antenna 1 and 3 resulted in a difference of approximately 10 dBm in this case, while the the separation between antenna 4 and 3 yielded a difference of

approximately 5 dBm. By looking at figure 6.8, there is, however, reasons to believe that the branches have different RSSI distributions as well as different means. Branch 1 experiences more variations than the other two. These variations lead to loss of packets at time 79 seconds while branch 3 and 4 are unaffected by whatever caused these variations. Figure 6.9 displays a period of apparent variations.

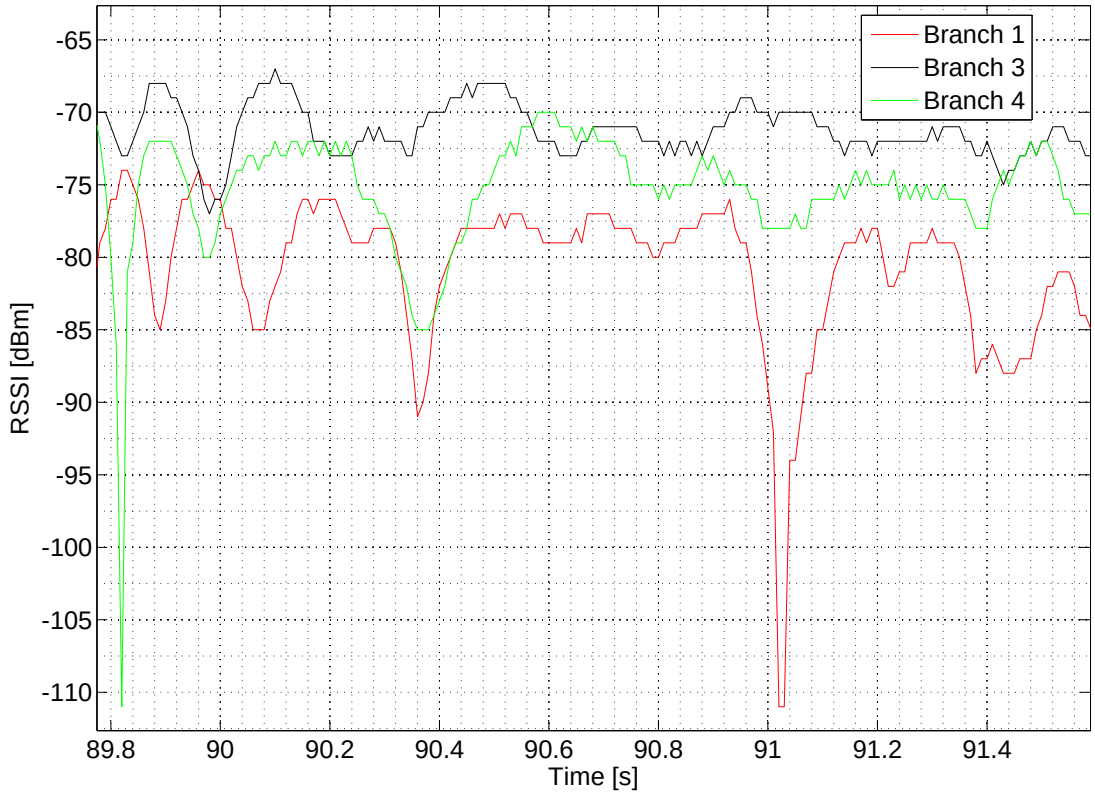

Figure 6.9: Segment of static RSSI measurement

As seen from this segment, branch 3 does not really vary significantly in terms of RSSI, while both branch 1 and 4 experience packet loss and more RSSI variation. The RSSI on branch 1 is subject to greatest variation. This example is very interesting when considering fading mitigation in such scenarios, which might be very typical in for example metering applications, where RX and TX are static. An implementation of PPS with any of these branches as input would have provided reduction in PER. In the extreme case with branch 1 and 3 as inputs, a great reduction could have been provided. This is an important observation since PPS is the cheapest form of fading mitigation. This is easily visualized by looking at figure 6.8 where RSSI values of -111 dBm corresponds to undetected packets. As seen, branch 1 experience many undetected packets. If PPS is configured to use branch 1 from the start, many lost packets might occur. However, when having erroneously demodulated a packet PPS might switch to branch 3 which in this example experienced only one undetected packet. The latter is not seen from this figure. As such, a great reduction in PER is achieved since branch 1 is used at minimal. The envelope covariance between the branches is presented in table 6.5.

The important observation from this table is that branch 3 is nearly uncorrelated with branch 1 while being little correlated with branch 4. Statistical envelope covariance between branches as function of antenna separation is not possible to determine for this type of measurement setting in general. For this particular case though, envelope covariance is decreasing with increasing separation.

Table 6.5: Envelope covariance between branches

	Branch 1	Branch 3	Branch 4
Branch 1	1	-0.0247	0.3985
Branch 3	-0.0247	1	0.1399
Branch 4	0.3985	0.1399	1

6.1.3.2 Channel Parameter Distributions

A histogram of the received RSSI[mW] and correlation values on branch 1 and 4 during this test are given in figure 6.10, while corresponding values for branch 3 are showed in figure 6.11.

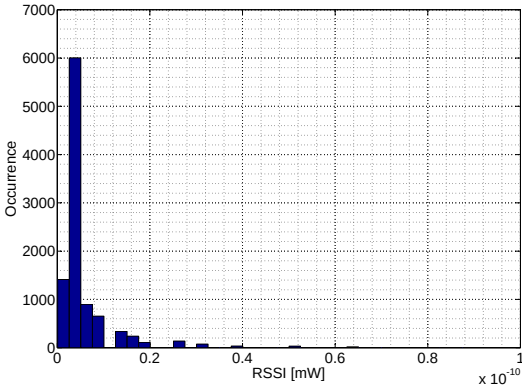

(a) RSSI distribution, branch 1

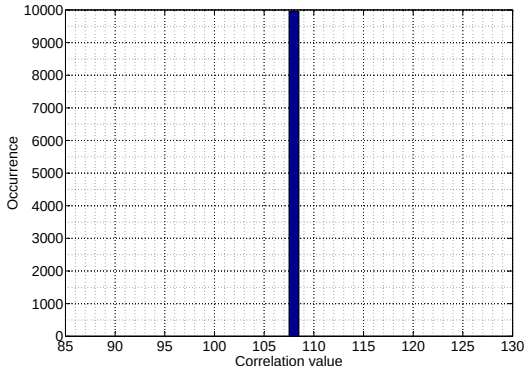

(b) Correlation value distribution, branch 1

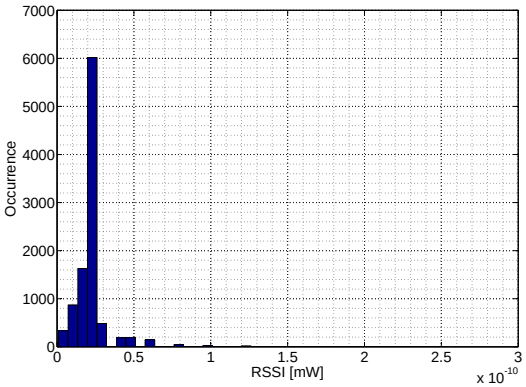

(c) Correlation value distribution, branch 4

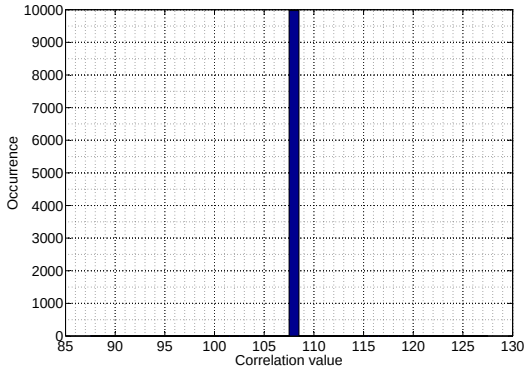

(d) Correlation value distribution, branch 4

Figure 6.10: Channel parameter distributions

The distributions of correlation values are once again constant end equal, while the corresponding RSSI distributions are different. The difference in mean RSSI corresponds to what can be observed in figure 6.8.

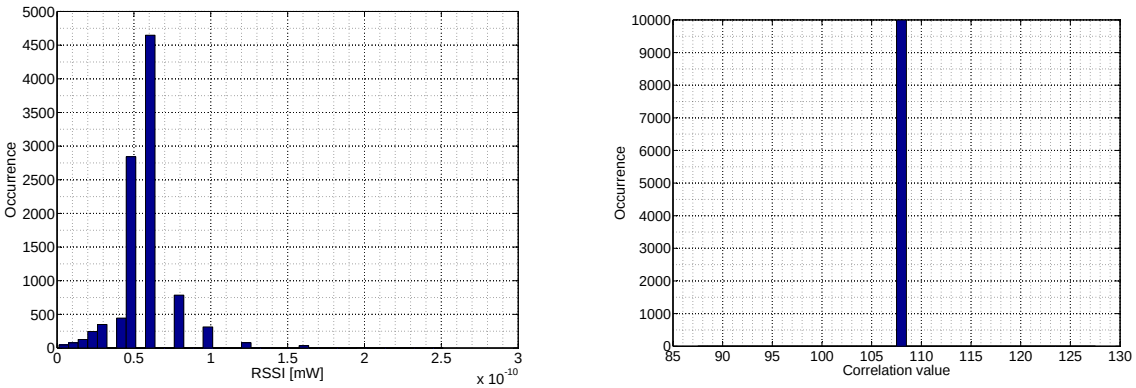

(a) RSSI distribution, branch 3

(b) Correlation value distribution, branch 3

Figure 6.11: Channel parameter distributions

Figure 6.11 reveals a very different RSSI distribution than earlier encountered for both the LOS and NLOS environments. The presence of a strong multipath component is obvious. The distribution of RSSI in figure 6.11 is more accurate than the ones in figure 6.10, since only one lost packet was associated with branch 3. The correlation values for branch 3 are the same as the ones for branch 1 and 4. Table 6.6 presents the Gamma distribution parameters.

Table 6.6: MLE for fit to Gamma distribution

Branch	m			$\frac{\overline{\Omega}}{m}$		
	MLE	Confidence Interval		MLE	Confidence Interval	
1	2.0923	2.0389	2.1471	2.9552e-012	2.8702e-012	3.0428e-012
3	8.9600	8.7194	9.2073	6.5241e-012	6.3440e-012	6.7093e-012
4	4.6098	4.4878	4.7350	4.8252e-012	4.6905e-012	4.9639e-012

The MLE values for m confirms the suspicion regarding different RSSI distributions. As noted earlier, branch 3 possessed less variation than the other two. From table 6.6 this is confirmed by a high value for m which translates to a K-value of 16.4. The deterministic component in this branch is therefore less affected by the remaining multipath power present during times of RSSI variation. Using the MLE values, the mean RSSI values varies from -82.08 dBm to -72.33 dBm.

6.1.3.3 Packet Error Dependencies

Branch 3 correctly received all packets except for one which was undetected. Packet error dependencies for branch 1 and 4 are shown figure 6.12.

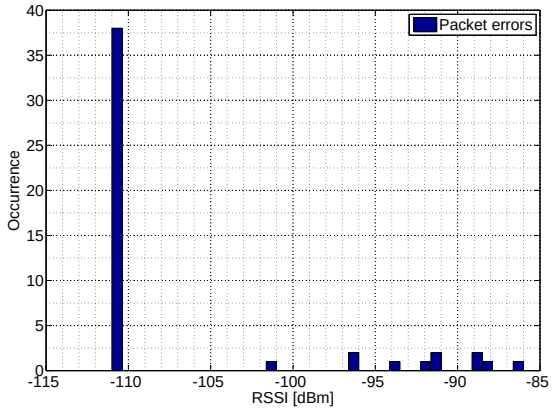

(a) Packet error as function of RSSI, branch 1

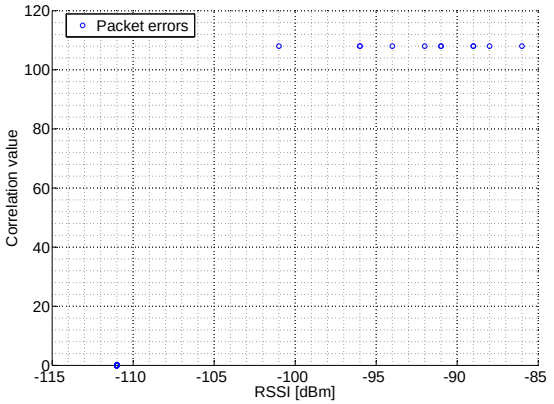

(b) Packet error as function of RSSI and correlation, branch 1

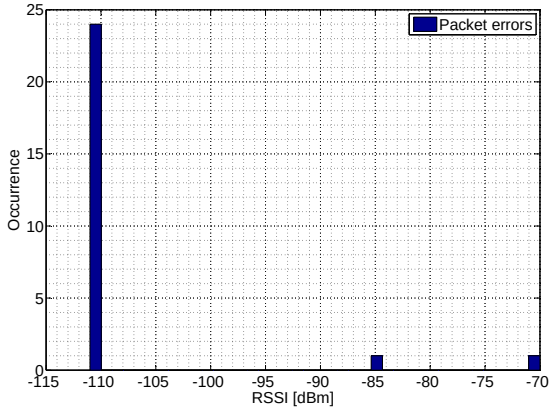

(c) Packet error as function of RSSI, branch 4

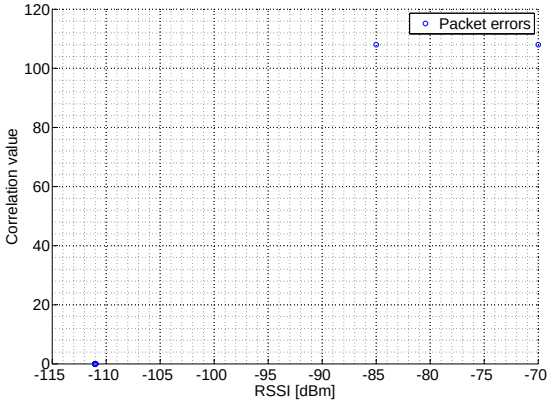

(d) Packet error as function of RSSI and correlation, branch 4

Figure 6.12: Packet error dependencies static RX/TX

As noted in previous tests, the correlation values remain constant in erroneously demodulated packets. Once again, undetected packets constitute the major part of PER. Using the MLEs for branch 1 and 4, the average RSSI values are -82.08 dBm and -76.53 dBm, respectively. The erroneously demodulated packets are not distributed around the mean on branch 1. Due to few erroneously demodulated packets, error distribution around the mean RSSI cannot be stated for branch 4 either, even though errors occur around the mean.

6.1.4 FPGA Setup, Office Environment

This section provides results on measurements conducted according to the methodology outlined in section 5.4.3 using the FPGA platform to receive packets. Due to the complications described in section 5.3.1.2, data is available for analysis from one branch only. All measurements resulted in many undetected or erroneously demodulated packets due to both multipath propagation as well as problems regarding the ADC interface. This amount of lost packets were far higher than for the Packet Sniffer implementation. Due to this, RSSI distribution estimates will not be given.

6.1.4.1 RSSI Dynamics

Figure 6.13 shows an error free sequence of RSSI values reported by the FPGA platform. Sequences of this length, corresponding to a movement of approximately 10λ, were hard to find among the data collected due to the frequent occurrence of undetected packets.

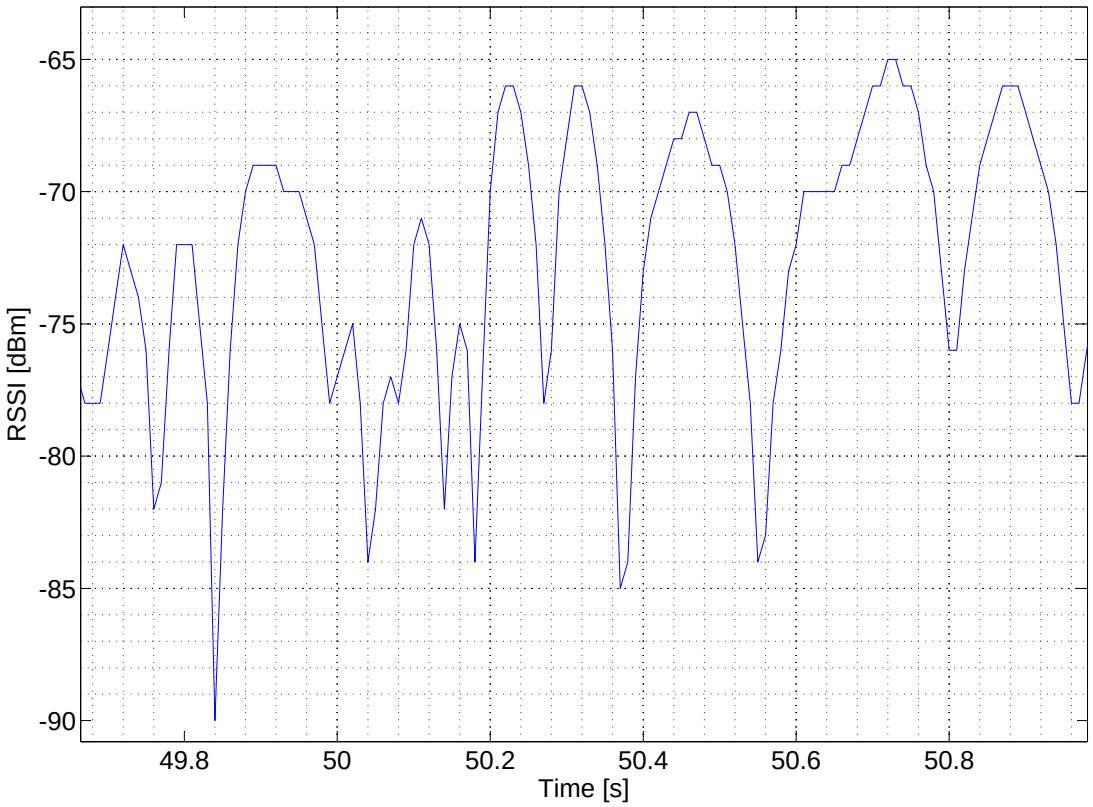

Figure 6.13: RSSI measurement made by the FPGA platform corresponding to approximately 10λ movement

The RSSI values were computed as given in section 5.1.1, and are hence comparable to values reported by the Packet Sniffer implementation. The time duration between the vertical lines correspond to the time required to receive 4 packets. As mentioned earlier, the targeted speed in the dynamic measurements was 1 ms^{-1}. This implies that the time duration between the vertical lines equal a distance of approximately 1/3 λ. As can be seen from this figure, the reported RSSI values were subject to frequent and large variations which could be caused by multipath fading. Similar variations in the simulated instantaneous SNR are observed in figure 4.2 for two Rayleigh fading channels. It is, however, not important that the example given in figure 4.2 represents the instantaneous SNR. It could represent any correlated sequence

of exponential distributed variables, such as the received power given by equation (3.23). The large variations can hence be supported by fading channel theory, even though the variation seen in figure 6.13 is very fast. There is, however, great uncertainty in this sequence of RSSI values due to the problems described in section 5.3.1.2. As such, the time variation seen may have been influenced by those problems as well.

6.1.4.2 Correlation Value Distribution

Even though the correlation values reported by the FPGA platform were averaged the same way as the ones reported by CC2520, large differences were seen. A histogram showing the distribution of the reported correlation values are given below.

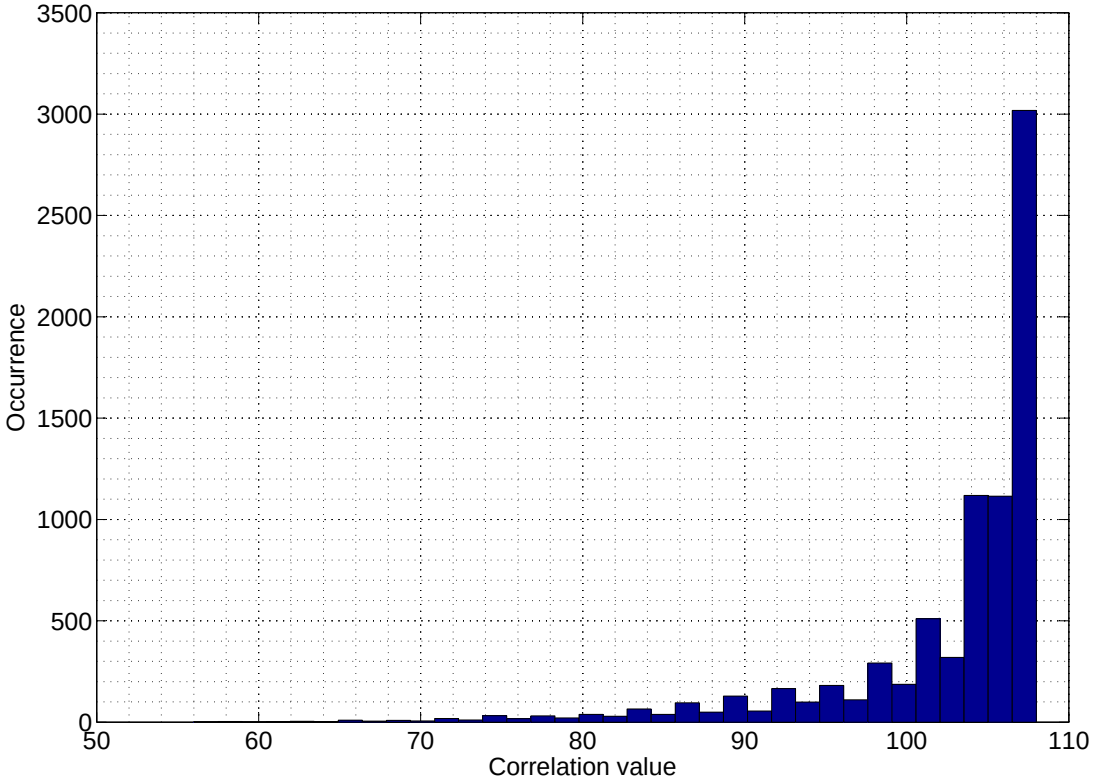

Figure 6.14: Correlation values reported by the FPGA platform corresponding to approximately 10λ movement

This histogram is very different from other histograms of correlation values given earlier. There is a span in the reported values that actually suits the description in section 5.1.2 quite well. However, if considering the Packet Sniffer implementation as an error free physical data source, the correlation value distribution in figure 6.14 displays some of the problems regarding the FPGA implementation described in section 5.3.1.2.

6.1.4.3 Packet Error Dependancies

This section will present examples on packet error dependencies for detected but erroneously demodulated packets.

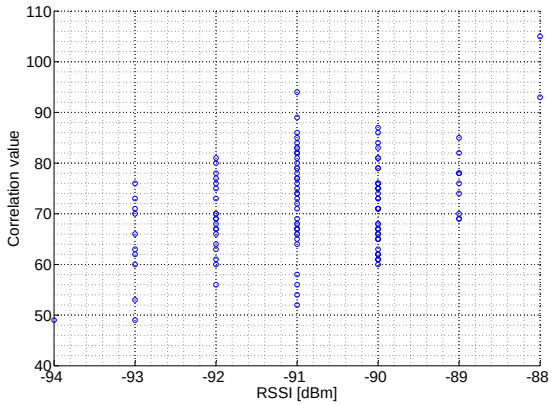

(a) Erroneously demodulated packets as function of RSSI and correlation

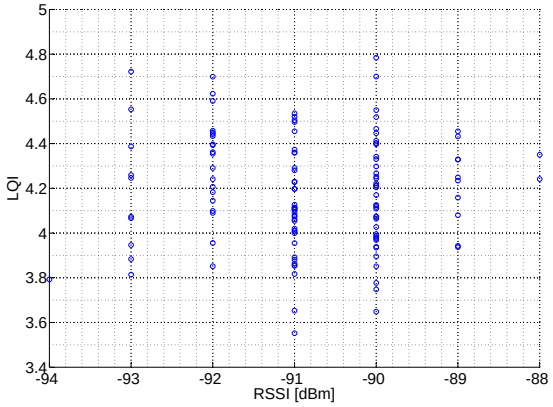

(b) Erroneously demodulated packets as function of RSSI and LQI

Figure 6.15: Erroneously demodulated packets as function of correlation and LQI values with fixed RSSI

As observed in the sections dealing with packet error dependencies earlier in this chapter, erroneously demodulated packets occur for low values of RSSI. There is, however, an underlying difference in these data that are not visible in the scatter plots. The RSSI values were in general much lower than what the Packet Sniffer implementation reported in the same measurement ranges. The errors are also shown varying over a range of correlation values. This is very different to the earlier made observations on packet error dependencies. Figure 6.15b also shows that packet errors are distributed over a range of LQI values. The mean LQI value in the data set, from which these results were generated, was 3.87. As seen from figure 6.15b, errors mostly occur above the mean LQI value. By analyzing the data collected with the FPGA platform, mean LQI values were all below 4 while the majority of the errors occurred above a LQI value of 4. These observations indicate that LQI might suit well as an argument for fading mitigation algorithms. It is, however, important to note that this observation is made on data obtained by using a hardware platform that did not perform satisfyingly.

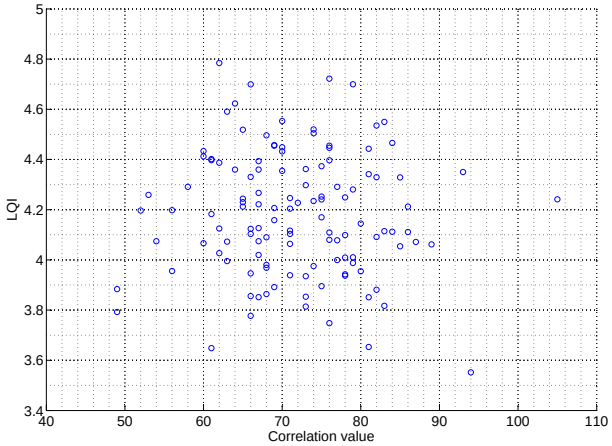

Figure 6.16: Erroneously demodulated packets as function of correlation and LQI

6.2 Performance Improvements

This section will analyze the performance improvements provided by a selection of the algorithms outlined in section 5.3.3 when applied to the four test environments described in section 5.4.3. The failing applicability of the correlation value as an argument for fading mitigation algorithms will first be used to reduce the algorithms subject to testing. SSC results will be presented as if SSC was implemented with one receiver chain, two antennas and a RF-switch. The problems regarding switching during packet reception as described in section 4.3.3.1 will be neglected. As such, the results provide an upper bound for what to expect from such an implementation. The channel arrays used to generate results were subject to absolutely minimal address filtering, as described in section 5.3.2. As such, they provide as much data as possible. Further, it has been verified that the data in the channel parameter arrays are synchronized.

Results on performance increases obtained by using the selected algorithms are presented as in section 4.5. There is, however, a distinct difference in how they should be interpreted. The simulation results on PER were provided for a range of average SNR values given the same fading channel statistics. As such, diversity gain and reduced PER could be calculated as explained in section 4.2.1. As noted in previous sections of this chapter the fading channels experienced during different measurements taken in one of the four environments are not likely to be the same. As such, it would be wrong to classify a potential diversity gain in a general case since different fading channels are mixed. The difficulties of performing such a classification becomes even worse when dealing with a limited data set, due to both issues regarding the confidence of the results and the number of tests conducted. In some cases though, it is possible to make some assumptions and approximate diversity gain. This can be done for tests that are close in mean RSSI and share the same tendencies with respect to channel statistics. Such determined diversity gains are, however, subject to uncertainties. An example of such diversity gain will be given.

The problems involving determination of obtainable diversity gain does not really matter that much. The algorithms can still be evaluated for the different tests in terms of the reduction they provide in PER. This reduction is connected to diversity gain. As such, proven reduction in PER maps to diversity gain, even though it is hard to establish the latter with confidence. Still, the data set is not big enough to evaluate reduction in PER as accurate as was done in section 4.5. However, different fading channels are not mixed when analyzing PER, hence yielding higher fidelity in discussions. Results on PER will be given graphically as function of RSSI, since this is the only variable parameter available. Results corresponding to an antenna separation of 0.5 and 1.0λ will be given. The results will not all be given with short comments. Results from the first environment tested will be commented to provide means on how to understand subsequent results. Key observations will be summarized in section 6.2.6.

6.2.1 Algorithms Subject to Test

The observations regarding the correlation values in previous sections of this chapter can be used to reduce the set of algorithms subject to test. Assuming a SC scheme where selection is based on correlation values alone will in the case of two branches with constantly different correlation values imply no diversity gain, since the same branch is selected at all times. As such, algorithm number 4 in section 5.3.3 is disregarded. If the selection is performed as algorithm number 2, there will be no diversity gain in the case of two branches with unequal correlation values. In the case of equal correlation values, decisions are based on RSSI which reduces algorithm number 2 to algorithm number 5. Since branches are observed having constant and unequal correlation values, algorithm number 3 cannot be reduced. The chosen realization of SSC and the correlation value properties reduce the SSC algorithms in a similar way to be evaluated for

number 7. PPS cannot be reduced. As such, 5 algorithms are subject to test. These are

- 1 - Double Receiver
- 3 - SC - Choose highest RSSI. If equal, choose highest correlation. If equal, keep current diversity branch.
- 5 - SC - Choose highest RSSI. If equal, keep current branch.
- 6 - PPS - If packet was received with errors, receive the next packet on the other branch.
- 7 - SSC - Switch to other branch if RSSI is under given threshold value.

The earlier described problems of selecting an appropriate RSSI switching threshold will be assessed by using 5 different and constant switching thresholds for all environments. These switching thresholds are -100 dBm, -95 dBm, -90 dBm, -85 dBm and -80 dBm and covers the span of RSSI values where most of the erroneously demodulated packets have occurred. It was impractical to label all the points corresponding to different RSSI switching thresholds. As such, the color order is (-100 dBm, black), (-95 dBm, blue), (-90 dBm, green), (-85 dBm, red) and (-80 dBm, cyan) and the symbol used is the Matlab triangle. They are plotted in the same order.

6.2.2 Forskningsparken, Main Cafeteria NLOS

Figure 6.17 shows the results obtained in the specified environment for an antenna separation of 0.5λ while figure 6.18 shows corresponding results for an antenna separation of 1.0λ.

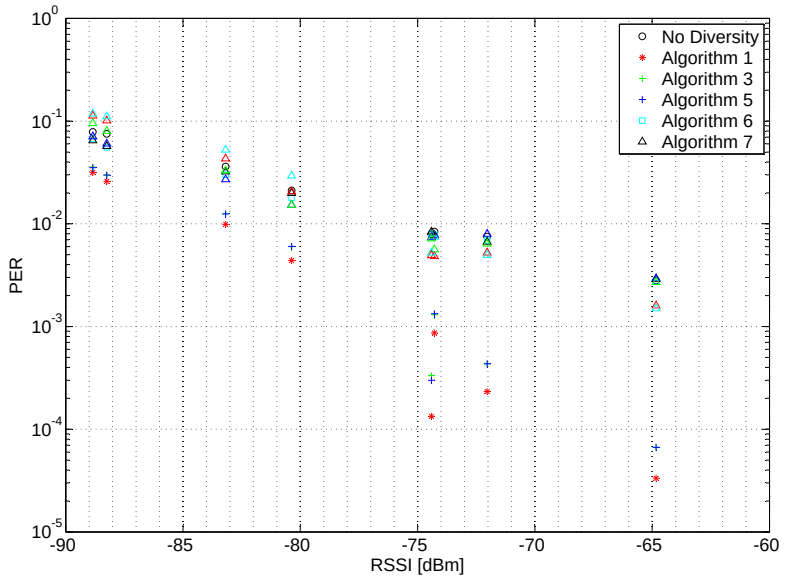

Figure 6.17: Measured PER curves at Forskningsparken, main cafeteria NLOS, antenna separation = 0.5λ

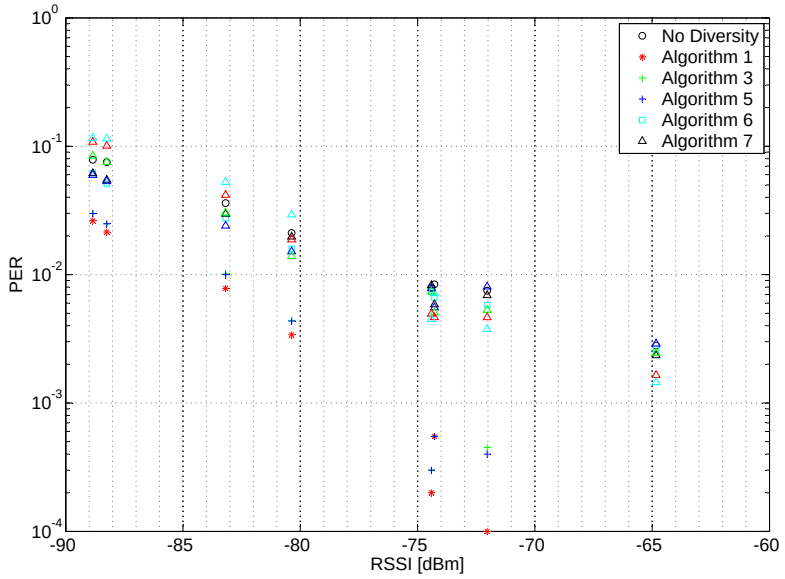

Figure 6.18: Measured PER curves at Forskningsparken, main cafeteria NLOS, antenna separation = 1.0λ

6.2.2.1 Comments

All the tests conducted in this environment are represented by symbols along a vertical line. The symbols represents the PER associated with a given algorithm. Even though these two figures display results generated from a limited set of data, they show a clear pattern. It is tempting to compare figure 6.17 with results from section 4.5. However, a closer investigation shows that the test conducted with a RSSI mean of -74.5 dBm deviates much from the pattern. This deviation is most likely a function of different fading channel statistics and perhaps a limited data set. As such, the difficulties regarding determination of diversity gain is visualized. However, in this environment it's possible to make a somewhat qualified determination of diversity gain by considering the tests with a mean RSSI of less than -80 dBm. As seen from both figures, these tests seem to share nearly the same channel statistics. Being aware of the uncertainty introduced, it seems that a diversity gain of a little less than 10 dB is achieved by using the double receiver or SC algorithms.

As explained earlier in section 6.2, evaluating reduction in PER provides more fidelity in the discussion of the results than qualified guesses on diversity gain. Considering the PER reported for the double receiver and the SC algorithms reveal results approximately analogous to what was reported by simulation results in section 4.5. The double receiver generally provides greater reduction in PER than the SC algorithms, but not as much as was predicted. By comparing the two figures it is also seen that PER is reduced if using an antenna separation of 1.0λ instead of 0.5λ. In fact, the test with a mean RSSI of approximately -65 dBm reports a PER equal to zero for both the double receiver and the SC algorithms.

For an antenna separation of 0.5λ the PPS algorithm performs somewhat identical to the case of no diversity. An antenna separation of 1.0λ yields slightly better results. The small performance increase is expected from the results presented in section 4.5, where the same packet rate was used.

The SSC algorithms using different thresholds perform close to a case of no diversity reception. A slight increase in performance is seen by using an antenna separation of 1.0λ instead of 0.5λ for low mean RSSI values. Further, low RSSI thresholds provide greater reduction in PER than higher threshold values at low mean RSSI values. At higher mean RSSI values, higher threshold values perform better than the lower.

6.2.3 Forskningsparken, Main Cafeteria LOS

Figure 6.19 shows the results obtained in the specified environment for an antenna separation of 0.5λ while figure 6.20 shows corresponding results for an antenna separation of 1.0λ.

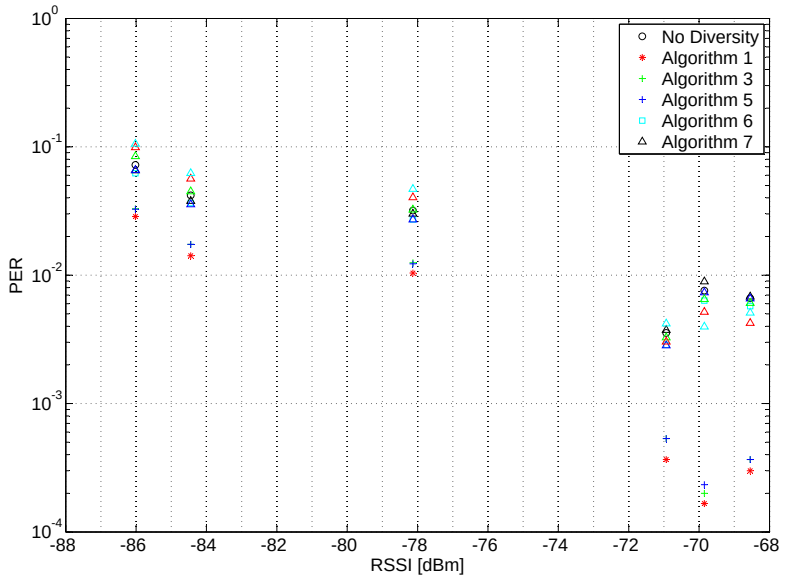

Figure 6.19: Measured PER curves at Forskningsparken, main cafeteria LOS, antenna separation = 0.5λ

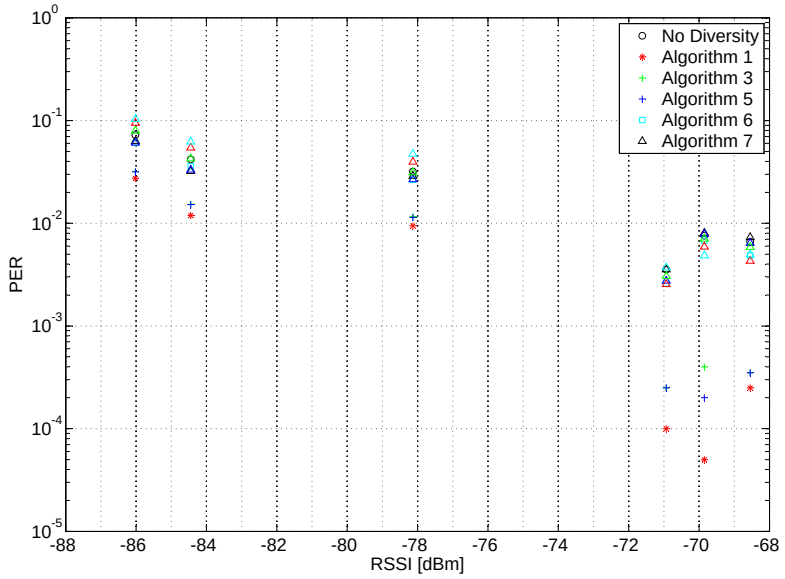

Figure 6.20: Measured PER curves at Forskningsparken, main cafeteria LOS, antenna separation = 1.0λ

6.2.4 Rikshospitalet, Garage House NLOS

Figure 6.21 shows the results obtained in the specified environment for an antenna separation of 0.5λ while figure 6.22 shows corresponding results for an antenna separation of 1.0λ.

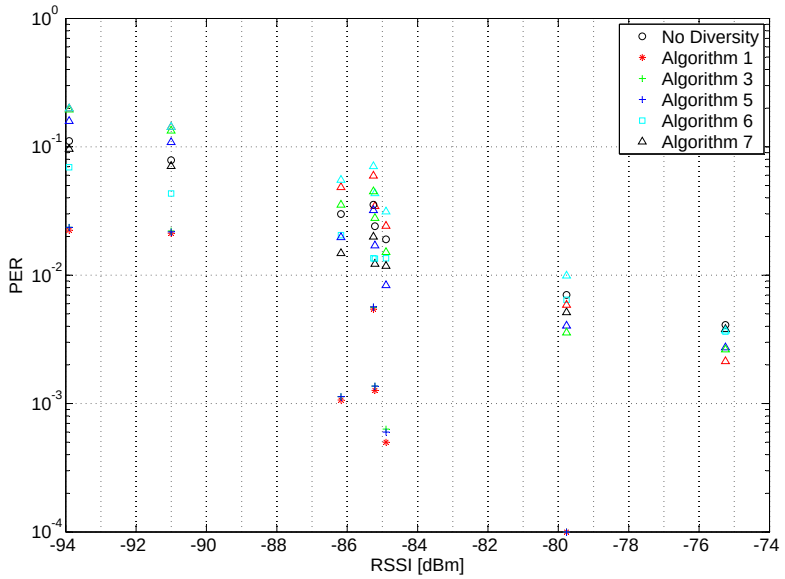

Figure 6.21: Measured PER curves at Rikshospitalet, garage house NLOS, antenna separation = 0.5λ

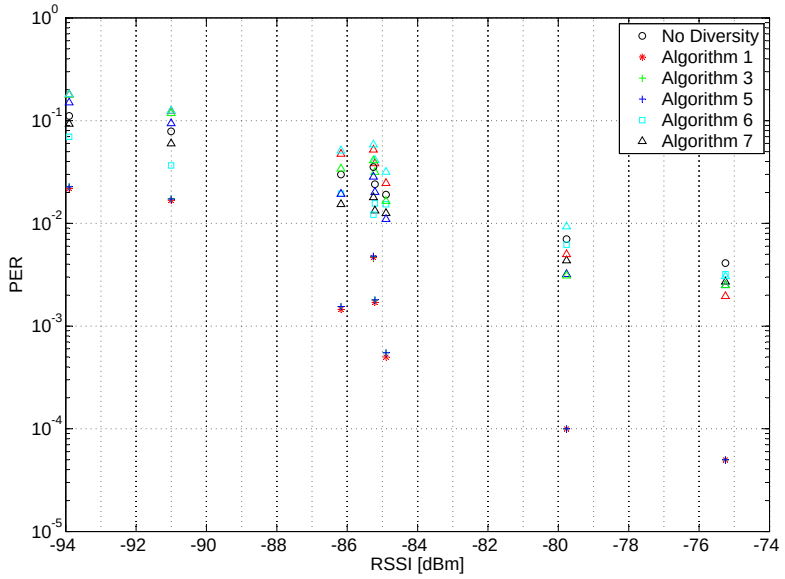

Figure 6.22: Measured PER curves at Rikshospitalet, garage house NLOS, antenna separation = 1.0λ

6.2.5 Rikshospitalet, Garage House LOS

Figure 6.23 shows the results obtained in the specified environment for an antenna separation of 0.5λ while figure 6.24 shows corresponding results for an antenna separation of 1.0λ.

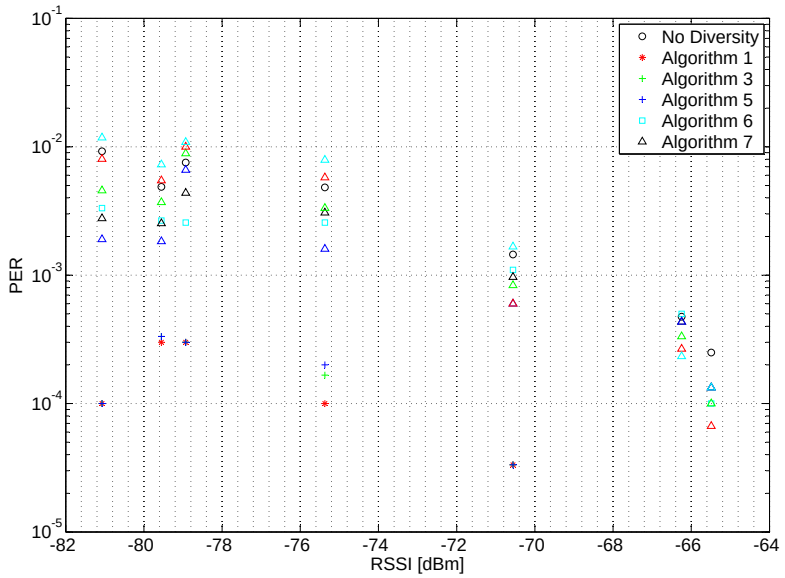

Figure 6.23: Measured PER curves at Rikshospitalet, garage house LOS, antenna separation = 0.5λ

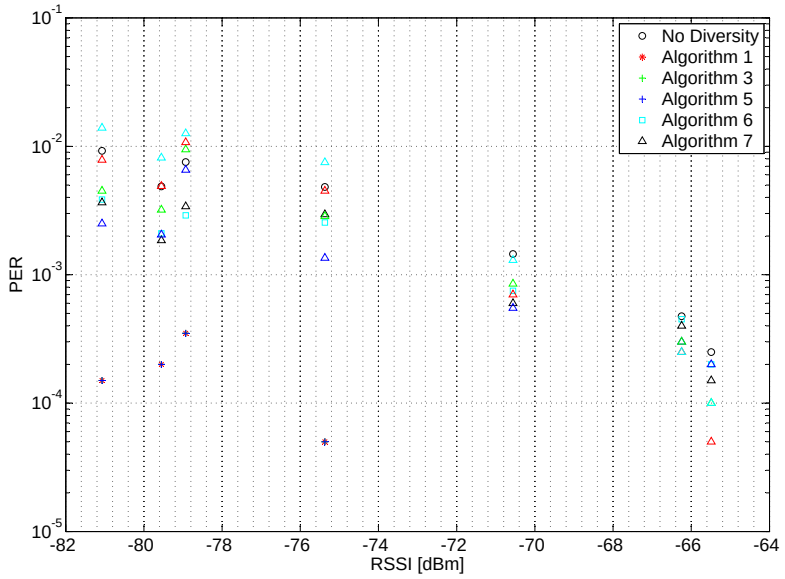

Figure 6.24: Measured PER curves at Rikshospitalet, garage house LOS, antenna separation = 1.0λ

6.2.6 Key Observations

By observing the results presented in figures 6.19 to 6.24, it is clear that a confident determination of obtainable diversity gain for the different environments is not possible due to different fading channel statistics and the uncertainty induced by a limited data set.

The reduction in PER provided by the double receiver and the SC algorithms is, however, easy to verify. This reduction in PER generally increases as RSSI increases with few exceptions. These exceptions are likely caused by the same two factors mentioned above. In most of the cases, the SC algorithms provide a reduction in PER close or equal to what is provided by the double receiver. Depending on environment and fading channel statistics, PER is reduced in the tests, independently of antenna separation, by a factor between approximately 2 to 100 by use of any of these algorithms.

The PPS algorithm provides greater reduction in PER for the environments encountered in the garage house at Rikshospitalet than the environments in Forskningsparken. This reduction in PER is somewhat larger than what was provided by simulation results for the same packet rate given in section 4.5. This might imply longer coherence time in the fading channels that were encountered in this type of environment compared to the fading channels encountered at Forskningsparken. The reduction in PER provided by PPS collapses as average RSSI increases. This is analogous to the simulation results provided in section 4.5, which showed the same behavior.

As can be seen from all the figures, the SSC algorithm based on different RSSI thresholds perform unpredictable. Generally, at lower average RSSI values SSC does not provide much performance increase. In fact, SSC might perform worse than not trying to mitigate fading at all. When average RSSI increases SSC tends to perform better but does not guarantee better performance than the no diversity case. The performance of the different RSSI thresholds are somewhat analogous to what was presented in chapter 4, where different SNR thresholds gave optimum diversity gain for different average SNR values. Low RSSI threshold values give greater reduction in PER for low average RSSI values, whereas higher threshold values yield the greatest reduction for higher average RSSI values. The largest reductions in PER given by SSC occur in figures 6.23 and 6.24, where PER in some cases is reduced by a factor of approximately 5. The garage house LOS environment provides as such an exception in the generally bad performance provided by SSC. This can be a function of more detected packets in this environment.

Comparison of test results obtained by the two antenna separations are troublesome. This is very nicely captured by comparing figures 6.21 and 6.22 to the others. Generally, there is a reduction in PER when comparing an antenna separation of 1.0λ to a separation of 0.5λ. This tendency is, however, strongly violated in some of the tests given in figures 6.21 and 6.22. Packet errors are actually induced when using an antenna separation of 1.0λ instead of 0.5λ. This behavior is caused by limitations of the data set, end will be interpreted in the discussion given in chapter 7.

Chapter 7

Discussion

7.1 Comparison Foundation

Before presenting the key observations obtained from the practical results, the assumptions made when theoretically evaluating the maximum obtainable diversity gain and corresponding reduction in PER for the PHY is revisited. The theory and simulations provided in chapter 4 gave promising results regarding diversity gain and reduction in PER given by various fading mitigation techniques. The underlying assumptions were a narrowbanded, flat fading channel that remained constant during packet reception and the use of an ideal estimator on radio link quality, the instantaneous SNR. The fading channel statistics were controlled and branches were uncorrelated. Further, all packets were assumed detected and a packet error only occurred when erroneously demodulated. As such, results were consistent and well established in theory while at the same time providing the maximum obtainable performance increase.

7.2 Algorithm Performance

When assessing the performance increase given by selected algorithms in section 6.2 using physical gathered data and non-ideal arguments for fading mitigation algorithms, results were not always analogous to what was expected from section 4.5. The SSC algorithm literally gave no reduction in PER in most of the environments tested when evaluated with different RSSI threshold values. In many tests an increase in PER was induced instead. SSC did, however, provide some reduction in PER in the LOS environment found in the garage house. SSC based on RSSI values has therefore been found very unpredictable and is in general disapproved. However, the SC algorithm always choosing the branch with the highest RSSI gave results equal or close to what a double receiver provided. As such, it seems that the RSSI value can successfully be used as an argument in SC. Both the double receiver and SC algorithms provided reductions in PER by a test-dependant factor between approximately 2 and 100, and can as such be regarded as successful fading mitigation algorithms. The least complex algorithm, PPS, provided reductions in PER in the garage house environment, but not the cafeteria environment at Forskningsparken. In most tests it performed equal or better than the SSC algorithm. Due to the different fading channel statistics observed between branches in static environments, PPS might have potential to provide greater reductions in PER in such situations by escaping the worst branch statistics. The difference in performance provided by the various algorithms is heavily colored by the large amount of undetected packets. The reduction in PER did generally increase with antenna separation but discrepancies regarding this trend was observed in figures 6.21 and 6.22.

7.3 Considerations On Observations

The following will discuss the results obtained and the confidence of the key observations given above. As explained earlier, time available to testing was heavily reduced due to problems in developing the FPGA platform. As a consequence, a limited data set of channel parameters were gathered with the Packet Sniffer implementation. As such, it is natural to start discussing the confidence of the results as a function of this.

7.3.1 Data Set Limitations

One of the most visible incidents where the limited data set affected the results was the discrepancy found in figures 6.21 and 6.22 regarding the trend in increasing reduction of PER as function of increasing antenna separation. These figures showed that PER increased when evaluated with an antenna separation of 1.0λ instead of 0.5λ. This incident exposed the limitations given by the data set, and the odd behavior observed in figures 6.21 and 6.22 can be explained by figure 7.1.

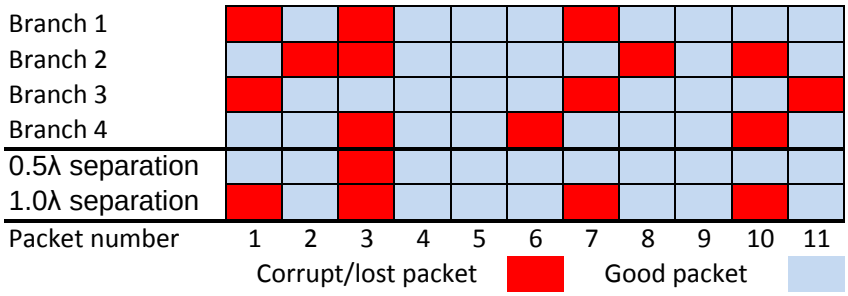

Figure 7.1: PER as function of antenna separation when data set limitations are exposed

The double receiver and SC algorithms have two signal branches as input. Packet errors occur if both branches have packet errors at the same time instants. When evaluating differences in PER as function of λ, the comparisons of branches are different. This is strongly exposed in figure 7.1 where comparisons for the 0.5λ case are made between branch 1 and 2, branch 2 and 3 and branch 3 and 4. When analyzing the 1.0λ case, comparisons are made between branch 1 and 3 and branch 2 and 4. In this example, a separation of 1.0λ yields more packet errors than a separation of 0.5λ. When using a small data set, situations like this are more probable to cause anomalies in the results. As such, the possible reduction in PER encountered when using a separation of 1.0λ instead of 0.5λ should not be emphasized too much. When considering an antenna separation of 0.5λ the accuracy of the reported PER is also higher than when considering an antenna separation of 1.0λ. This can also visualized by the above example. Noting that the 0.5λ separation is evaluated three times for the four signal branches, while the 1.0λ separation is evaluated only two times gives higher fidelity in the results provided for the 0.5λ separation. Thus, to classify reduction in PER, the 0.5λ measurements provide the best confidence. The earlier reported reductions in PER for the double receiver and SC algorithms are based on the 0.5λ separation.

The limited data set is also partly responsible for the differently estimated Gamma distribution parameters for the signal branches. When performing tests as outlined in section 5.4.3, all branches should experience the same distributions. However, another important factor contributing to these deviations is the hardware that was used. Since all packets were not detected, and the number of detected packets varied between branches, a different amount of low RSSI values were removed from the original sample distribution. As the number of undetected packets increase the validness of such distribution estimates decrease.

7.3.2 Uncertainties Induced By The RSSI

The uncertainties induced when performing both distribution estimation and covariance estimation between branches are explained in section 6.1 and will not be repeated here. This topic was placed in section 6.1 to provide a better understanding of what was about to be presented of results.

7.3.3 RSSI Dynamics

The examples on RSSI dynamics between the branches must be considered with reservation. As noted in section 5.1.1 this measure also contain interference, noise and effects of ISI. If neglecting these factors and considering the fading channels as narrowbanded, the observed RSSI variation is easily supported by statistical channel models. Similar and large variations in instantaneous SNR are depicted in figure 4.2 for the case of a Rayleigh fading channel with mean SNR equal to 10 dB. As such, figures showing RSSI dynamics supports the assumption of bad fading environments often found in indoor radio channels. The serious fading environment is also supported by estimated Gamma distributions, even though these possess uncertainty.

7.3.4 RSSI Distributions

As mentioned in section 7.3.1, the estimation of Gamma distribution parameters are troublesome due to many and unfortunate error sources coloring the estimates. However, when all packets were detected, the estimates provided stronger fidelity. By considering the histogram plots of RSSI given in section 6.1 and noting the relatively low amount of undetected packets in the packet error dependency subchapters, it is possible to make some key observations regarding the fading channel statistics experienced. Even though the RSSI samples used to make these figures are few, they show a tendency in the wide range of possibly different fading channel statistics experienced in indoor environments. In addition, the mean RSSI values in a static scenario have been shown differing by about 10 dBm while samples from the dynamic scenarios have shown greater differences in instantaneous RSSI between the branches, as in figure 6.2. These examples show the bad fading conditions often found in the indoor environments.

7.3.5 Packet Error Dependencies and Its' Algorithm Implications

Interesting to note about the packet error dependencies is the tendency of an increasing number of undetected packets with decreasing RSSI levels. This is, of course, very logical and not surprising. It does, however, give interesting conclusions when considered in relation to the different SSC implementations described in section 4.3.3.1 and the simulation results presented in 4.5. The analysis and simulation results were limited to a case where all packets were detected. As such, diversity gain was obtainable for low average SNR values. This gain was, however, dependant on the switching thresholds used. Failing to set an appropriate threshold could yield no diversity gain. Even though SNR cannot be mapped to RSSI or vice versa, the packet error dependencies in section 6.1 show that a large portion of PER can consist of undetected packets. This will hence decrease the obtainable diversity gain for SSC realized with one RF-front end and cause utterly inferiority with respect to SC and the double receiver. This might explain the behavior of SSC improving as average RSSI increases, since more packets are detected. The determination of a successful fixed switching threshold based on RSSI can be very difficult, if not impossible. The different thresholds used in section 6.2 provided variable PER as function of both mean RSSI and environment. This is analogous to the behavior of different fixed SNR-based thresholds in section 4.5. A RSSI threshold is, however, harder to determine

than a SNR threshold since the former contains a lot of unwanted effects, as described in section 5.1.1.

As such, there are mainly two reasons why the double receiver and SC algorithms outperform SSC. Firstly, the probability of detecting packets increases with two receiver chains. Secondly, the determination of a RSSI threshold is difficult and results by using such thresholds are unpredictable.

The performance of PPS was also affected by the relative big amount of undetected packets since a switch cannot be initiated if the packet is not detected. The PER results provided by PPS in figures 6.17 to 6.24 which correspond to a very dynamic environment will as such suffer from this in addition to the fact that branches were reported somewhat correlated. The latter will reduce the possible diversity gain by using PPS. The static scenario investigated in section 6.1.3 showed that PPS might provide great reductions in PER. This is, however, very dependant on the fading channel statistics associated with each branch and their covariance. Branches that have high positive covariance and approximately the same mean RSSI will most likely not benefit from PPS if PER mainly consists of undetected packets. In a similar way as with SSC, the simulation results provided in section 4.5 did not account for undetected packets. This is an another important factor to consider when reasoning about why results differed from theory.

7.3.6 FPGA Remarks

The FPGA platform provided great uncertainty in the data collected due to the problems described in section 5.3.1.2. The correlation values reported from this platform were very different from the ones reported from the Packet Sniffer implementation. If this platform had been used to evaluate obtainable performance increase, it would have provided very different results. Firstly, the number of undetected packets were much higher, which would imply smaller test ranges. As such, it would have been difficult to test various indoor environments at somewhat normal distances. Secondly, the distribution of correlation values would possibly have supported this value as argument for diversity combining. Even though erroneously demodulated packets were shown to mostly occur above a LQI value of 4, this property should be regarded as very uncertain due to the problems regarding the FPGA platform.

7.3.7 Future Work

As described earlier, problems regarding the development of the FPGA platform limited the time to conduct tests. To provide results with higher confidence, more tests should be conducted. The logical next step would be a physical implementation of PPS to further evaluate the performance improvement given by this algorithm, being the least complex algorithm studied.

Chapter 8

Conclusion

This thesis has investigated the obtainable performance increase associated with different fading mitigation techniques using spatial receiver diversity applied to the IEEE 802.15.4 2.4 GHz PHY. By using hardware from Texas Instruments, measurements were conducted in different indoor environments which conforms with the area of application for this wireless standard. Challenging fading environments have been observed with great differences in RSSI as function of λ. PER has been shown to mainly consist of undetected packets. The SSC algorithm using different RSSI thresholds and one RF-front end have as such been shown to perform somewhat equal to no diversity reception and is generally disapproved. PPS provided small reductions in PER in the dynamic environments encountered. PPS might, however, provide great reductions in PER in situations were RX and TX remain static and signal branches are little correlated and experience different mean RSSI values and distributions as function of λ. This is considered very likely from the observed data. In a general case, two RF-front ends are needed two predictably improve the quality of the radio link. Fading mitigation using a double receiver chain has been shown the most effective, while being closely approximated by a SC algorithm always choosing the antenna with the highest RSSI. These two approaches have reduced PER by a test-dependent factor between approximately 2 and 100. RSSI is hence approved as an argument in the SC algorithm. The close approximation of the double receiver chain given by the SC algorithm provides possible power reductions if two RF-front ends are used to synchronize with the preamble. If this is considered, more testing with different packets lengths should be conducted since reduction in PER also is a function of packet length. The results obtained in this thesis were obtained by using a PSDU length of 21 bytes.

Bibliography

[1] Mohamed-Slim Alouini. Switched diversity systems: Design, performance, and optimization. http://www.iet.ntnu.no/projects/beats/Documents/LoenAlouini.pdf, 2003.

[2] Kareem E. Baddour and Norman C. Beaulieu. Autoregressive modeling for fading channel simulation. http://ieeexplore.ieee.org/stamp/stamp.jsp?arnumber=01512123, 2005.

[3] ZigBee Alliance Bob Heile, Chairman. Zigbee alliance tutorial. http://www.zigbee.org/imwp/idms/popups/pop_download.asp?ContentID=6704, 2006.

[4] Robert K. Morrow David Patrick. *WiFi and BLUETOOTH COEXISTENCE*. McGraw-Hill Professional, 2004.

[5] Andrea Goldsmith. *Wireless Communications*. Cambridge University Press, 2005.

[6] P. Gorday. 802.15.4 multipath. https://mentor.ieee.org/802.15/dcn/04/15-04-0337-00-004b-802-15-4-multipath.ppt, 2004.

[7] Homayoun Hashemi. The indoor radio propagation channel. http://ieeexplore.ieee.org/stamp/stamp.jsp?tp=&arnumber=231342&isnumber=5980, 1993.

[8] Simon Haykin. *Communication Systems, 4th Edition*. John Wiley & Sons, INC, 2001.

[9] IEEE. Part 15.4: Wireless medium access control(mac) and physical layer (phy), specifications for low-rate wireless personal area networks (wpans). http://standards.ieee.org/getieee802/download/802.15.4-2006.pdf, 2006.

[10] Texas Instruments. Cc2520 datasheets. http://focus.ti.com/lit/ds/symlink/cc2520.pdf, 2007.

[11] Texas Instruments. Cc2530 evaluation module kit. http://focus.ti.com/docs/toolsw/folders/print/cc2530emk.html, 2009.

[12] Texas Instruments. Smartrf05 evaluation board user's guide. http://focus.ti.com/lit/ug/swru210/swru210.pdf, 2009.

[13] Texas Intruments. Smartrf^{TM} packet sniffer user manual, rev.1.9. http://focus.ti.com/lit/ug/swru187a/swru187a.pdf, 2005.

[14] Jennic. Co-existence of ieee 802.15.4 at 2.4 ghz application note. http://www.jennic.com/files/support_files/JN-AN-1079%20Coexistence%20of%20IEEE%20802.15.4%20In%20The%202.4GHz%20Band-1v0.pdf, 2008.

[15] Michel Daoud Yacoub José Cândido Silveira Santos Filho and Gustavo Fraidenraich. A simple accurate method for generating autocorrelated nakagami-m envelope sequences. http://ieeexplore.ieee.org/stamp/stamp.jsp?tp=&arnumber=4133906&isnumber=4133902, 2007.

[16] Jean-Paul M.G. Linnartz. Wireless communication reference website. http://wireless.per.nl/reference/chaptr03/2_4ghz.htm, 2004.

[17] Mohamed-Slim Alouini Marvin K. Simon. *Digital Communication over Fading Channels - A Unified Approach to Performance Analysis*. John Wiley & Sons, INC, 2000.

[18] MathWorks. gamfit. http://www.mathworks.com/access/helpdesk_r13/help/toolbox/stats/gamfit.html, 2009.

[19] F. Halsall P. Nobles. Delay spreads and received power measurements within a builing at 2ghz, 5ghz and 17 ghz. http://pdos.csail.mit.edu/decouto/papers/nobles97.pdf, 1997.

[20] Tadeusz A. Wysocki and Hans-Jürgen Zepernic. Characterization of the indoor radio propagation channel at 2.4 ghz. http://circuit.ucsd.edu/~curts/courses/ECE284_F05/references/Wys00.pdf, 2000.

[21] Kazunori Yokohata Yasutaka Ogawa and Kiyohiko Itoh. Spatial-domain path-diversity using an adaptive array for mobile communications. http://ieeexplore.ieee.org/stamp/stamp.jsp?arnumber=00497079, 2001.

Appendix

Appendix A

Inverted SC PDF

Deduction of the distribution of the instantaneous output SNR of a combiner that selects the minimum of two input instantaneous SNRs is provided for a Rayleigh fading channel in the following.

The two branches are assumed having equal SNR distributions. P() denotes cumulative distribution, while p denotes the PDF. To deduce the PDF of the inverted SC the cumulative distribution is first found as follows.

$$P(\gamma_{\sum} \leq \gamma) = 1 - P(\gamma_{\sum} \geq \gamma) \tag{A.1}$$

Assuming independent branches this becomes

$$\begin{aligned} P(\gamma_{\sum} \leq \gamma) &= 1 - (1 - P_{\gamma}(\gamma))^2 \\ &= 2P_{\gamma}(\gamma) - P_{\gamma}(\gamma)^2 \end{aligned} \tag{A.2}$$

Differentiating the equation gives the PDF

$$\begin{aligned} p_{\gamma_{\sum}}(\gamma) &= 2\frac{d}{d\gamma}P_{\gamma}(\gamma) - 2P_{\gamma}(\gamma)\frac{d}{d\gamma}P_{\gamma}(\gamma) \\ &= 2\frac{d}{d\gamma}P_{\gamma}(\gamma)\left(1 - P_{\gamma}(\gamma)\right) \\ &= 2p_{\gamma}(\gamma)\left(1 - P_{\gamma}(\gamma)\right) \end{aligned} \tag{A.3}$$

In a Rayliegh fading channel, the pdf of γ is exponential distributed

$$p_{\gamma,Rayleigh}(\gamma) = \frac{1}{\overline{\gamma}}e^{-\gamma/\overline{\gamma}} \tag{A.4}$$

with cumulative distribution

$$P_{\gamma,Rayleigh}(\gamma) = 1 - e^{-\gamma/\overline{\gamma}} \tag{A.5}$$

Inserting these into equation (A.3) yields

$$\begin{aligned} p_{\gamma_{\sum}}(\gamma) &= 2p_{\gamma}(\gamma) - 2\left(p_{\gamma}(\gamma) - \frac{1}{\overline{\gamma}}e^{-2\gamma/\overline{\gamma}}\right) \\ &= \frac{2}{\overline{\gamma}}e^{-2\gamma/\overline{\gamma}} \end{aligned} \tag{A.6}$$

which is an exponential distribution where $\overline{\gamma}$ has been reduced by a factor of two compared to the single branch Rayleigh case.